MARTIN MARIETTA ENERGY SYSTEMS LIBRARIES
3 4456 0364306 5

cy. 3
CENTRAL RESEARCH LIBRARY
DOCUMENT COLLECTION

ORNL-3099
UC-25 – Metals, Ceramics, and Materials
TID-4500 (20th ed.)

IN-PILE RADIATION CORROSION EXPERIMENTS WITH ZIRCONIUM, TITANIUM, AND STEEL ALLOYS IN 0.17 *m* UO_2SO_4 SOLUTIONS AT 280°C

G. H. Jenks
J. E. Baker

CENTRAL RESEARCH LIBRARY
DOCUMENT COLLECTION
LIBRARY LOAN COPY
DO NOT TRANSFER TO ANOTHER PERSON
If you wish someone else to see this document, send in name with document and the library will arrange a loan.

OAK RIDGE NATIONAL LABORATORY
operated by
UNION CARBIDE CORPORATION
for the
U.S. ATOMIC ENERGY COMMISSION

Printed in USA. Price: $1.75 Available from the
Office of Technical Services
U. S. Department of Commerce
Washington 25, D. C.

LEGAL NOTICE

This report was prepared as an account of Government sponsored work. Neither the United States, nor the Commission, nor any person acting on behalf of the Commission:

A. Makes any warranty or representation, expressed or implied, with respect to the accuracy, completeness, or usefulness of the information contained in this report, or that the use of any information, apparatus, method, or process disclosed in this report may not infringe privately owned rights; or

B. Assumes any liabilities with respect to the use of, or for damages resulting from the use of any information, apparatus, method, or process disclosed in this report.

As used in the above, "person acting on behalf of the Commission" includes any employee or contractor of the Commission, or employee of such contractor, to the extent that such employee or contractor of the Commission, or employee of such contractor prepares, disseminates, or provides access to, any information pursuant to his employment or contract with the Commission, or his employment with such contractor.

ORNL-3099
UC-25 – Metals, Ceramics, and Materials
TID-4500 (20th ed.)

Contract No. W-7405-eng-26

REACTOR CHEMISTRY DIVISION

In-Pile Radiation Corrosion Experiments with Zirconium, Titanium, and Steel Alloys in 0.17 *m* UO_2SO_4 Solutions at 280°C

G. H. Jenks J. E. Baker

Other Contributors

E. G. Bohlmann
S. E. Bolt
J. W. Brown
R. A. Lorenz
J. R. McWherter
A. R. Olsen
M. L. Picklesimer
H. C. Savage
F. J. Walter
S. H. Wheeler

DATE ISSUED

JUN 24 1963

OAK RIDGE NATIONAL LABORATORY
Oak Ridge, Tennessee
operated by
UNION CARBIDE CORPORATION
for the
U. S. ATOMIC ENERGY COMMISSION

MARTIN MARIETTA ENERGY SYSTEMS LIBRARIES

3 4456 0364306 5

CONTENTS

Abstract 1

1. Introduction 2

2. Methods and Procedures 3

3. Equipment and Materials 6
   - 3.1 Loop Specifications 6
   - 3.2 Specimens to Test Corrosion and Other Factors 7
   - 3.3 Loop Areas 7
   - 3.4 Solution Compositions 7

4. Results and Specific Evaluations 7
   - 4.1 Preparatory Operation 7
   - 4.2 In-Pile Operation, Solution Analyses 16
   - 4.3 In-Pile Operation, Oxygen Consumption 16
   - 4.4 Radiolytic-Gas Pressure 24
   - 4.5 Uranium Balance 28
   - 4.6 Results of Qualitative Examination of Loops 28
     - 4.6.1 Experiment L-2-15 28
     - 4.6.2 Experiment L-4-16 31
   - 4.7 Metallographic Examinations 34
   - 4.8 Results of Fission-Power Determination 42
     - 4.8.1 Induced Activities 42
     - 4.8.2 Cesium-137 45
     - 4.8.3 Heat from Absorption of Fission and Gamma-Ray Energy 50
     - 4.8.4 Comparison of Average Fission-Power Values from Cs^{137}, Gamma-Ray Heat, and Induced Activities 50
   - 4.9 Results of Quantitative Examination of Loops 51
     - 4.9.1 Analyses of Scale from Low-Power-Density Regions 51
     - 4.9.2 Results of Specimen Weight Measurements 52

5. Summary and Discussion of Results 62
   - 5.1 Solution Composition and Stability 62
   - 5.2 Zirconium Alloys 64
   - 5.3 Other Zirconium Alloys 66
   - 5.4 Nickel- and Platinum-Clad Zircaloy-2 66
   - 5.5 Titanium Alloys 66
   - 5.6 Stainless Steel 66

IN-PILE RADIATION CORROSION EXPERIMENTS WITH ZIRCONIUM, TITANIUM, AND STEEL ALLOYS IN 0.17 *m* UO_2SO_4 SOLUTIONS AT 280°C

G. H. Jenks J. E. Baker

ABSTRACT

In-pile loop experiments L-2-15 and L-4-16 were two of a series designed to test the radiation corrosion of Zircaloy-2 and other possible reactor construction materials in UO_2SO_4 solutions under various conditions of radiation intensities, temperatures, solution compositions, and velocity of flow past specimens. The solutions employed were 0.17 *m* UO_2SO_4, 0.015 *m* $CuSO_4$, and 0.03 *m* H_2SO_4 in H_2O for experiment L-2-15, and 0.17 *m* UO_2SO_4, 0.015 *m* $CuSO_4$, and 0.025 *m* H_2SO_4 in H_2O for experiment L-4-16. The mainstream temperature in the experiments ranged from 278 to 280°C. The experiments were exposed in the LITR beam holes HB-2 and HB-4 respectively. Construction material for the loops was type 347 stainless steel. Specimens of types 347 and 309SCb stainless steels, titanium-55A and -110AT, platinum, Zircaloy-2, crystal-bar zirconium, and a variety of other zirconium alloys were tested. The power density at core specimens ranged from 19.8 to 4.6 w/ml in L-2-15 and from 5.7 to 1.3 w/ml in L-4-16. For loop L-2-15, the total time of high-temperature operation with UO_2SO_4 was 792 hr, during in-pile exposure, and the reactor energy was 1632 Mwhr; for loop L-4-16, 1032 hr and 2325 Mwhr. During both experiments most of the reactor energy was accumulated at the 3-Mw power level.

In general, stainless steel corrosion results from these experiments were comparable to those observed in other in-pile loop experiments. Corrosion was confined primarily to the core areas and was power-density dependent. Some variations in attack, both positive and negative, with velocity of solution flow past specimens have been observed in other experiments, but there was no apparent effect of varying velocities in the range 10 to 40 fps on either the core-channel or in-line channel specimens in the present experiments. The core-annulus steel specimens in L-2-15 corroded at rates very much greater than those in the channel. This difference may have resulted, in part, from the differences in velocities; however, it may have also been a result of galvanic action between the steel annulus specimens and adjacent platinum specimens. In previous 250°C experiments the occurrence of a change in the stainless steel corrosion rate was correlated with a decrease in acidity and/or increase in the nickel concentration. The results for the oxygen consumption rates on steel during radiation exposure in the present experiments varied with radiation time in a manner qualitatively similar to that observed at the lower temperature. However, the concentration of excess acid in the present experiments probably remained fairly constant throughout the radiation exposures, and correlations similar to those obtained at the lower temperature could not be established. The acid concentration in the 280°C experiments was greater than the concentrations prevailing when corrosion rate changes occurred in the 250°C experiments. The difference in acid tolerance is probably a result of the increased temperature, since a similar beneficial effect of temperature occurs out-of-pile. No overall correlation has been established for the various factors found to have influenced steel corrosion in previous experiments. Results of the present experiments provide additional evidence in support of previous findings but do not further their interpretation.

Zircaloy-2 corrosion results from both loops have been discussed and correlated elsewhere in terms of the 280°C relationship between the corrosion rate R (mils per year, mpy), power density P (w/ml), and uranium sorption factor α: $1/R = 2.23/P\alpha + 1/40$. The data from these experiments obey this relationship. The values of α for core-annulus specimens exposed to velocities of about 0.8 fps in both experiments were 3.3 for L-2-15 and about 2.6 for L-4-16. For the exposed surfaces in the channel specimens from L-2-15 and for those channel specimens located in the convergent section of the channel in L-4-16, α is estimated at about 1. Specimens located in the divergent section of the channel in L-4-16 exhibited higher α values.

Core-annulus coupons of zirconium alloyed with niobium, palladium, or platinum from experiment L-4-16 exhibited corrosion rates varying from 40 to 90% of the rates observed for core-annulus coupons of Zircaloy-2 at similar power densities when the specimen materials were heat-treated at 900°C for 3 hr and then water-quenched. Other specimens of the same alloys subjected to the same heat treatment and to additional treatment at 600°C for 48 hr and then air-cooled exhibited rates varying from 80 to 230% of those observed for the Zircaloy-2 core-annulus coupons. Two core-annulus impact specimens of Zr–15% Nb subjected to these heat treatments and a third impact specimen of Zircaloy-2 heat-treated at 650°C for 30 min exhibited rates from 130 to 140% of those observed for the Zircaloy-2 core-annulus coupons.

Two Zircaloy-2 coupons clad with nickel and then platinum and exposed in the core annulus of experiment L-2-15 and two similar coupons from the line-annulus position exhibited very high weight losses as a result of the loss of nickel layer. Platinum specimens from L-2-15 exhibited negligible corrosion rates.

Results for Ti-55A specimens indicate that in-pile titanium corrosion was affected to a greater extent by some uniform change in the solution under radiation than by fission recoil irradiation of specimen surfaces or by the fissioning which takes place in the solution immediately adjacent to specimens. The average corrosion rate (based on radiation time and total area) for the core-channel coupons from experiment L-4-16 was 0.22 mpy, and 0.20 mpy for the in-line channel coupons. The average rate for the core-channel coupons in experiment L-2-15 was 1.2 mpy. In-line channel coupons from this experiment exhibited an average weight increase of 1.1 mg/cm^2. However, at the generally low rates prevailing for titanium, it is likely that the in-line results were affected appreciably by retained scale. Impact, tensile, and stress specimens of Ti-110AT in the core-annulus regions of both experiments exhibited higher rates than core-annulus coupons of Ti-55A.

Analyses of bulk scale from various parts of loop L-4-16 show wide variations in composition and are considered only qualitative. The results indicate that nearly all the zirconium that was oxidized in the core was transported to portions of the loop outside the core and deposited in the scale. The analyses also indicate that appreciable amounts of nickel are incorporated in the loop scales. Also, in these and other experiments, the difference between amounts of steel corrosion indicated by oxygen and dissolved-nickel data reveals that nickel is retained in the scales and, consequently, that the amount of dissolved nickel cannot be used as an accurate measure of steel corrosion in these systems.

There was no evidence of solution instability in these experiments. Some fluctuations in analytical results were ascribed to sampling and analytical errors.

---

1. INTRODUCTION

Solutions of uranyl sulfate at temperatures in the neighborhood of 250 to 300°C and contained by or in contact with various structural materials such as zirconium, titanium, and stainless steel alloys have been of interest as possible fuel systems for aqueous homogeneous reactors. A series of 18 in-pile loop experiments has been carried out with the primary objective of testing the effects of reactor radiations on corrosion in these systems. Also investigated in some of the experiments were the effects of the in-pile exposure on impact and tensile properties of various structural materials, solution stability under irradiation, rate constants for recombination of radiolytic gas by copper sulfate in solution, and the general reliability of equipment operating under the test conditions.

The methods, equipment, and procedures employed in these experiments have been described in detail elsewhere.[1] Each experiment has also been reported or summarized in quarterly progress reports of the Homogeneous Reactor Project. Results and conclusions were included; however, detailed reports of each experiment are planned, and some have been prepared and issued for several experiments.[2–6] The present paper describes two of these experiments (L-2-15 and L-4-16) which employed exposure temperatures of 280 and 295 to 298°C in the mainstream and pressurizer, respectively, 0.17 *m* UO_2SO_4 solutions, and were exposed to reactor radiations in the LITR. Experiments L-2-15 and L-4-16 were exposed in beam holes HB-2 and HB-4, respectively, in order to obtain data over a wide range of thermal-neutron fluxes and to provide a basis for direct comparison between experiments in the two holes. (The unperturbed thermal-neutron flux in HB-2 is about 3 to 4 times greater than that in HB-4.) In addition, operation of these experiments at 280°C provided a comparison of stainless steel and of zirconium and titanium alloy corrosion data with data obtained in previous 250°C experiments that employed comparable solutions. Some general information on the composition of the solutions employed and the operating-time data are given in Table 1.

2. METHODS AND PROCEDURES

An overall experiment included: (1) preparing the loop for operation and proving its satisfactory performance in out-of-pile operation, (2) exposing and operating the loop in the LITR, and (3) dismantling the loop and examining corrosion specimens and other portions of the loop for evidence of corrosive attack.

A brief listing of the different types of examinations, operations, and measurements for the results included in this report is given below. In the interest of brevity, only purposes are indicated; the general objectives of these measurements are discussed in ref 2. Reports on the in-pile operation of these experiments have been published.[7,8]

1. Sampling and chemical analyses of loop solutions during out-of-pile preparatory operations. Also, measurements of oxygen consumption during high-temperature operations with some of the solutions. Materials and equipment checkout.

---

[1] H. C. Savage and W. D. Reel, *In-Pile Corrosion Test Loops for Aqueous Homogeneous Reactor Solutions*, ORNL-2977 (Nov. 10, 1960).

[2] G. H. Jenks and J. E. Baker, *In-Pile Loop Corrosion Experiments with Uranyl Sulfate Solutions at 235 and 250°C*, ORNL-3131 (in press).

[3] J. E. Baker and G. H. Jenks, *HRP Radiation Corrosion Studies: In-Pile L-4-8*, ORNL-2042 (Aug. 8, 1956).

[4] J. R. McWherter and J. E. Baker, *HRP Radiation Corrosion Studies: In-Pile Loop L-4-11*, ORNL-2152 (June 11, 1958).

[5] G. H. Jenks and J. E. Baker, *In-Pile Loop Investigation of Corrosion of Zircaloy-2 and Other Possible Reactor Materials in 0.04* m UO_2SO_4 *at 280°C*, ORNL-2962 (in press).

[6] G. H. Jenks and J. E. Baker, *Determination of the Effect of High Sulfuric Acid Concentration on the Radiation Corrosion of Zircaloy-2 and Titanium in 0.17* m UO_2SO_4, ORNL-2943 (in press).

[7] F. J. Walter, *HRP In-Pile Corrosion Test Loops, Operation of In-Pile Loop L-2-15*, ORNL CF-57-8-42 (Aug. 27, 1957).

[8] F. J. Walter, *HRP In-Pile Corrosion Test Loops, Operation of In-Pile Loop L-4-16*, ORNL CF-57-8-11 (Aug. 26, 1957).

Table 1. Test-Solution Compositions and Operating-Time Data for Loop Experiments L-2-15 and L-4-16

Experiment Number	Date Exposed in Reactor	Temperature During In-Pile Exposure (°C)		Initial and Final Solution Compositions for In-Pile Corrosion (M at STP)					pH[a]	Makeup Solution Composition (M at STP)				pH	Time at Temperature with UO_2SO_4 Solutions (hr)		Radiation Exposure Time (3-Mwhr LITR Energy)
		Mainstream	Pressurizer	UO_2SO_4	$CuSO_4$	Ni	Cr	Excess H_2SO_4		UO_2SO_4	$CuSO_4$	Excess H_2SO_4	Cr as CrO_3		Preparatory	Enriched	
L-2-15	In 11-2-56	280	298	0.168	0.0143	0	<0.0005	0.030	1.51	0.166	0.0137	0.070	<0.0005	1.50	124	450	258
	Out 11-23-56			0.178[b]	0.0149[b]	0.0032[b]	0.0025	0.030	1.80								
	In 11-25-56			0.168	0.0143	0	<0.0005	0.030	1.51	0.164	0.0131	0.021	0.0030	1.51		306	248
	Out 12-8-56			0.188[b]	0.0152[b]	0.0033[b]	0.0022[b]		1.60								
L-4-16	In 12-28-56	280	295	0.170	0.0141	0	Negative	0.023	1.50	0.170	0.0138	0.060	0.0033	1.15	167	961	708
	Out 2-11-57			0.181[b]	0.0144[b]	0.0018[b]	0.0017[b]	0.027	1.80								

[a]Uncorrected for dilution of samples from loop stream.
[b]Average of two final samples.

2. Sampling of loop solution at regular intervals during in-pile operation, and analyses for various constituents including U, SO_4, Cu, Ni, Cr, Fe, Zr, Mn, and Cs^{137}. Lithium sulfate tracer was used to measure dilution during sampling. The LITR operation and sampling schedule is shown in Fig. 1. Solution composition and generalized corrosion.
3. Determinations of pressures of excess oxygen and of radiolytic gases in the pressurizer. Generalized corrosion and recombination.
4. Sampling of solution in weigh tank (solution dump tank). Solute inventory.
5. Qualitative inspection of loop and specimens after radiation exposure.
6. Determination of specimen weight losses resulting from corrosion.
7. Determination of thermal-neutron fluxes adjacent to core specimens from measurements of induced activities of samples.

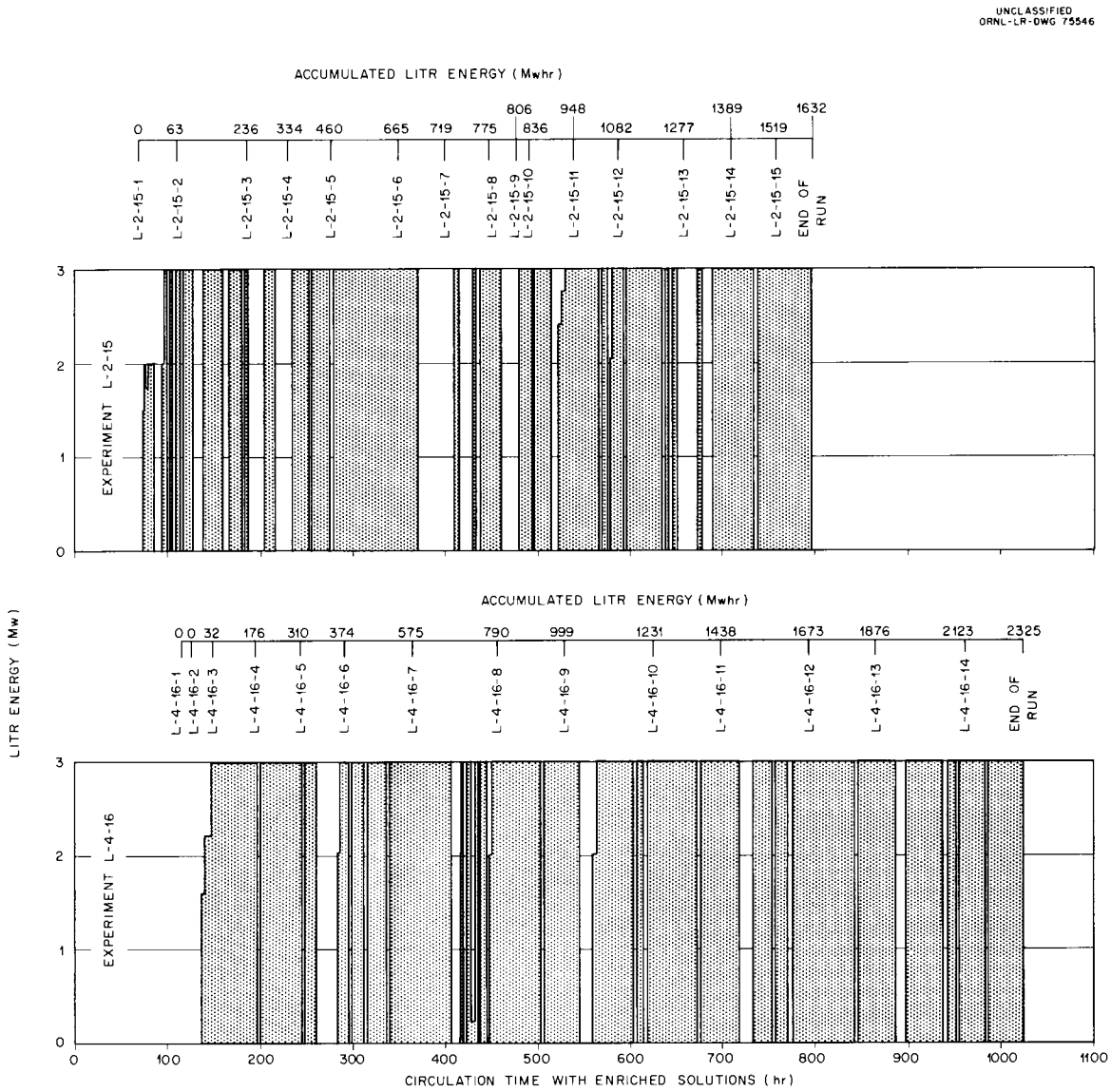

Fig. 1. LITR Operation and Loop Sampling Schedule.

8. Metallographic examination of specimens and portions of loops.
9. Analyses of bulk scales scraped from L-4-16 surfaces after irradiation. Determination of the distribution of corrosion products in the loop.
10. Testing of mechanical property specimens. These tests were carried out by the Metallurgy Group of the HRP, and the results are reported elsewhere.[9,10]

3. EQUIPMENT AND MATERIALS

3.1 Loop Specifications

Specifications for each loop, including volumes and materials of construction of pump and specimen holders, are listed in Table 2.

[9] G. M. Adamson *et al.*, *HRP Quart. Progr. Rept. Oct. 31, 1957*, ORNL-2432, p 134.

[10] G. M. Adamson *et al.*, *HRP Quart. Progr. Rept. Apr. 30 and July 31, 1958*, ORNL-2561, p 250.

Table 2. Loop Construction Data

	Loop L-2-15	Loop L-4-16
Loop volume (including pressurizer), ml	1518	1566
Pressurizer volume, ml	561	570
Volume of solution in pressurizer, ml	407	431
Empty-core volume, ml	372	372
Loaded-core volume, ml	308	311
Flow rates		
Pressurizer, ml/sec	7.5	7.5
Core, gpm	5.3	5.4
Pump design	ORNL outboard bearing	ORNL outboard bearing
Pump bearing material	Al_2O_3	Al_2O_3
Pump journal material	Al_2O_3	Al_2O_3
Loop construction material	347 stainless steel	347 stainless steel
Core and in-line channel coupon holders[a]	Z-2	S-1
Core-annulus coupon holders[a]	T-1	S-1
In-line annulus coupon holders[a]	T-1	S-1
Core impact specimen holders[a]	S-1	S-1
In-line impact specimen holders[a]	S-1	S-1
Core tensile specimen holders[a]	S-1	S-1
In-line tensile specimen holders[a]	S-1	S-1
Core stress specimen holders[a]	T-1	
In-line stress specimen holders[a]	T-1	
Design pressure, psi	2000	2000

[a] Refer to Table 3*a* for material code.

3.2 Specimens to Test Corrosion and Other Factors

The numbers and types of corrosion and mechanical property specimens employed in the loops are shown in Table 3*a*. The specimen materials are listed by a code shown at the bottom of the table. Material item numbers are also shown, and the corresponding compositions are listed in Table 3*b*. When compositions are not given, nominal ones are assumed.

All the corrosion coupons had the dimensions 0.25 × 0.50 × 0.06 in., except the platinum-nickel-clad coupons, which were 0.50 × 0.50 × 0.06 in., and the platinum coupons, which were 0.25 × 0.50 × 0.02 in. The clad specimens were tested at the request of the HRP Metallurgy Group, who supplied these specimens. The cladding was comprised of nickel plated on Zircaloy-2 to a depth of about 1 mil, and platinum plated on the nickel to a depth of about 0.2 mil. The specimens were cut from a bar following the plating operation, and, hence, all three metals were exposed on at least an edge of the coupon.

The arrangements of channel and annulus coupons are shown in Figs. 2 and 3. Figure 4 is a photograph of the core-channel holder and coupons in loop L-4-16. Figure 5 is a photograph of the core specimen assembly in loop L-4-16.

Abbreviations used in this report in referring to different types of specimens are the following: CC, core channel; CA, core annulus; LC, in-line channel; LA, in-line annulus.

3.3 Loop Areas

Internal surface areas of each loop and total areas of specimens of different materials are listed in Tables 4–8. Individual specimen and holder areas are included in Tables 21 and 22.

3.4 Solution Compositions

The compositions of the solutions charged to and recovered from loops are listed in Table 1. The compositions of the solutions used to replace those removed in sampling are also listed. The reliability of these analytical results is considered in the discussion section.

4. RESULTS AND SPECIFIC EVALUATIONS

4.1 Preparatory Operation

The solutions and other experimental conditions employed in preparatory operations are listed in Table 9 together with the results of analyses for corrosion products and chlorine in the various solutions. Values are also listed for the average corrosion rates of steel loop surfaces calculated from the results for nickel accumulation in solution and, where available, from oxygen consumption. In calculating the rate values it was assumed that there was no selective oxidation of any of the components of stainless steel and that oxidized nickel was dissolved quantitatively.

As discussed below (Sec 4.7), the nickel layers on the four nickel-platinum-clad Zircaloy-2 coupons in loop L-2-15 were badly attacked or completely dissolved during the experiment. Estimates of stainless steel corrosion rates for this experiment, based on nickel concentrations in solution, have not been corrected for the appreciable amount of nickel from this source.

Table 3*a*. Corrosion Specimens Exposed in Loop Experiments

Location	Materials and Number of Specimens																
	S-1	S-2	T-1	T-2	Z-1	Z-2	Z-3	Z-4	Z-5	Z-6	Z-7	Z-8	Z-9	Z-10	Z-11	Z-12	P
Experiment L-2-15																	
Core-channel coupons	8		8			8											
Line-channel coupons	8		8			8											
Core-annulus specimens																	
Corrosion coupons	3	2		2		3	2										2
Impact specimens					2	2											
Tensile specimens					2												
Stress specimens				2													
Line-annulus specimens																	
Corrosion coupons	3	2		2		3	2										2
Impact specimens					2	1											
Tensile specimens					1												
Stress specimens				2													
Experiment L-4-16																	
Core-channel coupons	8		8		8	8											
Line-channel coupons	8		8			8											
Core- and line-channel holders	2																
Core-annulus specimens																	
Corrosion coupons	2					4		2[a] 1[b]	2[a] 1[b]	2[a] 1[b]	2[a]	2[a]	2[a]	2[a] 1[b]	2[a] 1[b]	2[a] 1[b]	
Impact specimens			1[c]	1[c]		1[d]				1[a] 1[e]							
Tensile specimens				1[c]													
Line-annulus specimens																	
Corrosion coupons	1					2		1[a] 1[b]	1[a] 1[b]	1[a] 1[b]	1[a]	1[a]	1[a]	1[a]	1[a]	1[a]	
Impact specimens				1[c]		1[d]				1[a]							
Tensile specimens				1[c]													

[a]Held at 900°C for 3 hr, water-quenched.
[b]Held at 900°C for 3 hr, water-quenched; held at 600°C for 48 hr, air-cooled.
[c]Commercial anneal.
[d]Held at 1200°F for 30 min.
[e]Held at 900°C for 3 hr, water-quenched; held at 600°C for 3 hr, water-quenched.
Specimens fabricated from materials Z-4 through Z-12 were chemically polished; all others were "as-machined."

Material code:
- S-1 Type 347 stainless steel (L-2-15) item No. 1149, (L-4-16) item No. 1149
- S-2 Type 309SCb stainless steel (L-2-15) item No. 252
- T-1 Titanium-55A (L-2-15) item No. 1165, (L-4-16) item No. 1165
- T-2 Titanium-110AT (L-2-15) item No. 1176, (L-4-16) item No. 1176
- Z-1 Crystal-bar zirconium (L-2-15) item No. 1591-8
- Z-2 Zircaloy-2 (L-2-15) item No. 1157, (L-4-16) item Nos. 1157 and 1153
- Z-3 Nickel- and platinum-clad Zircaloy-2
- Z-4 85% Zr sponge, 15% Nb
- Z-5 67% Zr crystal bar, 33% Nb
- Z-6 85% Zr crystal bar, 15% Nb
- Z-7 95% Zr crystal bar, 5% Pt
- Z-8 95% Zr crystal bar, 5% Pd
- Z-9 75% Zr crystal bar, 20% Nb, 5% Pd
- Z-10 80% Zr crystal bar, 15% Nb, 5% Pt
- Z-11 83% Zr crystal bar, 15% Nb, 2% Pt
- Z-12 83% Zr crystal bar, 15% Nb, 2% Pd
- P Platinum

Table 3*b*. Composition of Specimen Materials (%)

Element	Material and Item Number					
	347 Stainless Steel, 1149	309SCb Stainless Steel, 252	Zircaloy-2 1157	Zircaloy-2 1163	Titanium-55A, 1165	Zirconium Crystal Bar, 1591-8
Cr	12.8	23.19	0.2	HRT plate No. 8		0.05
Cu			0.05			0.05
Fe	69.2		0.5		0.047	0.5
Ni	10.2	14.46	0.1			0.05
Sn			1.5			0.05
C	0.043	0.06			0.027	
Si	0.50	0.54				
Mn	1.43	1.76				
Mo	0.11					
Nb/Ta	0.79					
N_2					0.020	
H_2					0.004	
P		0.014				
S		0.020				
Nb		0.89				

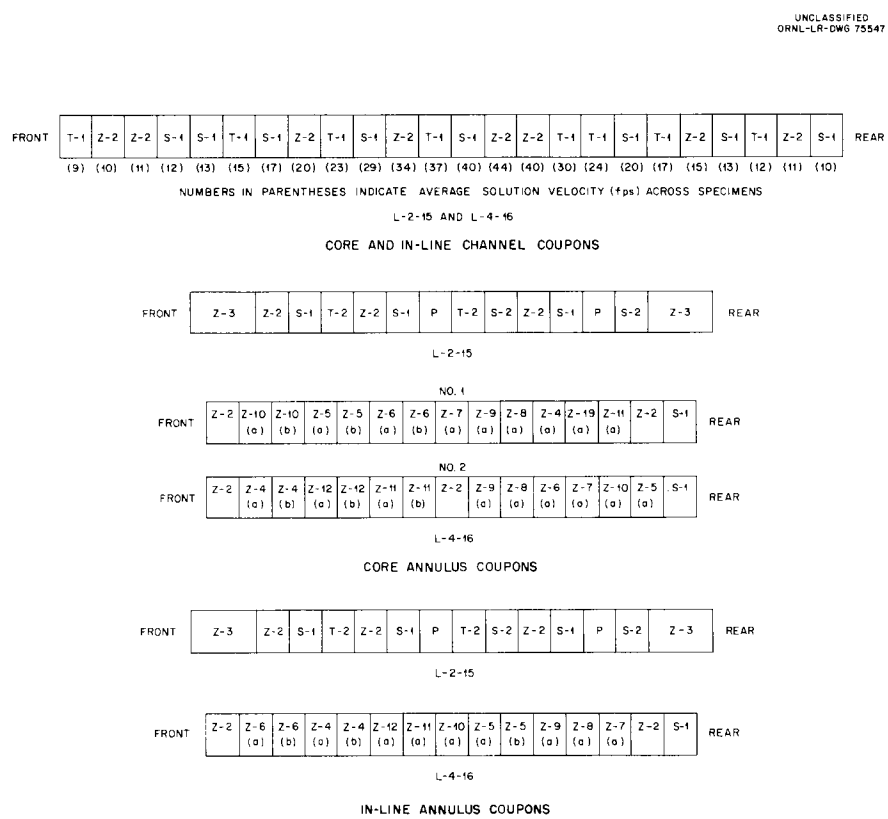

Fig. 2. Core and In-Line Coupon Specimen Arrangement in L-2-15 and L-4-16.

UNCLASSIFIED
ORNL-LR-DWG 75548

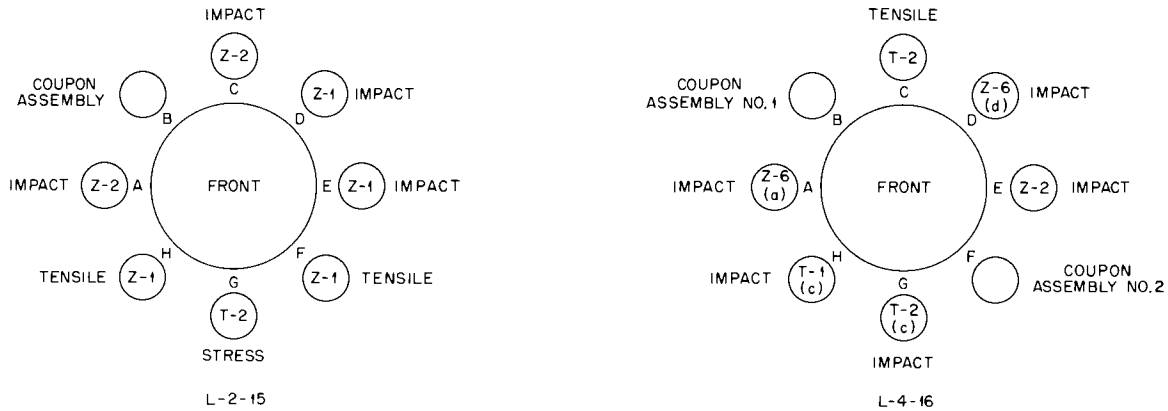

CORE SPECIMENS

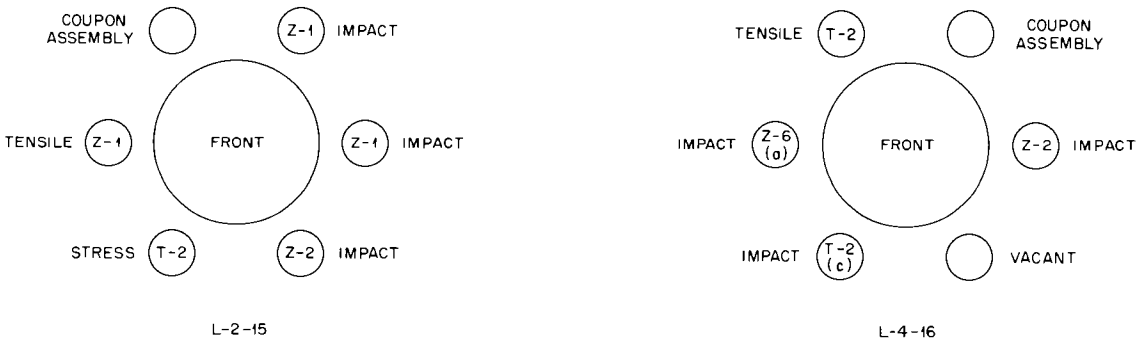

IN-LINE SPECIMENS

Fig. 3. Core and In-Line Tensile, Impact, Stress, and Annulus Coupon Specimen Arrangements in L-2-15 and L-4-16.

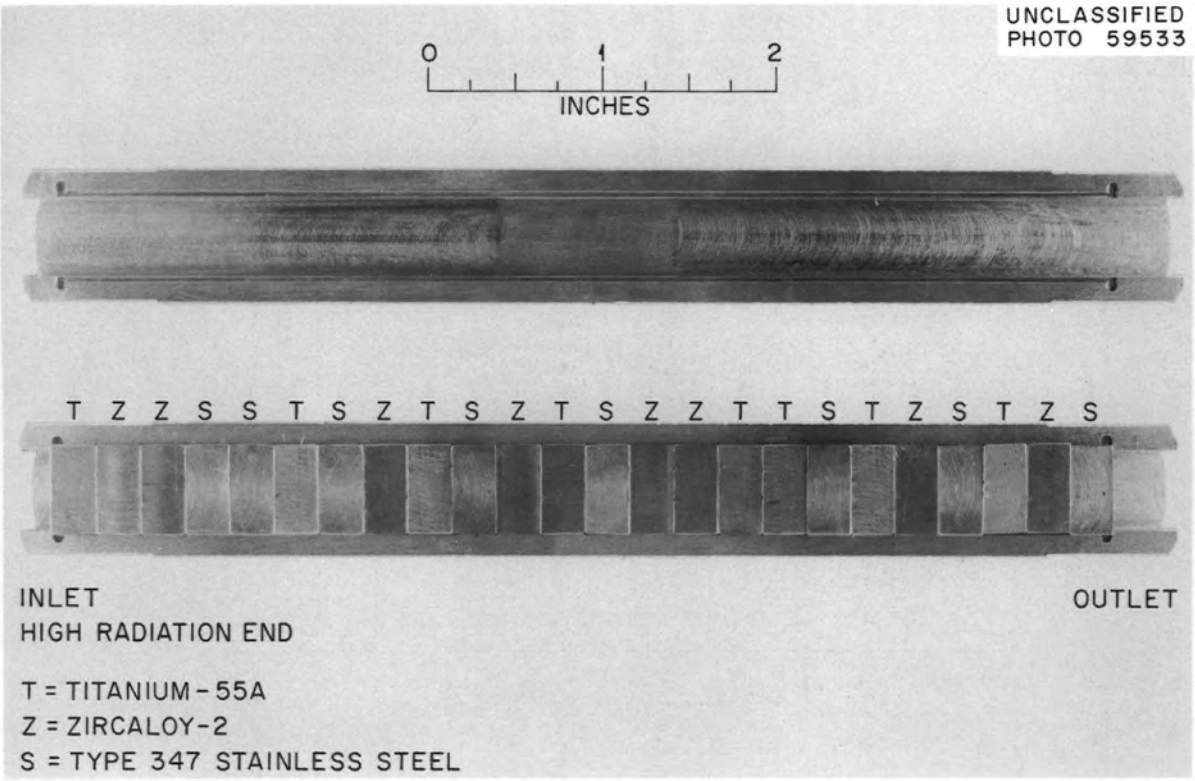

Fig. 4. Tapered-Channel Core Coupon Holder – In-Pile Loop L-4-16.

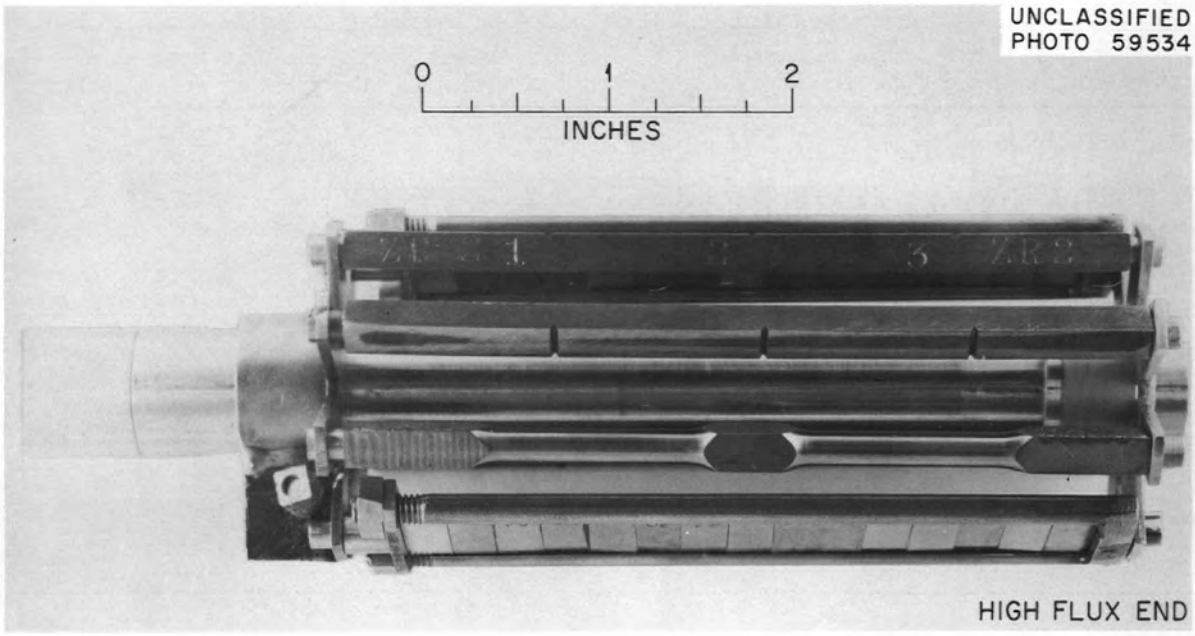

Fig. 5. Annulus Coupon, Impact, and Tensile Specimens in Core – In-Pile Loop L-4-16.

Table 4. Loop Areas Exposed to High-Temperature Solution: Type 347 Stainless Steel

Component	Area Exposed (cm^2)	
	L-2-15	L-4-16
Total main circulation lines (not including pump and core)	1450	1516
Pressurizer		
Total	(708)	(708)
Area wetted	504	469
Pressurizer lines	243	293
Core	318	318
Pump		
Scroll	236	236
Impeller	215	215
Total area	2966	3047

Table 5. Total Areas Exposed to High-Temperature Solution: Stainless Steel Specimens

Component	L-2-15				L-4-16	
	347		309SCb		347	
	Number	Area (cm^2)	Number	Area (cm^2)	Number	Area (cm^2)
Core-channel coupons	8	17.6			8	17.6
Line-channel coupons	8	17.6			8	17.6
Core- and line-channel holders					2	380
Core-annulus coupons	3	6.6	2	4.4	2	4.4
Line-annulus coupons	3	6.6	2	4.4	1	2.2
Core- and line-annulus holders					3	124.8
Core spider	1	19.4			1	19.4
Core- and line-channel holder clamp bands	4	58.0			4	58.0
Core and line special holders	4	116.8			4	116.8
Total		242.6		8.8		744.1

Table 6. Total Areas Exposed to High-Temperature Solution: Titanium

Component	L-2-15				L-4-16			
	Ti-55A		Ti-110AT		Ti-55A		Ti-110AT	
	Number	Area (cm^2)	Number	Area (cm^2)	Number	Area (cm^2)	Number	Area (cm^2)
Core-channel coupons	8	17.6			8	17.6		
Line-channel coupons	8	17.6			8	17.6		
Core-annulus coupons			2	4.4				
Core-annulus holder	1	41.6						
Line-annulus coupons			2	4.4				
Line-annulus holder	1	41.6						
Core impact specimens					1	23.9	1	23.9
Line impact specimens							1	23.9
Core tensile specimens							1	21.2
Line tensile specimens							1	21.2
Core stress specimens			2	20.0				
Core stress specimen holder	1	20.0						
Line stress specimen			2	20.0				
Line stress specimen holder	1	20.0						
Total		75.2		48.8		29.1		90.2

Table 7. Total Areas Exposed to High-Temperature Solution: Zirconium and Zirconium Alloy Specimens

Material	Component																	
	Core-Channel Coupons		Line-Channel Coupons		Core- and Line-Channel Holders		Core-Annulus Coupons		Core Impact Specimens		Core Tensile Specimens		Line-Annulus Coupons		Line Impact Specimens		Line Tensile Specimens	
	No.	Area (cm^2)	No.	Area (cm^2)	No.	Area (cm^2)	No.	Area (cm^2)	No.	Area (cm^2)	No.	Area (cm^2)	No.	Area (cm^2)	No.	Area (cm^2)	No.	Area (cm^2)
L-2-15																		
Crystal-bar zirconium									2	53.4	2	42.4			2	53.4	1	21.2
Zircaloy-2	8	17.6	8	17.6	2	380	3	6.6	2	53.4			3	6.6	1	26.7		
Zircaloy-2[a]																		
Nickel- and platinum-clad Zircaloy-2							2	4.4					2	4.4				
Total		17.6		17.6		380		11.0		106.8		42.4		11.0		80.1		21.2
L-4-16																		
Zircaloy-2	8	17.6	8	17.6			4	8.8					2	4.4				
Zircaloy-2[a]									1	26.7					1	26.7		
Nickel- and platinum-clad Zircaloy-2																		
85% Zr sponge, 15% Nb[b]							2	4.4					1	2.2				
85% Zr sponge, 15% Nb[c]							1	2.2					1	2.2				
67% Zr crystal bar, 33% Nb[b]							2	4.4					1	2.2				
67% Zr crystal bar, 33% Nb[c]							1	2.2					1	2.2				
85% Zr crystal bar, 15% Nb[b]							2	4.4	1	26.7			1	2.2	1	26.7		
85% Zr crystal bar, 15% Nb[c]							1	2.2					1	2.2				
85% Zr crystal bar, 15% Nb[d]									1	26.7								
95% Zr crystal bar, 5% Pt[b]							2	4.4					1	2.2				
95% Zr crystal bar, 5% Pd[b]							2	4.4					1	2.2				
75% Zr crystal bar, 20% Nb, 5% Pt[b]							2	4.4					1	2.2				
80% Zr crystal bar, 15% Nb, 5% Pt[b]							2	4.4					1	2.2				
80% Zr crystal bar, 15% Nb, 5% Pt[c]							1	2.2										
83% Zr crystal bar, 15% Nb, 2% Pt[b]							2	4.4					1	2.2				
83% Zr crystal bar, 15% Nb, 2% Pt[c]							1	2.2										
83% Zr crystal bar, 15% Nb, 2% Pd[b]							2	4.4					1	2.2				
83% Zr crystal bar, 15% Nb, 2% Pd[c]							1	2.2										
Total		17.6		17.6				61.6		80.1				30.8		53.4		

[a]Held at 1200°F for 30 min.
[b]Held at 900°C for 3 hr, water-quenched.
[c]Held at 900°C for 3 hr, water-quenched; held at 600°C for 48 hr, air-cooled.
[d]Held at 900°C for 3 hr, water-quenched; held at 600°C for 3 hr, water-quenched.

Table 8. Total Areas Exposed to High-Temperature Solution: Miscellaneous Specimens

Material	Component				Total Area (cm^2)
	Core-Annulus Coupons		Line-Annulus Coupons		
	Number	Area (cm^2)	Number	Area (cm^2)	
Platinum					
L-2-15	2	1.8	2	1.8	3.6

Table 9. Analyses of Samples from Loop Inventory and Overall Corrosion Rates During Preparatory Operations[a]

Solution	Atmosphere	Temperature (°C)	Total Circulation Time for Each Solution (hr)	Inventory at Time of Sampling (ml)	Concentration and Total Weight of Constituents																Average Stainless Steel Corrosion Rate (mpy)		pH
					Uranium		Sulfate		Copper		Nickel		Iron		Chromium		Aluminum		Chlorine				
					(mg/ml)	(g)	(mg/ml)	(g)	(μg/ml)	(mg)	(μg/ml)	(mg)	(μg/ml)	(mg)	(μg/ml)	(mg)	(μg/ml)	(mg)	(μg/ml)	(mg)	Nickel	O_2	
L-2-15																							
3% Na_3PO_4	He	95	5.6	1250					<1	<1	<1	<1	5	6	<1	<1	<2	<2	<2	<2			11.4
5% HNO_3	He	95	23.5	1250					5	6	75	94	110	138	8	10	14	18	<1	<1			0.3
H_2O	O_2	280–305	6.1	1013					<1	<1	<1	<1	<1	<1	<1	<1	<1	<1	<1	<1			8.0
H_2O	O_2	280–305	36.3	1014					<1	<1	3	3	<1	<1									3.7
0.17 *m* UO_2SO_4,	O_2	280–305	46.0		41.0[b]		21.0		2000		2		1		8		1		<2		4.3		1.9
0.03 *m* $CuSO_4$, 0.02 *m* H_2SO_4				1014[c]	36.6	37.1	20.5	20.8	1960	1990	90	91	10	10	46	46	31	31	<3	<3			2.1
0.17 *m* UO_2SO_4,	O_2	280–305	78.2		41.0[b]		20.0		1950		5		10		1		8		8		1.8	2.0	1.9
0.03 *m* $CuSO_4$, 0.02 *m* H_2SO_4				1015[c]	38.6	39.2	21.8	22.1	1800	1830	64	65	24	24	16	16	23	23	<2	<2			1.8
H_2O	O_2	280–305	5.1	1013																			
L-4-16																							
3% Na_3PO_4	He	94	3.9	1250					<1	<1	<1	<1	11	14	<1	<1	4	4	8	10			11.0
5% HNO_3	He	95	24.2	1170					<4	<4	18	21	75	88	10	12	20	23	<2	<2			0.03
H_2O	O_2	280–295	16.1	1050					<1	<1	<1	<1	<1	<1	<3	<3	<1	<1	<1	<1			2.6
0.17 *m* UO_2SO_4,	O_2	280–295	53.3		40.0[b]		19.0		480		0		3		0		5		<2		1.0	4.0	1.5
0.025 *m* H_2SO_4, 0.0075 *m* $CuSO_4$				1065[c]	38.8	41.3	18.7	19.9	470	501	48	51	32	34	46	49	29	31	<2	<2			1.6
0.17 *m* UO_2SO_4,	O_2	280–295	114.3		40.0[b]		19.5		450		0		12		0		13		<2		0.3	1.1	1.5
0.025 *m* H_2SO_4, 0.0075 *m* $CuSO_4$				1065[c]	39.5	42.1	19.5	20.8	480	511	23	25	21	22	32	34	28	30	<2	<2			1.5

[a]Constituent concentrations and totals shown are not cumulative but represent the quantities present for operation with each solution.
[b]Entries on this line are for the original solution.
[c]Entries on this line are for the final solution.

4.2 In-Pile Operation, Solution Analyses

The results of analyses for constituents other than fission products are given in Table 10, and for free acid in Table 11. In general, the listings include the reported concentration of a constituent in a sample, the concentration in the sample prior to dilution by wash water which contained Li_2SO_4 tracer, and the calculated total amount of a given constituent in the loop solution. The calculated values for total amounts of a constituent at the time of a given sampling include corrections, where applicable, for the amounts withdrawn in prior sampling.

Table 11 includes the free-acid concentration calculated from the results of pH measurements[11] and from inventory balances of acid additions and removals, assuming removal of acid mole per mole by the nickel and manganese found in solution.

The reported, corrected, and calculated concentrations of uranium, sulfate, and copper in the several experiments are shown and compared graphically in Fig. 6.

The nickel data given in the above table are plotted against circulation time in Fig. 7. Values of steel corrosion which correspond to given amounts of nickel (calculated as described in Sec 4.1) are also shown.

Plots of the free-acid concentration determined by analyses and from pH measurements are plotted vs radiation exposure time in Figs. 8 and 9.

4.3 In-Pile Operation, Oxygen Consumption

The results of oxygen consumption measurements during radiation exposure are shown in Figs. 10 and 11 in plots of calculated rates of consumption by steel vs megawatt-hours of LITR energy accumulated during exposure. Each datum was obtained during periods in which the reactor operated at the 3-Mw power level (the usual level) and in which the rate of pressure loss was essentially constant for 10 hr or more. The plotted times are midpoints of such periods. The consumption rates are in units of volume of oxygen per 3 Mwhr. Also shown in each figure are values for the average consumption rates on the zirconium and titanium alloys determined from weight data. The steel rates were obtained by reducing the observed consumption rates by these listed amounts. Values are also shown in each figure for the relationships between oxygen consumption rates and steel corrosion rates in mils per year when it is assumed in one case that all steel surfaces in contact with high-temperature solution corroded uniformly, and in another case that only the steel surfaces in the core consumed oxygen. The actual distribution of the corrosion in a loop will be considered in the discussion section.

Data for the total amounts of oxygen consumed during the in-pile exposures are listed in Table 12. The corresponding steel penetration values calculated, assuming uniform corrosion of steel surfaces, with no corrections for corrosion of other materials, are also listed. These oxygen consumption results corrected for consumption by other materials are shown graphically and compared with the nickel results in Fig. 7 as functions of total times at operating temperature.

---

[11] G. H. Jenks and J. E. Baker, *In-Pile Loop Corrosion Experiments with Uranyl Sulfate Solutions at 235 and 250°C*, ORNL-3131 (in press).

Table 10. Analyses of Samples from Loop Inventory During Enriched-Solution Operation[a]

Sample	Total Circulation Time (hr)	Accumulated LITR Energy (Mwhr)	Inventory Volume at Time of Sample, 25°C (ml)	Lithium[b] (mg/ml)	Sample Dilution Factor[c]	Uranium Rep (mg/ml)	Uranium Cor[d] (mg/ml)	Uranium Calcd[e] (mg/ml)	Sulfate Rep (mg/ml)	Sulfate Cor[f] (mg/ml)	Sulfate Calcd[g] (mg/ml)	Copper Rep (mg/ml)	Copper Cor[d] (mg/ml)	Copper Calcd[h] (mg/ml)	Chromium Rep (mg/ml)	Chromium Calcd Total[i] (g)	Nickel Rep (mg/ml)	Nickel Calcd Total[j] (g)	Chlorine Rep (mg/ml)	Chlorine Calcd Total[j] (g)	Iron Rep (mg/ml)	Iron Calcd Total[i] (g)	Zirconium Rep (mg/ml)	Zirconium Calcd Total[i] (g)	Aluminum Rep (mg/ml)	Aluminum Calcd Total[j] (g)	Manganese Rep (mg/ml)	Manganese Calcd Total[j] (g)	pH	Specific Gravity	H_2SO_4[k] Concentration (m)
														L-2-15																	
First original charge	0	0	1016	ND	1.0	39.6	39.6	39.6	20.9	20.9	20.9	0.91	0.91	0.91	0.012	0.013	ND	ND	ND	ND	0.056	0.057	0.006	0.006					1.51	1.057	0.031
L-2-15-1[l]	69.4	0	1016	0.145	1.19	33.4	39.6	39.6	18.4	20.7	20.9	1.07	1.27	0.91			0.093	0.112	ND	ND	0.145	0.175							1.95		0.013
L-2-15-2	110.7	62.8	1016	0.162	1.21	32.1	38.9	39.6	17.5	19.8	20.9	0.53	0.64	0.91			0.073	0.090	ND	ND	0.056	0.070	0.012	0.015					2.15		0.008
L-2-15-3	183.7	235.7	1016	0.182	1.24	34.1	42.4	39.6	18.4	21.4	20.9	0.91	1.13	0.91	0.037	0.047	0.100	0.128	ND	ND	0.144	0.182	0.012	0.015			ND	ND	1.75		0.022
L-2-15-4	230.2	334.4	1018	0.146	1.19	36.7	43.6	39.4	19.3	21.7	20.8	0.87	1.03	0.90	0.053	0.064	0.135	0.166	ND	ND	0.081	0.098	0.056	0.068			ND	ND	1.90		0.015
L-2-15-5[l]	278.2	459.6	1016	0.210	1.29			39.4			20.8			0.90			ND	ND											1.80		0.021
L-2-15-6	350.4	664.7	1016	0.156	1.17	34.4	40.3	39.4	18.6	20.7	20.8	0.87	1.02	0.90			0.157	0.192	ND	ND	0.032	0.039	ND	ND			ND	ND	1.80		0.019
L-2-15-7[l]	402.0	719.1	1017	0.145	1.19	36.6	43.4	39.3	20.0	22.5	20.9	0.74	0.88	0.90	0.110	0.132	0.162	0.206	ND	ND	0.033	0.041	0.048	0.058			ND	ND	1.80		0.019
L-2-15-8	449.5	775.3	1015					39.3			21.0			0.90					ND	ND									1.80		0.019[m]
Average concentration							41.3			21.1			0.89																		
Second original change	0	0	1018	ND	1.0	39.6	39.6	39.6	20.9	20.9	20.9	0.91	0.91	0.91	0.012	0.013	ND	ND	ND	ND	0.056	0.057	0.006	0.006					1.51	1.057	0.031
L-2-15-9[l]	476.3	805.5	1018	0.158	1.21	33.1	39.9	39.5	19.2	21.8	20.8	0.80	0.97	0.90	0.127	0.156	0.023	0.028	ND	ND	0.293	0.360	0.135	0.163					1.65		0.027
L-2-15-10	490.6	836.4	1018	0.148	1.19	37.6	44.7	39.5	20.6	23.3	20.8	0.93	1.11	0.90	0.171	0.207	0.039	0.047	ND	ND	0.055	0.065	0.076	0.092					1.80		0.019
L-2-15-11	538.8	948.0	1016	0.166	1.22	38.1	46.4	39.5	19.5	22.3	20.9	0.86	1.05	0.90	0.161	0.199	0.019	0.024	ND	ND	0.094	0.117	0.002	0.002					1.75		0.022
L-2-15-12	587.2	1082.0	1016	0.160	1.21	35.6	43.0	39.5			20.9			0.90			0.086	0.107	ND	ND									1.80		0.019
L-2-15-13	658.3	1276.8	1016	0.140	1.18	37.1	43.7	39.5	19.8	22.2	20.9	0.85	1.01	0.90	0.143	0.171	0.199	0.239	ND	ND	0.081	0.097	0.019	0.023			ND	ND	1.75		0.021
L-2-15-14	706.4	1388.9	1018	0.146	1.19	34.8	41.2	39.4	18.8	21.1	20.9	0.79	0.93	0.90	0.045	0.054	0.125	0.154	ND	ND	0.070	0.085	ND				ND	ND	1.80		0.019
L-2-15-15	754.6	1518.6	1016	0.135	1.17	40.2	47.0	39.4			20.9			0.90															1.60		0.029
Average concentration							43.7			22.1			1.01																		
														L-4-16																	
Original charge	0	0	1056	ND	1.0	39.9	39.9	39.9	19.0	19.0	19.0	0.90	0.90	0.90			ND	ND	0.001	0.001	ND	ND	ND	ND	ND	ND	ND	ND	1.50	1.056	0.032
L-4-16-1[l]	113.1	0	1046	0	1.0	39.2	39.2	39.9	19.2	19.2	19.0	0.69	0.69	0.90	0.013	0.014	0.021	0.022			0.044	0.046	0.007	0.007					1.85		0.014
L-4-16-2[l]	122.4	0	1056	0.107	1.13	39.0	44.0	39.9	20.5	22.4	19.1	0.96	1.08	0.90	0.042	0.051	0.037	0.045			0.027	0.033	0.067	0.080					1.80		0.018
L-4-16-3	145.6	32.2	1056	0.112	1.14	40.4	46.0	39.9	20.3	22.2	19.2	0.94	1.07	0.90	0.028	0.034	0.034	0.043			0.053	0.063	0.064	0.077			0.029	0.035	1.90		0.015
L-4-16-4	193.1	175.7	1056	0.117	1.14	41.0	46.9	39.9	21.8	24.1	19.4	0.91	1.04	0.90			0.100	0.123			0.093	0.119	0.020	0.024			ND	ND	1.75		0.021
L-4-16-5	241.1	309.9	1057	0.133	1.17	38.3	44.7	39.9	21.7	24.3	19.5	0.83	0.97	0.90	0.015	0.019	0.052	0.070			0.104	0.128	0.100	0.124			ND	ND	1.80		0.019
L-4-16-6	289.1	374.2	1056	0.119	1.15	37.8	43.4	39.9	20.0	22.0	19.6	0.86	0.99	0.90	0.022	0.026	0.038	0.054			0.035	0.042	0.038	0.047			ND	ND	1.85		0.016
L-4-16-7	361.9	575.0	1056	0.117	1.14	36.5	41.8	39.9	18.9	20.7	19.7	0.82	0.99	0.90	0.101	0.122	0.078	0.102			0.039	0.048	0.075	0.094			ND	ND	1.60		0.029
L-4-16-8	457.6	789.5	1057	0.143	1.18	38.4	45.4	39.8	21.7	24.5	19.8	0.96	1.13	0.10	0.054	0.068	0.089	0.152			0.040	0.050	0.043	0.054			ND	ND	1.75		0.021
L-4-16-9	529.4	999.0	1057	0.136	1.17	38.7	45.4	39.8	21.3	23.8	19.8	1.05	1.13	0.10	0.018	0.022	0.121	0.192	ND	ND	0.044	0.055	0.024	0.030			ND	ND	1.65		0.026
L-4-16-10	625.0	1229.8	1056	0.090	1.11	36.7	40.7	39.8	21.1	22.7	19.9	0.94	1.14	0.89	0.089	0.105	0.757	0.346			0.007	0.101	0.020	0.023			ND	ND	1.75		0.020
L-4-16-11	697.0	1438.1	1056	0.100	1.12	36.0	40.4	39.8	20.1	21.7	20.0	0.81	0.71	0.89	0.074	0.088	0.173	0.255			0.149	0.176	0.077	0.041			ND	ND	1.85		0.016
L-4-16-12	793.0	1672.9	1056	0.141	1.18	37.5	44.2	39.8	21.2	23.8	20.1	1.01	1.19	0.88	0.061	0.076	0.225	0.331			0.153	0.190	0.040	0.050			ND	ND	1.70		0.024
L-4-16-13	865.1	1876.4	1056	0.113	1.14	36.5	41.5	39.8	20.9	23.0	20.2	0.88	1.10	0.88	0.021	0.146	0.235	0.342			0.140	0.168	ND	ND			ND	ND	1.70		0.023
L-4-16-14	961.1	2122.5	1057	0.129	1.16	37.5	43.6	39.8	19.5	21.7	20.2	0.72	0.83	0.89	0.049	0.060	0.312	0.447			0.142	0.174	0.013	0.016			0.032	0.039	1.80		0.019
Average concentration							43.4			22.6			1.00																		

[a]Where no values are given, either an analysis was not requested or the analytical results were not reliable. ND, not detected.
[b]Wash water contained Li_2SO_4 at 0.068 *m*.
[c]Dilution factors calculated on lithium concentration found in sample.
[d](Reported concentration) × (dilution factor).
[e]Determined from calculated uranium and inventory balance.
[f](Reported concentration) × (dilution factor); corrected for SO_4 from Li_2SO_4.
[g]Determined from calculated sulfate and inventory balances – does not include amount introduced by Li_2SO_4.
[h]Determined from calculated copper and inventory balances.
[i](Reported concentration) × (dilution factor) × (inventory volume).
[j](Reported concentration corrected for sample dilution and amounts withdrawn in previous samples) × (inventory volume).
[k]Determined from pH and corrected for sample dilution.
[l]Sample taken with reactor down.
[m]Using an estimated value of 1.18 for the dilution factor.

Table 11. Reported, Corrected, and Calculated Free H_2SO_4 in Solution

Sample Number	Inventory (ml)	Circulation Time (hr)	Reported Free Acid in Solution at Time of Sample (*m*)	Free Acid[a] from pH (*m*)	Corrected Free Acid in Solution at Time of Sample (*m*)	Nickel[b] and Manganese[b] Produced at Time of Sample (moles)	Calculated Free Acid in Solution at Time of Sample (*m*)
				L-2-15			
Original charge	1016	0.0	0.030	0.031	0.030	0.0	0.030
L-2-15-1	1016	69.4		0.011		0.002	0.028
L-2-15-2	1016	110.7		0.007		0.002	0.029
L-2-15-3	1016	183.7		0.018		0.002	0.028
L-2-15-4	1018	230.2		0.013		0.003	0.027
L-2-15-5	1016	278.2	0.020	0.016	0.024	0.003[c]	0.027
L-2-15-6	1016	350.4		0.016		0.003	0.027
L-2-15-7	1017	402.0		0.016		0.004	0.028
L-2-15-8	1015	449.5	0.026	0.016	0.030[d]		0.029
Second original charge	1018	0.0	0.030	0.031	0.030	0.0	0.030
L-2-15-9	1018	476.3		0.022		0.001	0.030
L-2-15-10	1018	490.6		0.016		0.001	0.030
L-2-15-11	1016	538.8		0.018		0.001	0.030
L-2-15-12	1016	587.2	0.027	0.016	0.033	0.002	0.029
L-2-15-13	1016	658.3		0.018		0.004	0.027
L-2-15-14	1018	706.4		0.016		0.003	0.028
L-2-15-15	1016	754.6	0.029	0.025	0.034		
				L-4-16			
Original charge	1056	0.0	0.023	0.032	0.023	0.0	0.023
L-4-16-1	1046	113.1	0.025	0.014	0.025	0.001	0.022
L-4-16-2	1056	122.4	0.021	0.016	0.024	0.001	0.022
L-4-16-3	1056	145.6		0.013		0.001	0.022
L-4-16-4	1056	193.1	0.025	0.018	0.029	0.002	0.022
L-4-16-5	1057	241.1	0.021	0.016	0.025	0.001	0.024
L-4-16-6	1056	289.1	0.021	0.014	0.024	0.001	0.025
L-4-16-7	1056	361.9	0.021	0.025	0.024	0.002	0.024
L-4-16-8	1057	457.6	0.028	0.018	0.033	0.003	0.024
L-4-16-9	1057	529.4	0.029	0.022	0.034	0.003	0.024
L-4-16-10	1056	625.0	0.029	0.018	0.032	0.006	0.021
L-4-16-11	1056	697.0	0.028	0.014	0.031	0.004	0.023
L-4-16-12	1056	793.0	0.023	0.020	0.027	0.006	0.022
L-4-16-13	1056	865.1	0.024	0.020	0.027	0.006	0.023
L-4-16-14	1057	961.1	0.030	0.016	0.035	0.008	0.021

[a]Not corrected for sample dilution.

[b]Includes amounts withdrawn in previous samples.

[c]Estimated.

[d]Using an estimated value of 1.18 for the dilution factor.

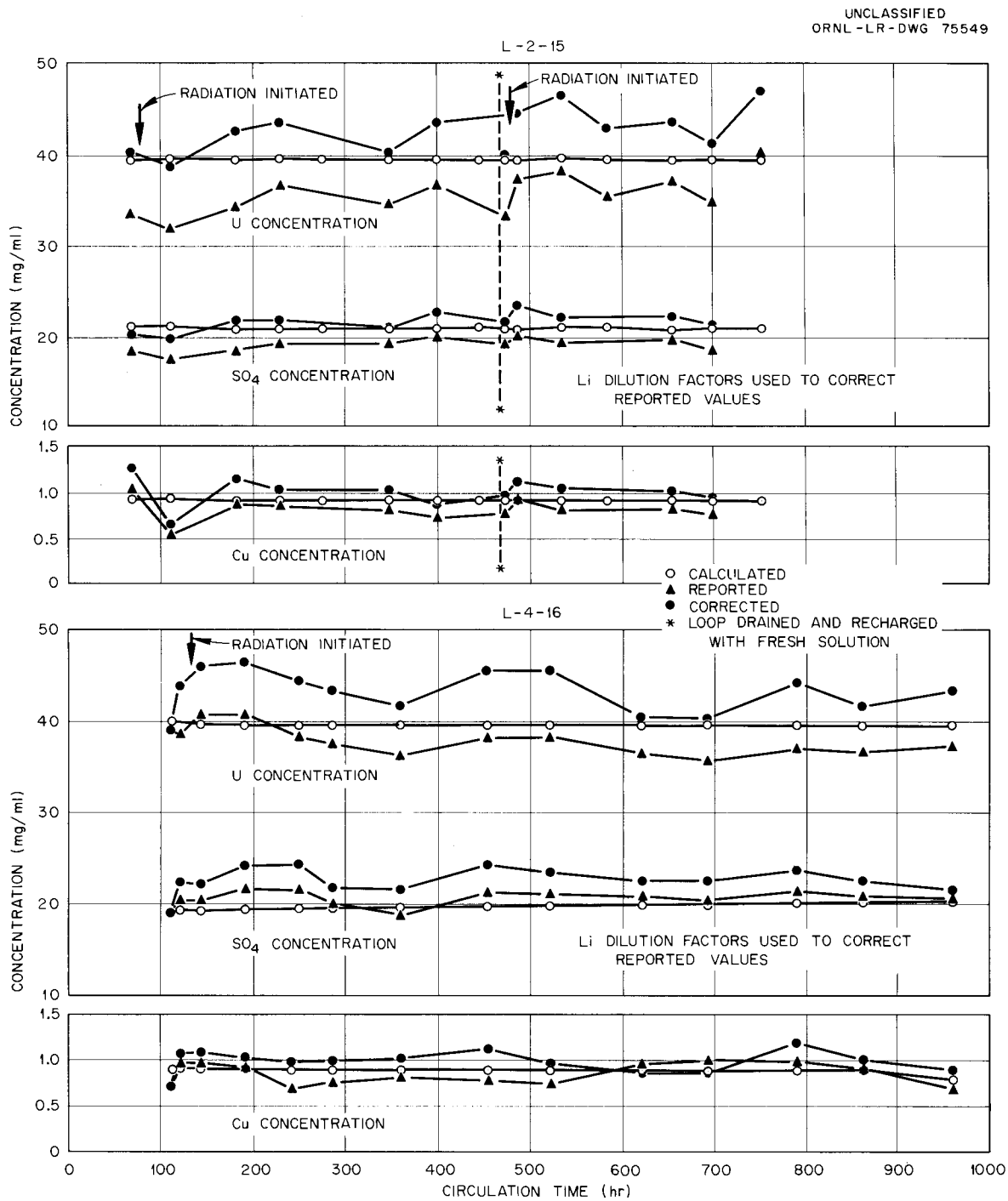

Fig. 6. Concentration of Uranium, Sulfate, and Copper in Solution Samples.

UNCLASSIFIED
ORNL-LR-DWG 75550

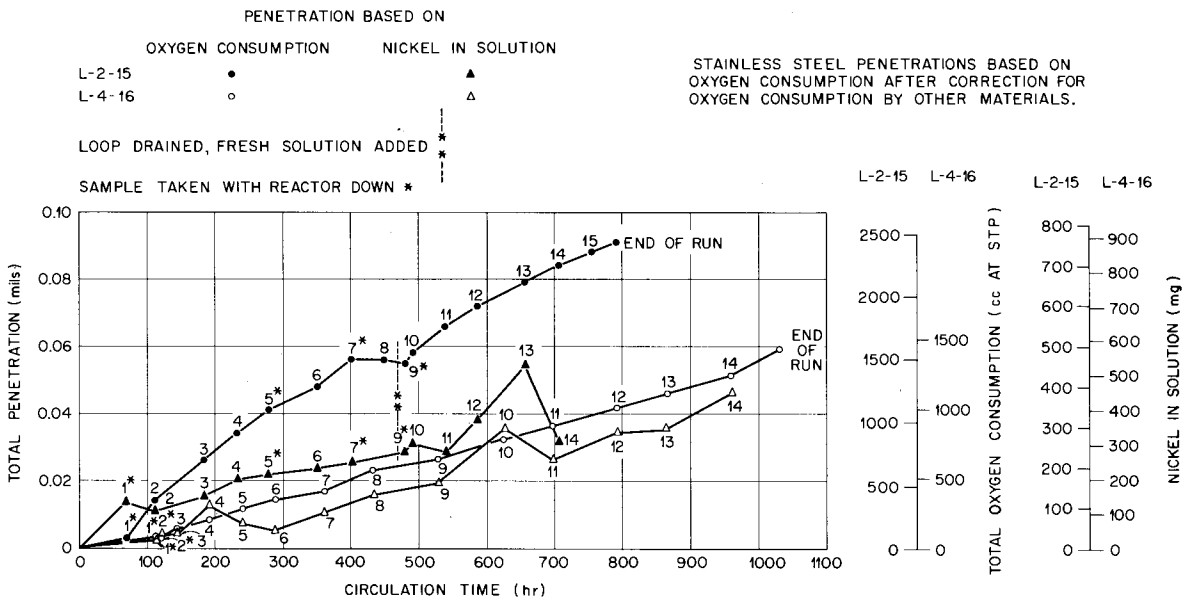

Fig. 7. Overall Corrosion Penetration of Type 347 Stainless Steel.

UNCLASSIFIED
ORNL-LR-DWG 75551

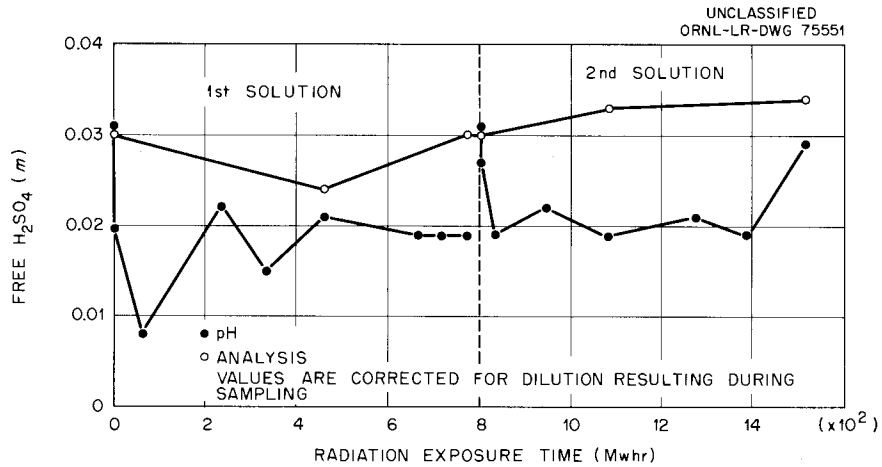

Fig. 8. Free-Acid Concentration in Solution vs Radiation Exposure Time (L-2-15).

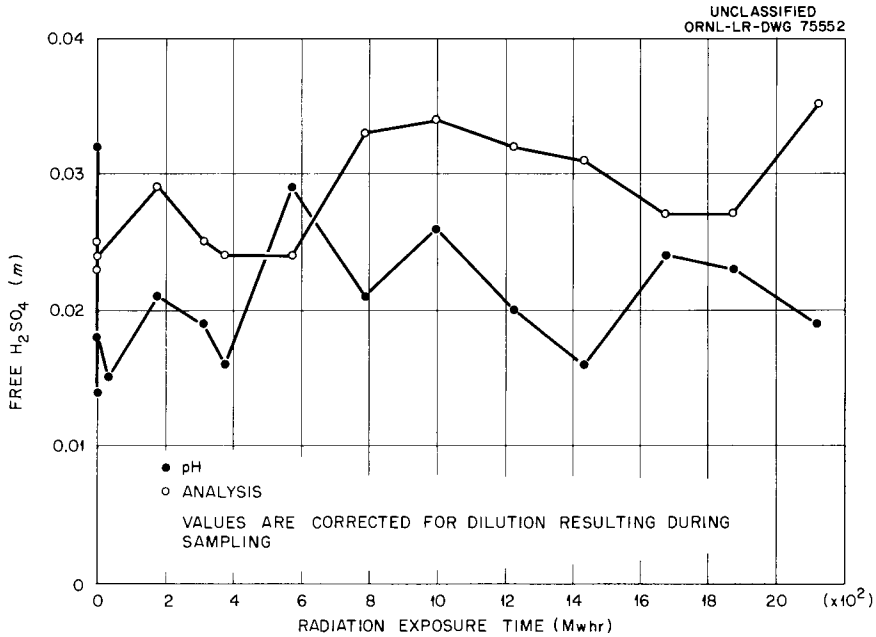

Fig. 9. Free-Acid Concentration in Solution vs Radiation Exposure Time (L-4-16).

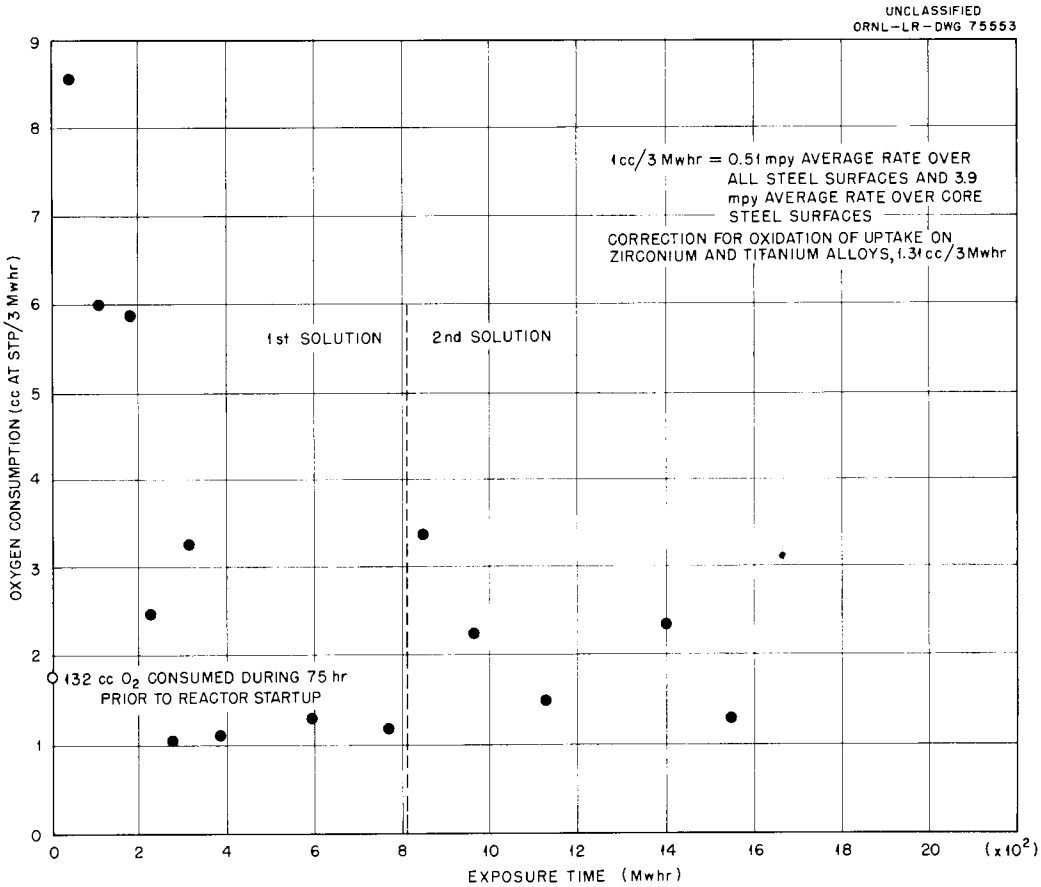

Fig. 10. Oxygen Consumption Rates on Stainless Steel in Loop L-2-15.

Table 12. Oxygen Consumption in Loop

Operation	Sample Number	LITR Energy (Mwhr)	Total Solution Circulation Time (hr)	O_2 Additions to Loop (cc at STP)	O_2 Withdrawn from Loop[a] (cc at STP)	Total O_2 Charged to Loop Less O_2 Withdrawn in Sampling (cc at STP)	O_2 Volume at Time of Sample (cc at STP)	O_2 Consumed Since Last Sample (cc at STP)	Total O_2 Consumed (cc at STP)	Calculated[b] Corrosion Penetration of Type 347 Stainless Steel (mils)
					L-2-15					
1st O_2 addition		0	0	1228	0	1228	0	0	0[c]	0
	L-2-15-1	0	69	0	6	1222	1103	119	119[c]	0.01
	L-2-15-2	63	111	0	5	1217	856	242	361[c]	0.02
	L-2-15-3	236	184	0	3	1214	561	292	653[c]	0.04
2d O_2 addition			208	861	0	2075	1332	743	743[d]	0.04
	L-2-15-4	334	230	0	7	2068	1229	96	839[d]	0.05
	L-2-15-5	460	278	0	6	2062	1040	183	1022[d]	0.05
	L-2-15-6	665	350	0	11	2051	831	198	1220[d]	0.07
3d O_2 addition			399	697	0	2748	1425	103	1323[e]	0.07
	L-2-15-7	719	402	0	19	2729	1405	1	1415[e]	0.08
	L-2-15-8	775	449	0	20	2709	1294	91	1458[e]	0.08
Drained loop and recharged with fresh solution			470	0	1251	1458		43	1458[e]	0.08
4th O_2 addition			470	1230	0	2688	1230	0	1458[f]	0.08
	L-2-15-9	806	476	0	7	2681	1204	19	1477[f]	0.08
	L-2-15-10	836	491	0	6	2675	1132	66	1543[f]	0.08
	L-2-15-11	948	539	0	5	2670	927	200	1743[f]	0.09
	L-2-15-12	1082	587	0	4	2666	773	150	1893[f]	0.10
	L-2-15-13	1277	658	0	3	2663	582	188	2081[f]	0.11
5th O_2 addition			682	775	0	3438	1300	57	2138[g]	0.11
	L-2-15-14	1389	706	0	7	3431	1209	84	2222[g]	0.12
	L-2-15-15	1519	755	0	6	3425	1076	127	2349[g]	0.13
End of run		1632	792	0	0	3425	983	93	2442[g]	0.14

Table 12 (continued)

Operation	Sample Number	LITR Energy (Mwhr)	Total Solution Circulation Time (hr)	O_2 Additions to Loop (cc at STP)	O_2 Withdrawn from Loop[a] (cc at STP)	Total O_2 Charged to Loop Less O_2 Withdrawn in Sampling (cc at STP)	O_2 Volume at Time of Sample (cc at STP)	O_2 Consumed Since Last Sample (cc at STP)	Total O_2 Consumed (cc at STP)	Calculated[b] Corrosion Penetration of Type 347 Stainless Steel (mils)
					L-4-16					
1st O_2 addition		0	0	1263	0	1263	1263	0	0[b]	0
	L-4-16-1	0	113	0	0	1263	1165	97	97[b]	0.01
	L-4-16-2	0	122	0	13	1250	1147	5	103[b]	0.01
	L-4-16-3	32	146	0	12	1237	1078	56	159[b]	0.01
	L-4-16-4	176	193	0	11	1226	994	72	231[b]	0.01
	L-4-16-5	310	241	0	10	1215	913	71	302[b]	0.01
	L-4-16-6	374	289	0	3	1212	849	61	363[b]	0.02
	L-4-16-7	575	362	0	9	1203	764	76	440[b]	0.02
2d O_2 addition			436	824	0	2027	1473	115	554[i]	0.02
	L-4-16-8	790	458	0	5	2022	1441	26	581[i]	0.02
	L-4-16-9	999	529	0	10	2012	1341	90	671[i]	0.03
	L-4-16-10	1230	625	0	9	2003	1195	137	808[i]	0.03
	L-4-16-11	1438	697	0	8	1995	1091	96	904[i]	0.04
	L-4-16-12	1673	793	0	7	1988	972	132	1036[i]	0.04
	L-4-16-13	1876	865	0	6	1981	848	97	1133[i]	0.05
3d O_2 addition			886	1054	0	3035	1864	38	1171[j]	0.05
	L-4-16-14	2122	961	0	14	3021	1762	89	1260[j]	0.05
End of run		2325	1032	0	0	3021	1594	168	1427[j]	0.06

[a]Calculated amount removed as O_2 dissolved in sample.
[b]Assumes oxygen consumption only by steel.
[c]12.34 std cc/psi.
[d]12.45 std cc/psi.
[e]12.80 std cc/psi.
[f]12.48 std cc/psi.
[g]11.57 std cc/psi.
[h]12.33 std cc/psi.
[i]12.65 std cc/psi.
[j]12.24 std cc/psi.

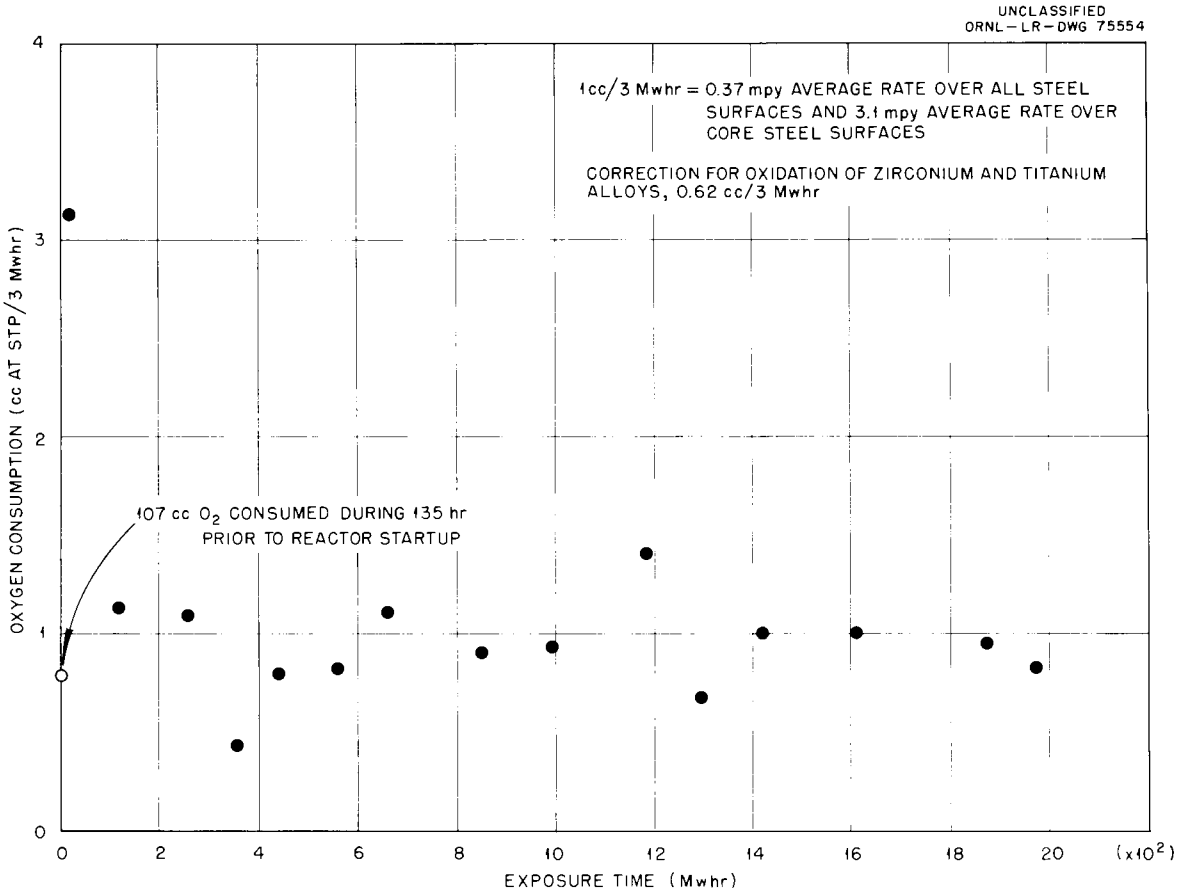

Fig. 11. Oxygen Consumption Rates on Stainless Steel in Loop L-4-16.

The total amounts of oxygen consumed by steel surfaces are shown vs megawatt-hours of LITR energy in Fig. 12. Again, the data have been corrected for consumption by zirconium and titanium alloys by the factors listed in Figs. 10 and 11. Shown for comparison in Fig. 12 are similarly corrected consumption data from in-pile loop experiment EE.[11] This 250°C experiment was operated with a solution 0.16 *m* in UO_2SO_4, 0.028 *m* in $CuSO_4$, and 0.02 *m* in H_2SO_4.

Values for overall stainless steel corrosion rates, based on corrected oxygen consumption data and circulation time, are given in Table 13. Rates during periods preceding and following reactor startups are also given.

4.4 Radiolytic-Gas Pressure

Average radiolytic-gas pressures in the pressurizers at 3-Mw reactor power, calculated from pressurizer pressure-temperature measurements before and after reactor shutdowns, are shown in Fig. 13. The average radiolytic-gas pressures at 3-Mw LITR power were 19.1 ± 1.4 and 5.1 ± 0.5 psi in experiments L-2-15 and L-4-16. There were no significant changes in radiolytic-gas pressures with time in either experiment. In experiment L-2-15, there was no significant difference between the average radiolytic-gas pressures before and after refueling.

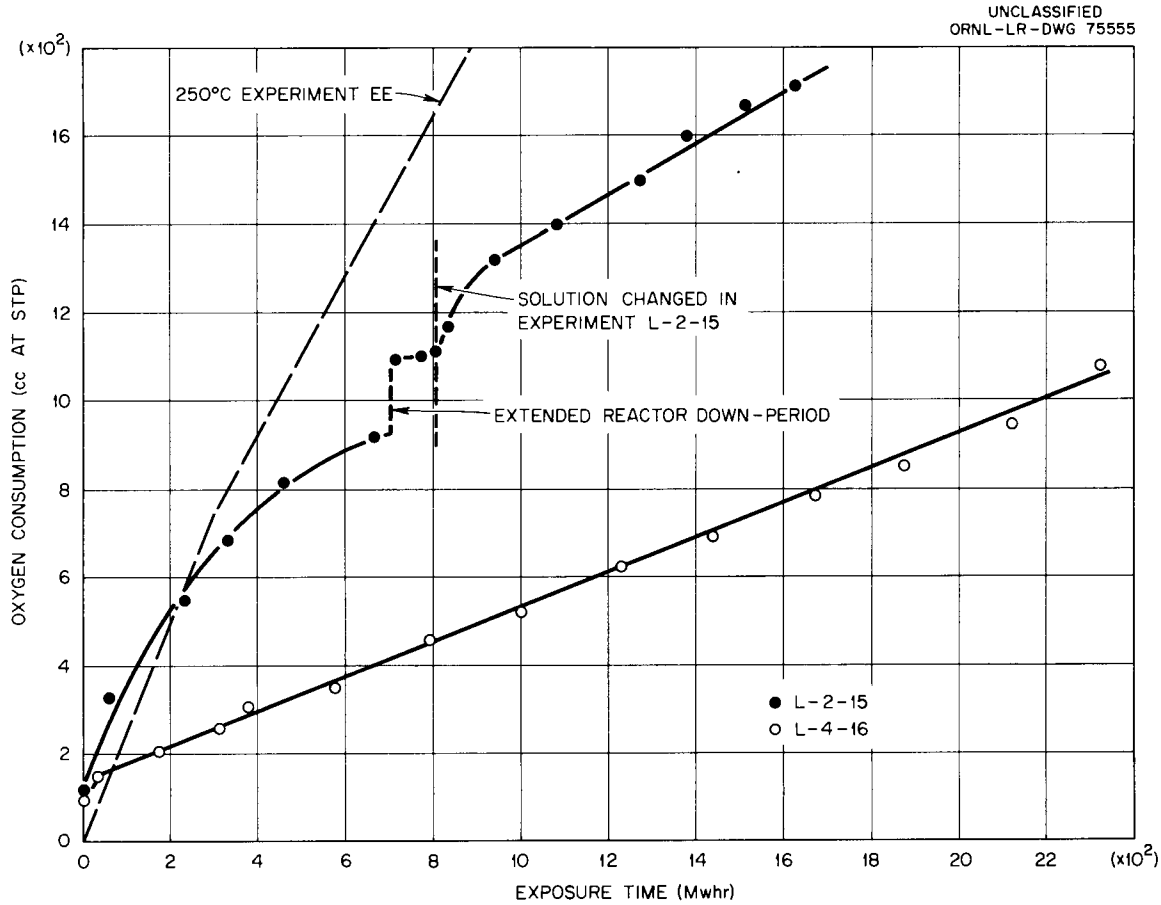

Fig. 12. Oxygen Consumption by Steel Surfaces in Experiments L-2-15 and L-4-16.

Table 13. Overoll Stainless Steel Corrosion Rates from Oxygen Consumption[a]

	Circulation Time Before Reactor Startup (hr)	Corrosion Rate (mpy)	Circulation Time Following Reactor Startup (hr)	Corrosion Rate (mpy)	Overall Corrosion Rate for Experiment (mpy)
L-2-15					
1st enriched solution	75	0.5	395	1.1	1.0
2d enriched solution	10	0	312	1.0	
L-4-16					
1st enriched solution	135	0.3	897	0.5	0.5

[a]Corrected for consumption by other materials.

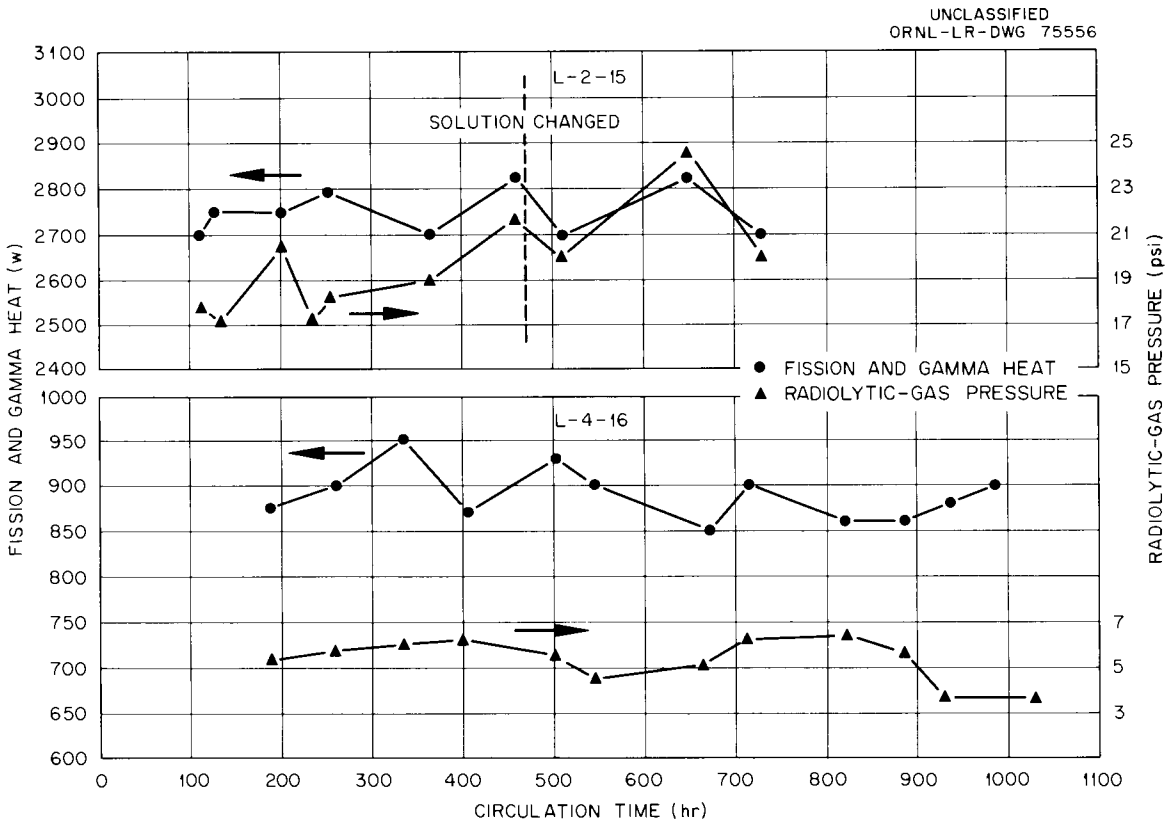

Fig. 13. Fission and Gamma Heat and Radiolytic-Gas Pressure vs Circulation Time.

The radiolytic pressure values were used to calculate the copper rate constants in the test solutions by the method previously described.[12] Values for the several factors employed in the calculation are listed in Table 14. The fission-power values are those determined from Cs^{137} analyses as described in Sec 4.8.2. The solubility constants for O_2 (α') and H_2 or D_2 (α) in the pressurizer solutions were obtained from a compilation of Battelle and ORNL solubility data by Banter.[13] The copper concentrations are those for the solutions as charged. Another factor employed in the calculation is the ratio of the rate constants in the mainstream and pressurizer. An activation energy of 22,000 kcal/mole for the copper activity was used to estimate these values. These rate constants appear to be in fair agreement with those calculated from the data from a group of in-pile experiments operated at 250°C.[11]

The final calculated values for the copper molar rate constant and the hydrogen concentration in the mainstream solutions are listed in the final columns.

---

[12] G. H. Jenks and J. E. Baker, *Apparent Copper Rate Constants Determined in In-Pile Loop Experiment L-2-22*, ORNL CF-60-3-88 (Mar. 23, 1960).

[13] J. C. Banter, private communication.

Table 14. Apparent Copper Molar Rate Constants

Experiment	Radiolytic-Gas Pressure in Pressurizer (psi)	P^a, Fission Power (w)	α, H_2 Solubility at Pressurizer Temperature (psi liter^{-1} cc^{-1})	α', O_2 Solubility at Pressurizer Temperature (psi liter^{-1} cc^{-1})	R', Flow Rate Through Pressurizer (psi liter^{-1} cc^{-1})	V_e, Solution Volume in Pressurizer (liter)	V_m, Solution Volume in Mainstream (liter)	L^b, Factor for Recombination of Radiolytic H_2 and O_2 in Pressurizer Exit Line (liter)	E^b, Factor for Recombination of Radiolytic H_2 and O_2 in Pressurizer Entrance Line ($e^{-K_s t}$)	[Cu] Copper Concentration in Solution Originally Charged to Experiment (m)	$[H_2]^*$, H_2 Concentration in Pressurizer (cc/liter)	$[H_2]$, H_2 Concentration in Mainstream (cc/liter)	K_m,[c] Apparent Copper Molar Rate Constant at Mainstream Temperatures (liter mole^{-1} hr^{-1})
L-2-15	19.1	2125	0.246	0.204	0.0055	0.251	0.581	0.989	0.867	0.0143	54.9	239.9	9,860
L-4-16	5.1	715	0.256	0.212	0.0055	0.257	0.615	0.982	0.864	0.0141	14.1	65.3	12,000

[a] Based on Cs^{137} analyses and 200 Mev/fission.
[b] K_s' and t' are, respectively, the estimated average rate constant in the pressurizer exit line (sec^{-1}) and the residence time in the line (sec); K_s'' and t'' are similarly defined factors for the entrance line.
[c] Mainstream and pressurizer temperatures were 279 and 298°C, respectively, for experiment L-2-15; temperatures for L-4-16 were 280 and 295°C.
Note: All volumes and concentrations are at STP.

$$[H_2]^* = \frac{K_1 \frac{R'}{V_e} E}{B\left(\frac{K_m[\mathrm{Cu}]}{3600}\right)^2 + \left(\frac{K_m[\mathrm{Cu}]}{3600}\right)\left(B\frac{R'}{V_m} + \frac{R'}{V_e}\right) + \frac{(R')^2}{V_m V_e}(1 - LE)},$$

where

$B = 1.9$ (L-2-15)
$= 1.7$ (L-4-16).

4.5 Uranium Balance

The method and results of estimating the balance between the amounts of charged and recovered uranium in each of the experiments are illustrated in Table 15. The differences between the charged and recovered amounts, –5% for L-2-15 and +2.5% for L-4-16, fall within the estimated uncertainty of the determinations of the recovered amounts.[11]

4.6 Results of Qualitative Examination of Loops

Results of qualitative inspection of loop and specimens for each experiment are given in the following paragraphs. Brief descriptions of the surface appearance of the coupons are included in Tables 21 and 22.

4.6.1 Experiment L-2-15

This loop was the first to use an air-demineralized water mixture to remove heat from the loop coolers. Air alone or water alone had been employed previously.[14] Because of this, particular attention was given to the condition of these components. Visual and metallographic examination of the cooler annuli showed no evidence of cracking. There was some staining of the metal and accumulation of light-colored scale near the inlet and outlet parts of both coolers.

In an attempt to determine the cause of the pump failure, the volute, stator, and rotor were removed from the pump. Examination of the volute and impeller showed no evidence of the impeller having dragged on any of the surfaces. The impeller appeared to have adequate end play; it would turn, but would not spin freely. Examination of the rotor, bearings, and journals, shown in Fig. 14, also failed to produce evidence of the cause of the pump failure. Journal and bearing diameters were the same as when installed, except for the front bearing, which showed a slight increase (0.003 in.) in inside diameter, probably as a result of wear. As shown in Fig. 15, a small chip of Al_2O_3 was missing from near the outer edge of the rear journal thrust surface, but there was no evidence of damage to the mating surface on the bearing. Information gained in subsequent experiments has shown that pump failures in loops L-2-15, L-4-16, and previous loops were caused by stator failures.[14]

As with previous loops, all the components outside the core region were covered with a brown rustlike scale. This scale was heavy on all surfaces that had been wetted by solution, but the scale was thin on the pressurizer surface that been exposed to vapor only. There was no evidence of localized attack on any of the loop components.

All specimens from the in-line positions were uniformly covered with the brown scale. Figure 16 is a view of the in-line holder coupons and tapered-channel, Zircaloy-2 coupon holder in the "as-removed" condition. The uniform nature of the scale is apparent in this photograph. As with previous loops, the standard cathodic defilming technique was only partially effective on the Zircaloy-2 coupons, and some of this scale was retained on all of the in-line annulus and channel holder coupons of this material.

---

[14] H. C. Savage and W. D. Reel, *In-Pile Corrosion Test Loops for Aqueous Homogeneous Reactor Solutions*, ORNL-2977 (Nov. 10, 1960).

Table 15. Actual Uranium Balance

	Enriched Solution Operation				
	Solution Weight (g)	Specific Gravity	Solution Volume (ml)	U Concentration by Analysis (mg/ml)	Weight of U (92.66% U^{235}) (g)
Solution Charged to L-2-15					
1st original solution charged to loop	1,073.5	1.057	1,015.6[a]	39.57	40.2[a]
2d original solution charged to loop	1,057.2	1.057	1,000.2[a]	39.57	39.6[a]
1st makeup solution charged to loop	247.0[a]	1.059	233.2	39.04	9.1[a]
2d makeup solution charged to loop	55.5[a]	1.057	52.5	38.48	2.0[a]
Excess solution from fuel reservoir	1,185.7[a]	1.058[b]	1,120.7	38.76[a]	43.4[a]
Total					134.3
Recovered from L-2-15					
Loop inventory samples sent to laboratory	39.6[c]	1.057[c]	37.5	32.1–40.2	1.3
Weigh-tank samples sent to laboratory	10.1[c]	1.0[c]	10.1	11.7–13.1	0.1
Weigh-tank contents (including solution from reservoir)	10,400[d]	1.0[c]	10,400[a]	12.1[b]	126
Total					127
					Balance = −5%
Solution Charged to L-4-16					
Original solution charged to loop	1,115.3	1.056	1,056.2[a]	39.85	42.1[a]
Makeup solution charged to loop (sum of fuel expansion plus solution for the line rinses)	479.9[a]	1.058	453.6	40.02	18.2[a]
Total					60.3
Recovered from L-4-16					
Loop inventory samples sent to laboratory	39.2[c]	1.057[b]	37.1	36.0–41.0	1.4[e]
Weigh-tank samples sent to laboratory	15.6[c]	1.0[c]	15.6	5.6–10.6	0.1[e]
Weigh-tank contents		1.0[c]	7,737[f]	7.6[b]	59.0[a]
Weigh-tank contents	7,900[d]	1.0[c]	7,900[a]	7.6[b]	60.0[d]
Total					60.5 61.5[d]
					Balance = +0.3% +1.9%[d]

[a]Calculated.
[b]Average from analyses.
[c]Assumed.
[d]Weigh-tank reading.
[e]Sum of individual analyses.
[f]Calculated from inventory data.

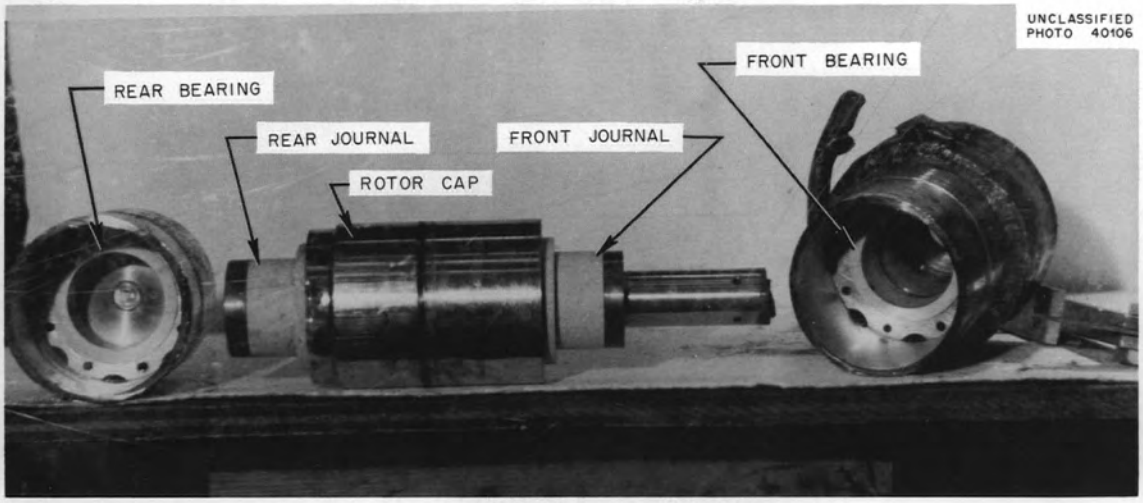

Fig. 14. In-Pile Loop L-2-15 – Pump Parts.

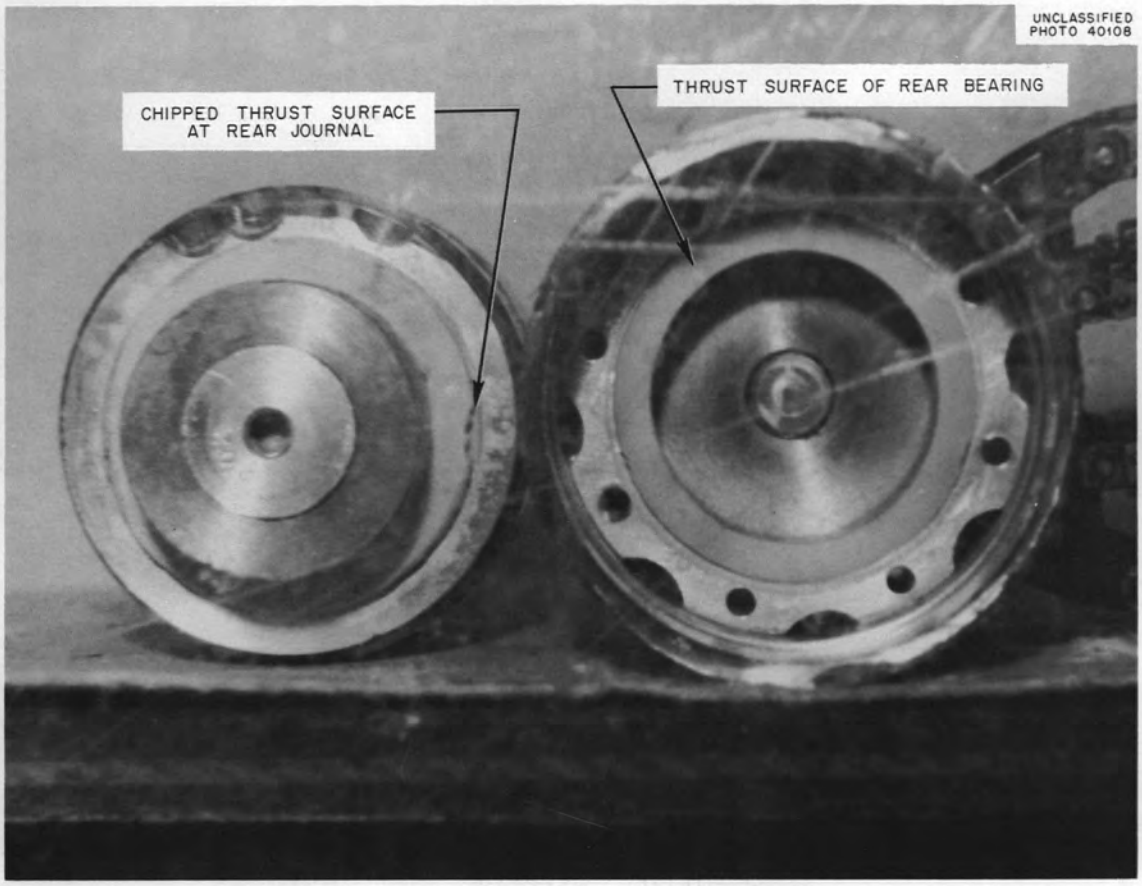

Fig. 15. In-Pile Loop L-2-15 – Rear-Bearing Assembly.

UNCLASSIFIED
PHOTO 19567

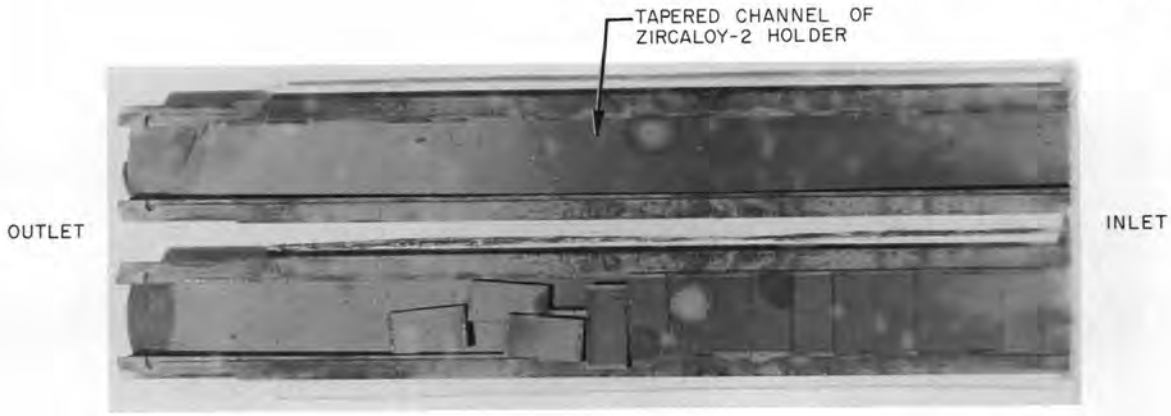

Fig. 16. In-Pile Loop L-2-15 – In-Line Coupon Array.

The inside surface of the type 347 stainless steel core body was generally covered with a thin, dark-brown, rustlike scale, the thickness of which increased from the high- to the low-flux end of the core. Along a line parallel to and near the core-annulus coupon assembly the scale was slightly discolored. A similar but more pronounced discoloration was noted in a similar region in loop L-2-10.[15]

All the stainless steel components and coupons in the core array were covered with a thin rustlike scale similar to that found on the core body. The titanium stress specimens and coupons were covered with the typical, thin brass-colored films. The Zircaloy-2 coupons, impact samples, and coupon holder were covered with a very thin iridescent film, while the crystal-bar zirconium impact and tensile specimens were covered with a similar thin film which was darker in color, ranging from light gray to black. All the zirconium and Zircaloy-2 surfaces in the core had a lightly etched appearance. Figures 17 and 18 are views of the complete core sample assembly in the "as-removed" condition. Figure 19 is a view of the opened core holder and holder coupons in the "as-removed" condition.

4.6.2 Experiment L-4-16

In an effort to locate the source of the pump failure, the L-4-16 pump was carefully sectioned and examined. Figure 20 is a sketch of the pump showing the cutting sequence and approximate location of various cuts. As with all previous pumps the seal weld was first cut (A-A') so that the volute could be removed. Visual examination of the interior of the volute and of the impeller surfaces shown in Fig. 21 revealed no indications of scoring or other signs of mechanical damage. The pump rotation was then tested with a long-handled screwdriver inserted into the impeller. The impeller did not spin freely, but there was no evidence of mechanical locking. The amount of end play appeared to be normal. A second cut was then made at B-B' through the cooling jacket, the front-bearing spacer, and the shaft. This cut permitted the removal of the thermal barrier and the impeller, with that section of the shaft in the area of the seal rings

[15] G. H. Jenks and J. E. Baker, *In-Pile Loop Investigation of Corrosion of Zircaloy-2 and Other Possible Reactor Materials in 0.04 m UO_2SO_4 at 280°C*, ORNL-2962 (in press).

UNCLASSIFIED
PHOTO 19566

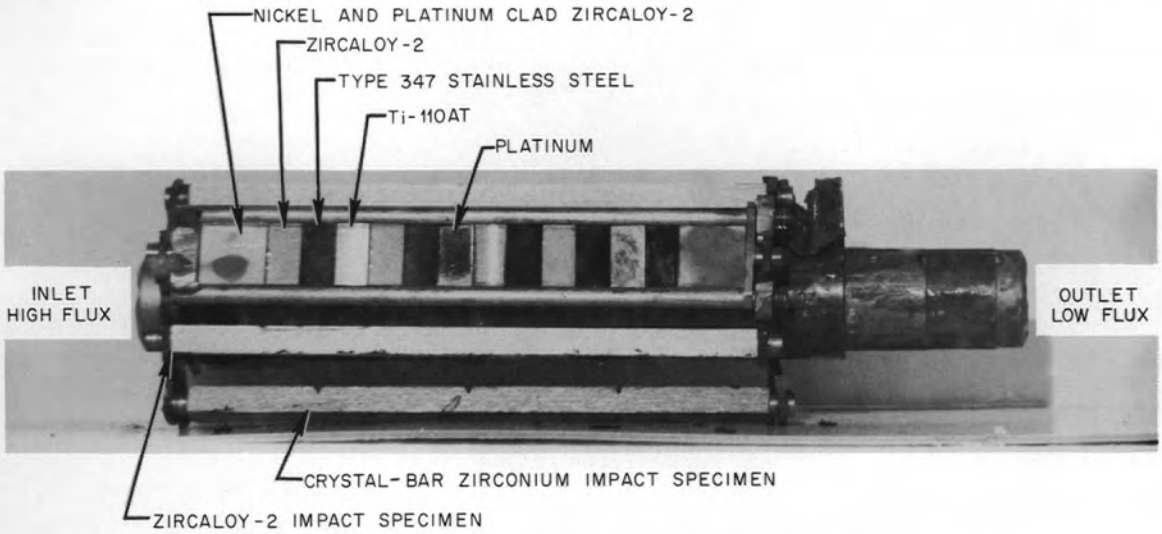

Fig. 17. In-Pile Loop L-2-15 – Core Specimen Assembly.

UNCLASSIFIED
PHOTO 19563

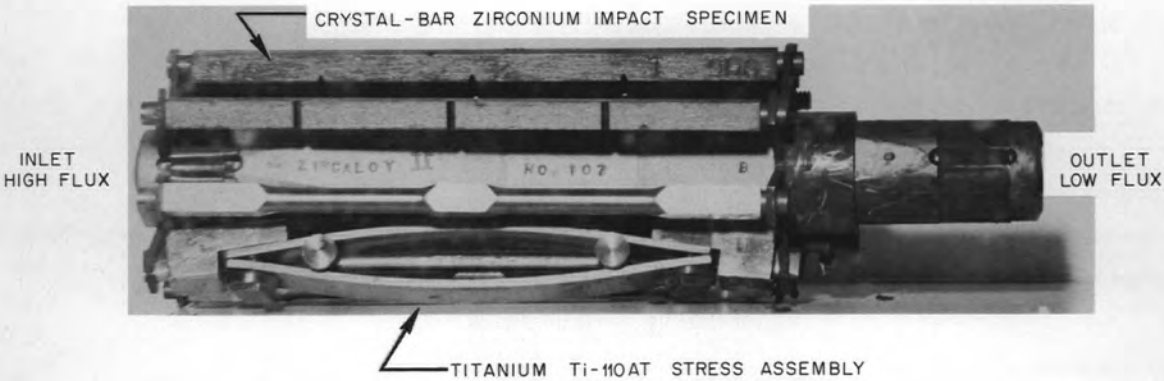

Fig. 18. In-Pile Loop L-2-15 – Core Specimen Assembly.

UNCLASSIFIED
PHOTO 19721

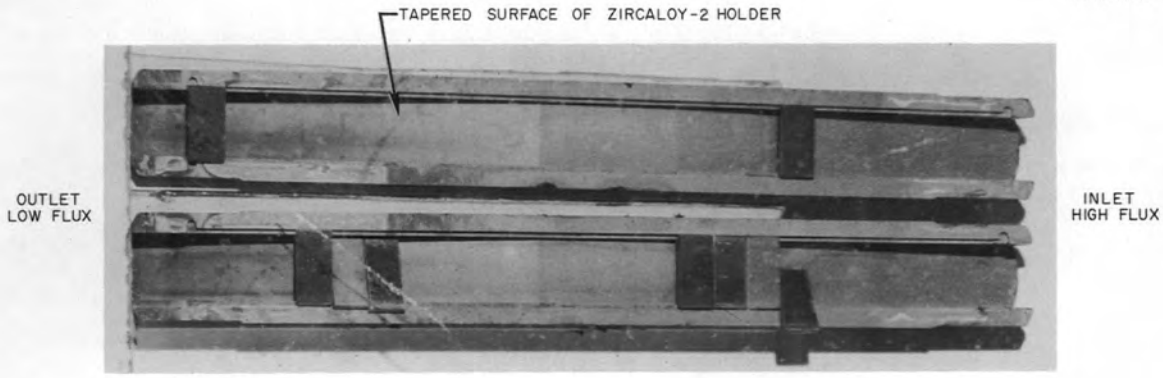

Fig. 19. In-Pile Loop L-2-15 – Core Coupon Holder.

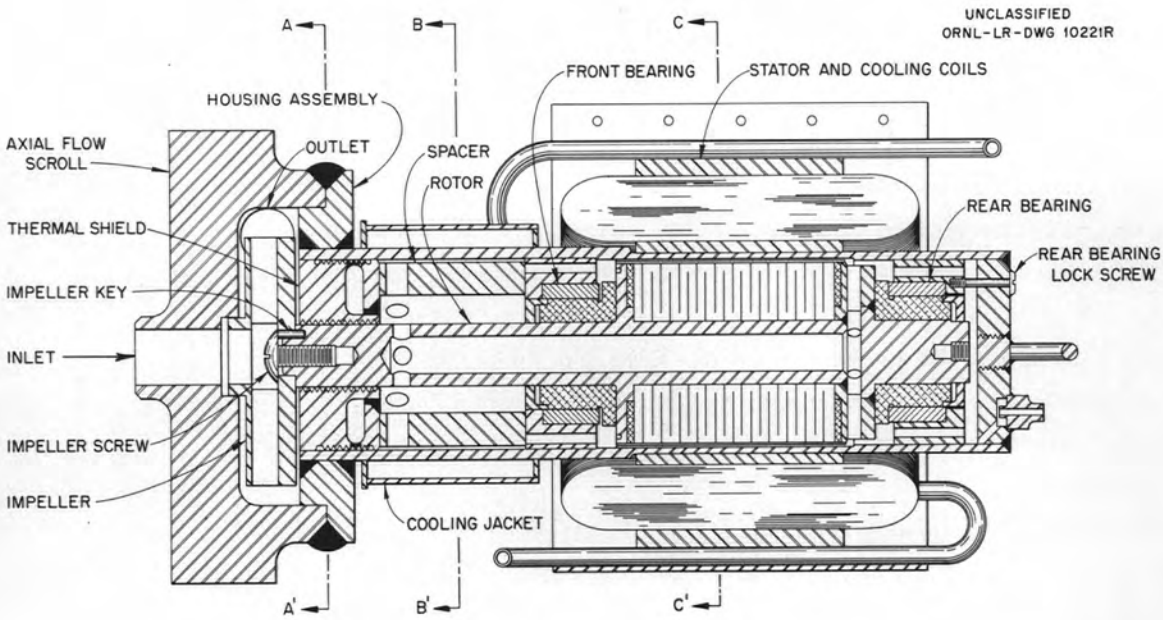

Fig. 20. In-Pile Loop Canned Rotor Pump.

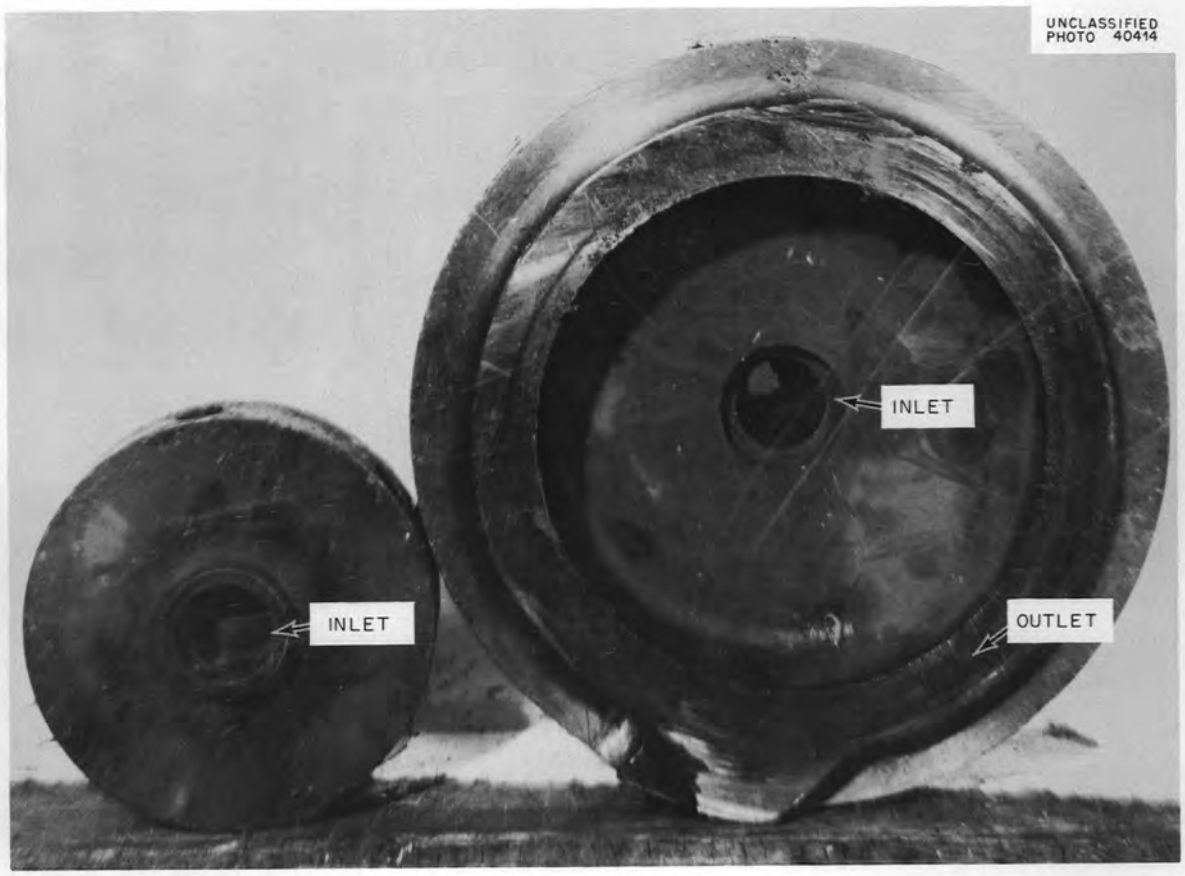

Fig. 21. In-Pile Loop L-4-16 – Pump Impeller and Volute.

still attached to the impeller. Figure 22 is a photograph of the units removed. Some scoring of the shaft adjacent to the rear seal rings was apparent, but this damage was quite shallow. The stator was then removed, and the seal can was cut at *C-C'*; this permitted the removal of the rotor assembly, shown in Fig. 23. Very careful visual examination of the rotor can, bearings, and journals showed no indications of wear or other damage. No dimensional measurements were made. From this examination it was concluded that there was no evidence of any mechanical failure which could have caused the pump failure. As stated in the previous section, it is now believed that stator failure was responsible for this pump failure.

As with previous loops, all the components outside the core were covered with a uniform dark-brown rustlike scale which was thin only in the vapor region of the pressurizer.

The tensile specimens, impact specimens, annulus coupons from the in-line holder, and coupons from the in-line tapered-channel holder were uniformly covered with a brown rustlike scale. As shown in Fig. 24, several coupons from the annulus array were held on one end only when removed from the loop. There was no evidence to indicate that these coupons were dislodged during removal of the assembly from the loop. They did not fall out during subsequent handling, indicating that they may have been dislodged while the loop was in operation.

As with previous loops, the standard cathodic defilming technique was only partially effective on the zirconium-alloy coupons.

The interior surface of the type 347 stainless steel core body was covered with a relatively thin rustlike film, ranging from a deep red-black color at the outlet or low-flux end. As with previous loops, this film gradually increased in thickness with decreasing neutron-flux exposure. This graduated-scale thickness was also observed on the stainless steel spiders, coupons, and core coupon holder. Machine marks on the interior surface of the core holder were found to decrease in distinctness in the direction of increasing neutron flux and were completely absent at the high-flux end.

Titanium specimens and coupons in the core were covered with the typical, thin brass-colored film. The Zircaloy-2 coupons and impact specimens were covered with a thin, iridescent, predominantly gray film. The remaining zirconium alloys were, in general, covered with an apparently heavier film which was much darker and in some places a distinct shiny black. Figures 25 and 26 show the core-annulus specimen arrays and core-channel coupon arrays as removed from the core.

4.7 Metallographic Examinations

Interior surfaces of typical sections of loop components, all surfaces of representative cross sections of representative coupons, and both the tension and compression surfaces of stress specimens were examined. In addition, coupon thicknesses were measured at both ends and near the center to determine general surface removal and the location and extent of regions of localized attack. Findings from the metallographic examinations for the components, coupons, and stress specimens from both experiments are summarized in Table 16. These examinations were carried out by Stiegler.[16,17]

---

[16] J. O. Stiegler, *Metallographic Examination of Components, Coupons and Stress Specimens from HRP In-Pile Loop L-2-15*, ORNL CF-57-5-103 (May 22, 1957).

[17] J. O. Stiegler, *Metallographic Examination of Components and Coupons from HRP In-Pile Loop L-4-16*, ORNL CF-57-9-99 (Sept. 30, 1957).

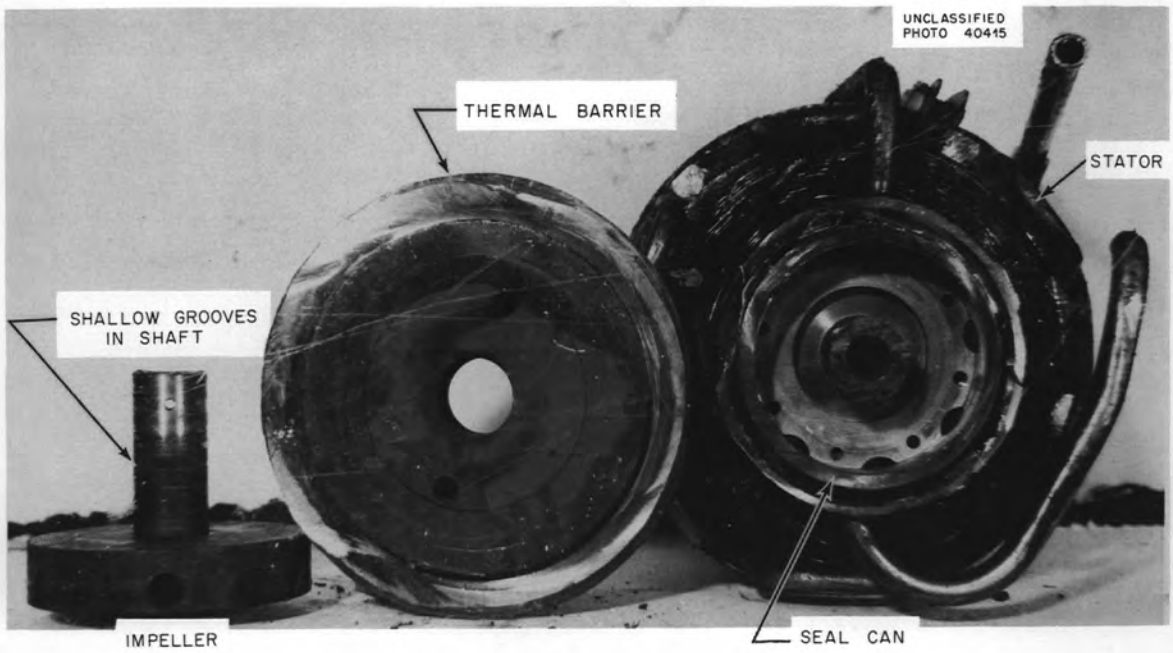

Fig. 22. In-Pile Loop L-4-16 – Pump Parts.

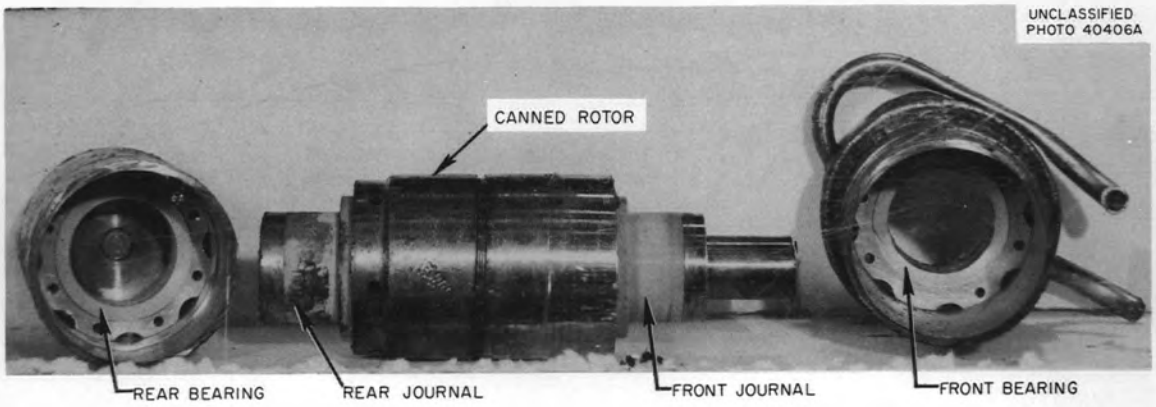

Fig. 23. In-Pile Loop L-4-16 – Pump Components.

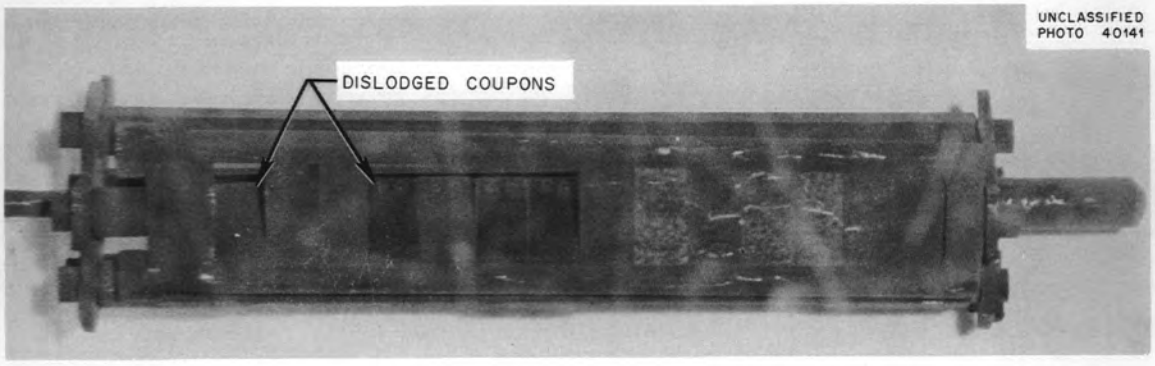

Fig. 24. In-Pile Loop L-4-16 – In-Line Annulus Coupon Array.

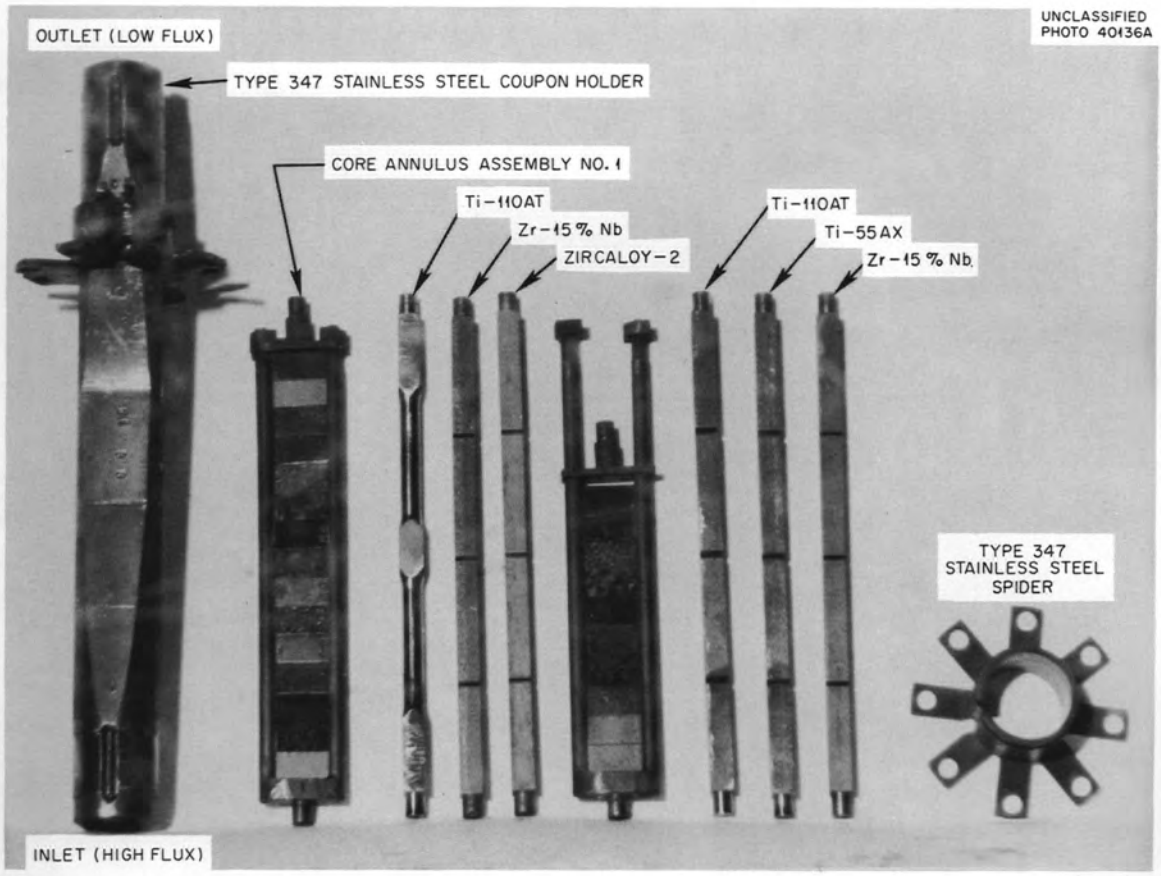

Fig. 25. In-Pile Loop L-4-16 – Core Specimen Arrays as Removed from the Loop.

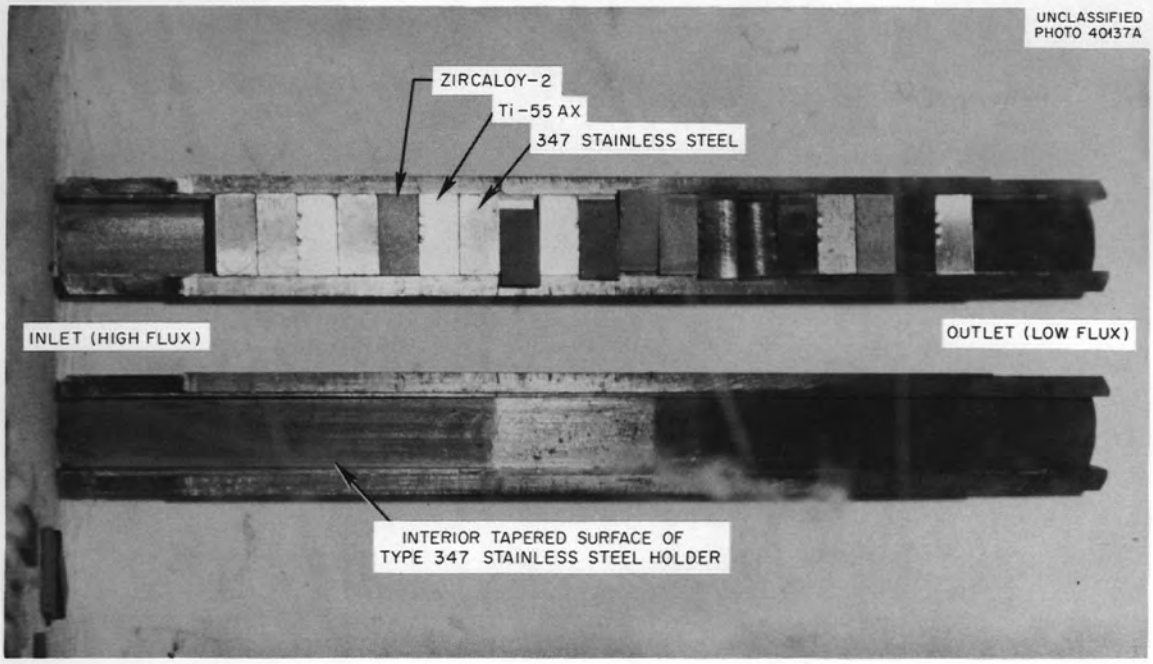

Fig. 26. In-Pile Loop L-4-16 – Core-Channel Coupon Array as Removed from the Loop.

Table 16. Summary of Metallographic Examination of Components, Coupons, and Specimens

Material and Specimen	Specimen Number	Calculated[a] Penetration (mils)	Specimen Thickness (in.) End	Center	End	Metallographic Observations	Figure Number
				L-2-15			
Type 347 SS components							
Interior surface of core cap						Interior surface appeared roughened but showed no evidence of intergranular corrosive attack or cracking; the initial surface probably rough	
Inlet end of pressurizer						Slight intergranular attack to maximum depth of $\frac{1}{4}$ mil; most of surface covered by $\frac{1}{8}$-mil film	26
Outlet end of pressurizer						Surface appeared smooth and covered by $\frac{1}{4}$-mil film	
Pressurizer heater inlet wall						Several cracks up to 3 mils in length emanated from the surface; a $\frac{1}{4}$-mil film covered most of specimen	29
Pressurizer heater U-bend						Smooth; free of film	
Small loop cooler jacket						Rough and uneven but no cracks evident	
Pump outlet piping						Smooth with no evidence of localized attack	
Pump outlet piping weld						Smooth with no evidence of localized attack	
Type 347 SS coupons							
Core channel	1241A	0.63	0.059	0.060	0.060	1-mil pits both sides and ends, but most cases on ends	
	1261A	0.03	0.059	0.060	0.060	Smooth, no attack	
Core annulus	1249A	2.20	0.059	0.036–0.048	0.057	Attacked along entire length; more severe near center	27
Line annulus	1252A	0.03	0.059	0.059	0.060	Smooth, no attack	
Type 309SCb SS coupons							
Core annulus	C-76	1.56	0.059	0.058	0.059	Ends and sides rough	30 and 31
	C-77	4.56	0.010	0.046	0.008	Attacked over entire surface, but most severe at edges and ends	
Line annulus	C-79	0.03	0.060	0.060	0.061	Smooth, no attack	
Zircaloy-2							
Core channel	ZB-14	0.42	0.060	0.060	0.060	Smooth, no attack	
	ZB-18	0.24	0.060	0.060	0.060	Smooth, no attack	
Core annulus	ZB-28	0.79	0.058	0.058	0.058	Six to eight isolated $\frac{1}{2}$-mil pits, otherwise smooth	
Line channel	ZB-22	+ 3.7 mg	0.061	0.061	0.061	Smooth, no film visible	
Line annulus	ZB-81	+ 0.4 mg	0.061	0.061	0.061	Smooth, no film visible	
Nickel- and platinum-clad crystal-bar zirconium coupons							
Core annulus	ZV-1		0.058	0.058	0.058	Dull gray with plating breaking off in spots; nickel removed from between zirconium and platinum; nickel removal confined by etching for nickel	
Line annulus	ZV-3		0.058	0.058	0.058	Uniform brown scale on all surfaces; nickel removed from between zirconium and platinum; nickel removal confined by etching for nickel	
Titanium-55A coupons							
Core channel	Ti-132	0.08	0.059	0.059	0.059	Smooth, no attack	
	Ti-138	0.08	0.059	0.058	0.059	Smooth, no attack	
Line channel	Ti-140	+ 1.9 mg	0.059	0.059	0.059	Smooth, no visible film	
Titanium-55A stress specimens							
Core annulus	TD-8	0.08				Both tension and compression surfaces appeared smooth with no cracking; pitting a localized attack	
	TD-9	0.10					
Line annulus	TD-6	0.02					
	TD-7	0.02					

Table 16 (continued)

Material and Specimen	Specimen Number	Calculated[a] Penetration (mils)	Specimen Thickness (in.) End	Center	End	Metallographic Observations	Figure Number
				L-4-16			
Type 347 SS components							
Pressurizer heater inlet wall						Cracks up to 2 mils long, originating at interior surface, randomly located; cracking probably transgranular; surfaces between cracks were smooth	
Pressurizer heater U-bend						Cracks up to 2 mils long, originating at interior surface, randomly located; cracking probably transgranular; surfaces between cracks were smooth	34
Pressurizer heater outlet wall						No cracking detected	
Pump outlet piping weld						Intergranular penetration (< 1/4 mil in depth) on piping interior on one side of weld, none on opposite side; no attack on weld; no surface film detected on sections examined	
Type 347 SS coupons							
Core channel	1069A	0.15	0.060	0.064	0.062	Six or eight 1/2-mil pits on edges of coupon; erosion near both ends of coupon about 3 mils deep; apparently most of weight loss accounted for by general surface removal near ends	28
	1076A	0.06	0.062	0.065	0.061	One 1-mil pit on end; remaining surfaces smooth	
Line channel	1409A	0.05	0.061	0.064	0.060	Edges smooth; both ends and one corner roughened	
Titanium-55A coupons							
Core channel	T-203	0.03	0.058	0.058	0.058	Slight (1/2 mil) uniform roughening on all surfaces and three corners	
	T-204	0.02	0.058	0.059	0.059	Slight roughening, less than on T-203; all corners smooth	
	T-205	0.01	0.059	0.059	0.059	Slight roughening, less than on T-203; all corners smooth	
Line channel	T-224	0.04	0.059	0.060	0.059	Severe roughening; maximum surface height variation of 1 mil	
	T-230	0.01	0.059	0.059	0.059	Several 1/2-mil pits on edges, ends, and corners	
Zircaloy-2 coupons							
Core channel	ZB-53	0.19	0.060	0.060	0.060	All surfaces smooth	
	ZB-61	0.11	0.060	0.060	0.060	Slight roughening; maximum surface height variations of < 1/4 mil	
Line channel	ZB-67	+1.4 mg	0.061	0.061	0.060	Roughening similar to ZB-61; three corners rounded; no surface film visible	
Line annulus	ZB-59	+0.4 mg	0.060	0.060	0.060	All surfaces smooth; no surface film visible	
Crystal-bar Zr–15% Nb coupons							
Core annulus	69-1	0.22	0.053–0.054	0.055	0.056	All surfaces smooth	
	69A-1	0.39	0.052	0.054–0.055	0.057	All surfaces smooth	
Line annulus	69-3	+1.7 mg	0.054	0.056	0.057	All surfaces smooth	
Sponge Zr–15% Nb coupons							
Core annulus	21-2	0.27	0.060	0.060	0.060	All surfaces smooth	
	21A-1	0.52	0.059	0.059	0.059	All surfaces smooth	
Line annulus	21-3	+1.5 mg	0.060	0.061	0.060	Slight roughening; two 3-mil pits near one end	
Crystal-bar Zr–15% Nb–2% Pd coupons							
Core annulus	27-2	0.16	0.056	0.057	0.058	All surfaces smooth	
	27A-1	0.29	0.054	0.056	0.057	All surfaces smooth	
Crystal-bar Zr–15% Nb–2% Pt coupons							
Core annulus	54A-1	0.40	0.058	0.059	0.057	Slight roughening over most surfaces; severe roughening on corners	35
Crystal-bar Zr–33% Nb							
Core annulus	42A-1	0.74	0.057–0.058	0.058–0.059	0.055	Pitting on all surfaces; more severe near ends	36
Line annulus	42A-2	+0.8 mg	0.060	0.061	0.060	Eight or ten pits; randomly distributed; up to 2 mils deep on edges	

[a]Based on total specimen area and defilmed weight change.

In general, corrosion estimates from thickness measurements and metallographic observations of the corrosion coupons were in near agreement with the weight-loss data.

Photomicrographs of cross sections of the inner walls of the L-2-15 pressurizer heater inlet tubing, the L-4-16 pressurizer heater inlet tubing U-bend, and of a section removed from the L-2-15 pressurizer body near the inlet end are shown in Figs. 27–29. Slight intergranular attack to a maximum depth of $\frac{1}{4}$ mil was observed along the entire surface of the pressurizer body specimen. Eight or ten intergranular cracks of 3-mil maximum length were distributed uniformly around the pressurizer heater inlet wall. The randomly scattered 2-mil cracks observed in the L-4-16 pressurizer heater U-bend specimen provide no definite evidence of intergranular attack. The cracks, appearing in the work-hardened surface metal, are believed to have resulted from fabrication techniques.

Figure 30 is a cross-section view of a portion of type 347 stainless steel CA coupon 1249A (L-2-15), showing severe attack near the center of the specimen.

Type 309SCb stainless steel CA coupon C-77 (L-2-15) was attacked along its entire length, but was most severely attacked at the edges and ends. This coupon exhibited the highest corrosion rate of all stainless steel specimens in the experiment. Figures 31 and 32 are macro- and microphotographs of the coupon. Figure 32 is a cross-section view at one corner of the specimen.

Fig. 27. L-2-15 Pressurizer Heater Inlet Wall. 250X.

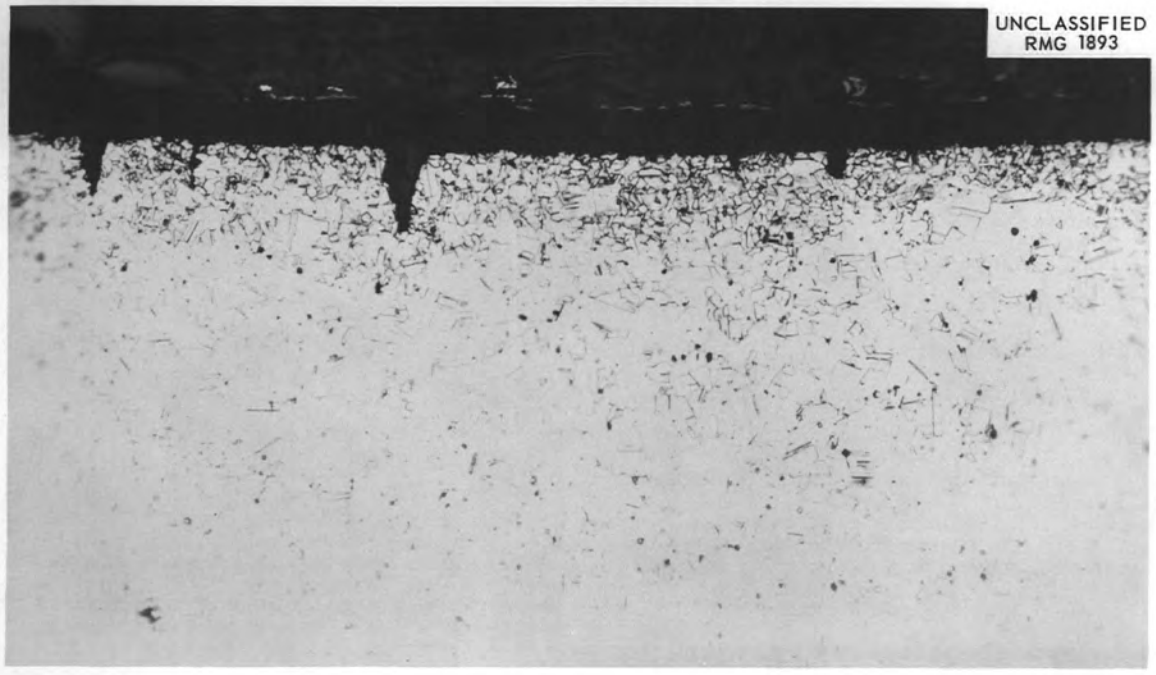

Fig. 28. L-4-16 Pressurizer Heater U-Bend. 250X.

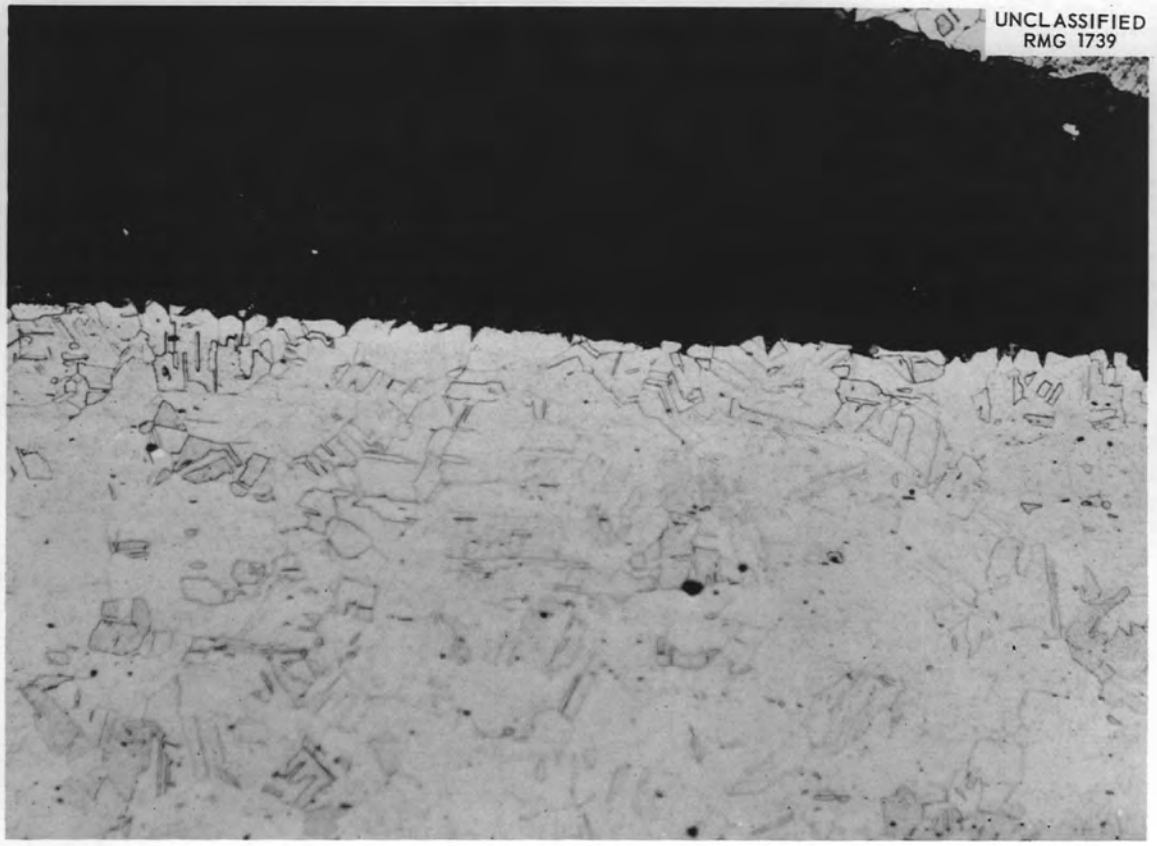

Fig. 29. L-2-15 Pressurizer – Inlet End. 250X.

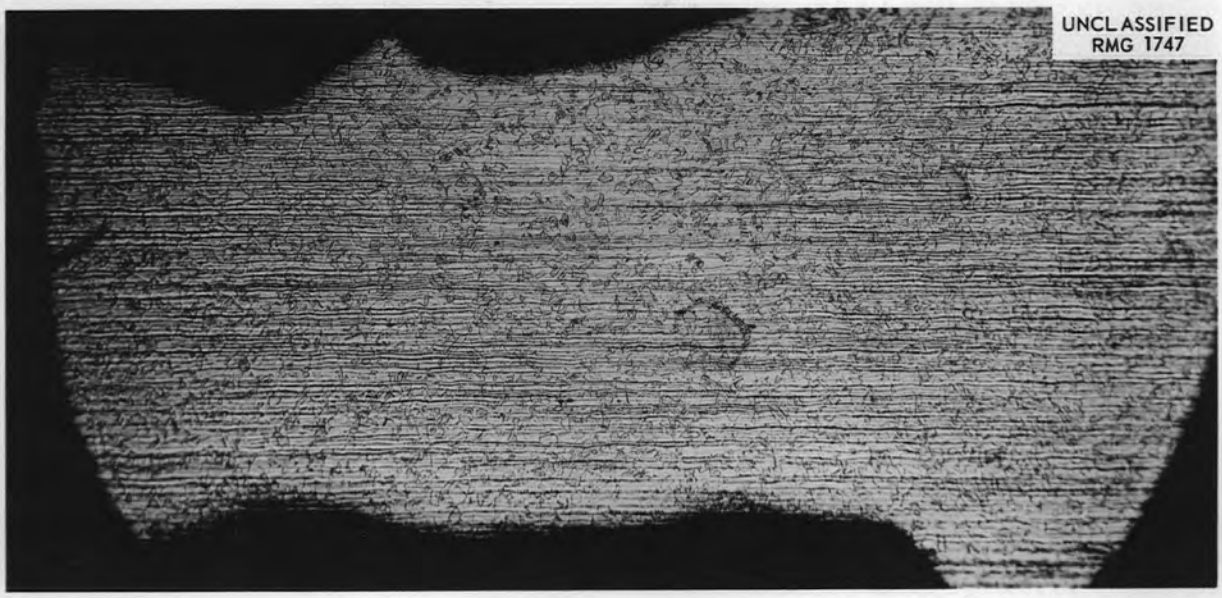

Fig. 30. Center of Type 347 Stainless Steel CA Coupon 1249A (L-2-15). 250X.

Fig. 31. Type 309SCb Stainless Steel CA Coupon C-77 (L-2-15). ~8X.

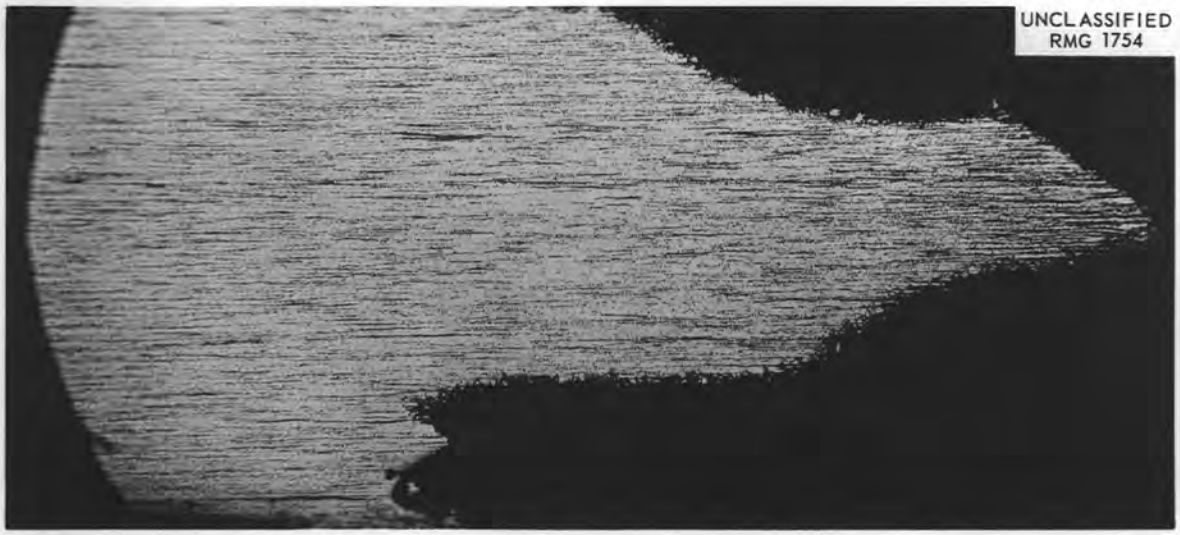

Fig. 32. Type 309SCb Stainless Steel CA Coupon C-77 (L-2-15). 50X.

Photographs of the two CA and LA nickel-platinum-clad Zircaloy-2 coupons from L-2-15 are shown in Figs. 33 and 34. The remaining two coupons were not examined metallographically. As shown, the cladding appeared intact around coupon ZV-3 but was bowed and broken at the corners of ZV-1. No nickel-platinum boundary could be detected in the cladding. Etching for nickel yielded negative results, implying that the cladding remaining was only platinum. Each coupon was plated with 1.0 mil of nickel (~80 mg) and approximately 0.2 mil of platinum.

Figure 35 is a low-magnification cross-section view of one end of type 347 stainless steel CC coupon 1069A (L-4-16), showing several of the isolated ½-mil pits and the rounded appearance of the coupon end.

Surface roughening was observed on the edges and corners of Zr–15% Nb–2% Pt CA coupon 54-A-1 (L-4-16), as shown in Fig. 36.

A pitting type of attack was visible on all surfaces of Zr–33% Nb CA coupon 42-A-1 (L-2-15). The region near the ends of the coupon appeared to be more severely attacked than the central portion. Only eight or ten pits less than 2 mils deep were observed on an LA coupon of this material. Figure 37 is a photomicrograph of coupon 42-A-1.

4.8 Results of Fission-Power Determination

4.8.1 Induced Activities

The results of flux determinations made from comparisons between the induced activities of representative core specimens and control specimens irradiated as known fluxes are listed in Table 17. The flux values are also shown in Fig. 38, where the logarithm of the flux is plotted vs the axial position in the core. The fission-power density in solution adjacent to a specimen was computed from the flux value indicated by the lines in Fig. 38, together with values of 580 barns and 200 Mev/fission for the fission

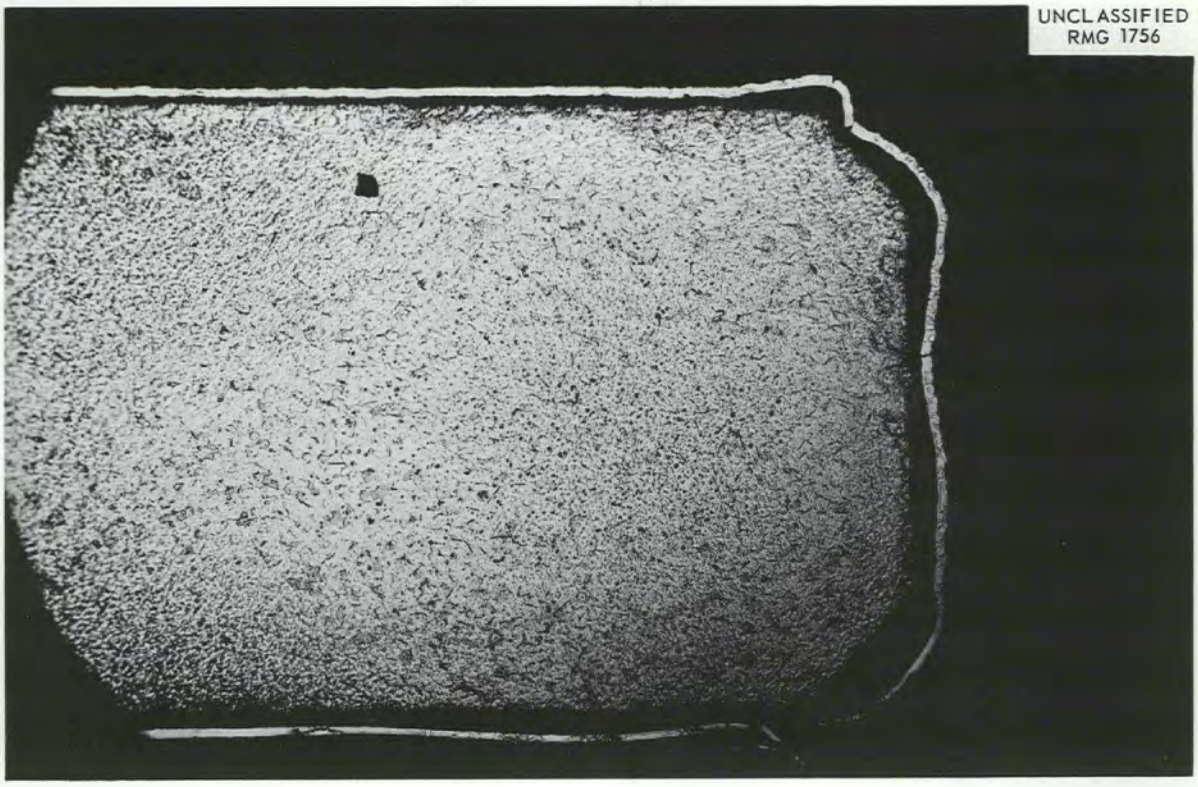

Fig. 33. Nickel- and Platinum-Clad Zircaloy-2 CA Coupon ZV-1 (L-2-15). 50X.

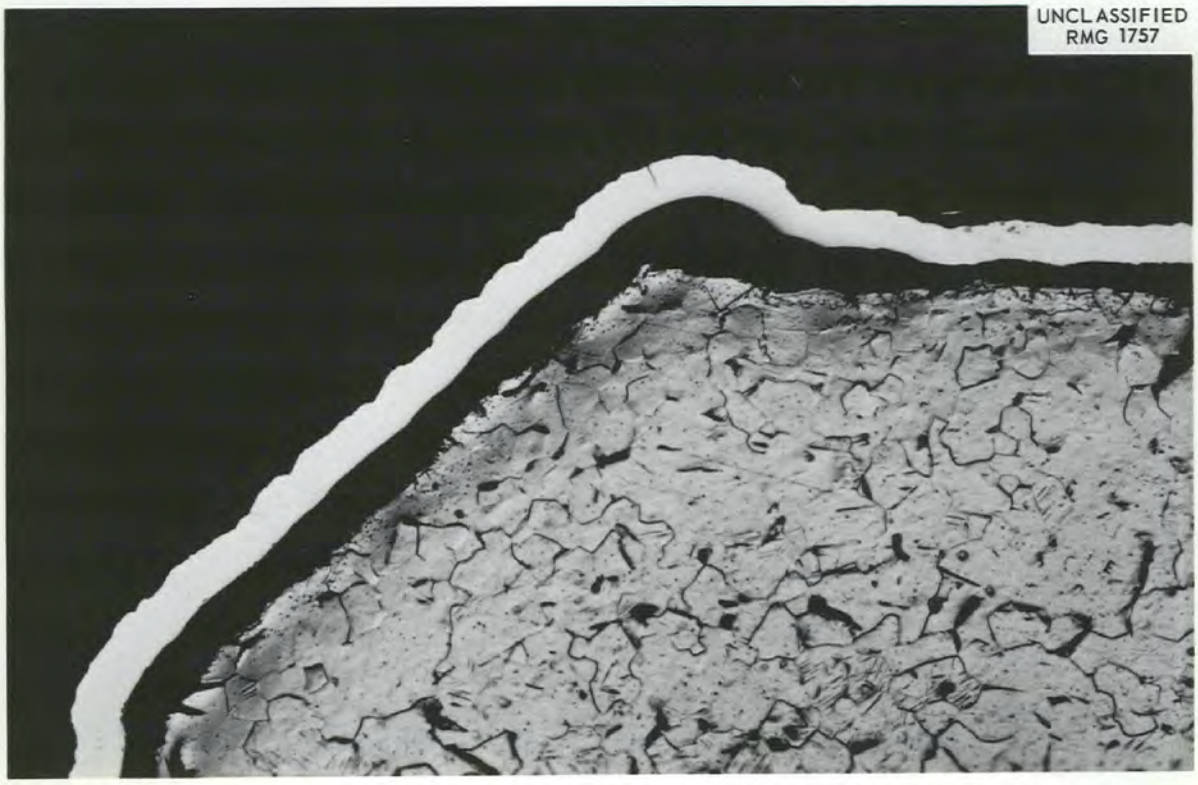

Fig. 34. Nickel- and Platinum-Clad Zircaloy-2 LA Coupon ZV-3 (L-2-15). 250X.

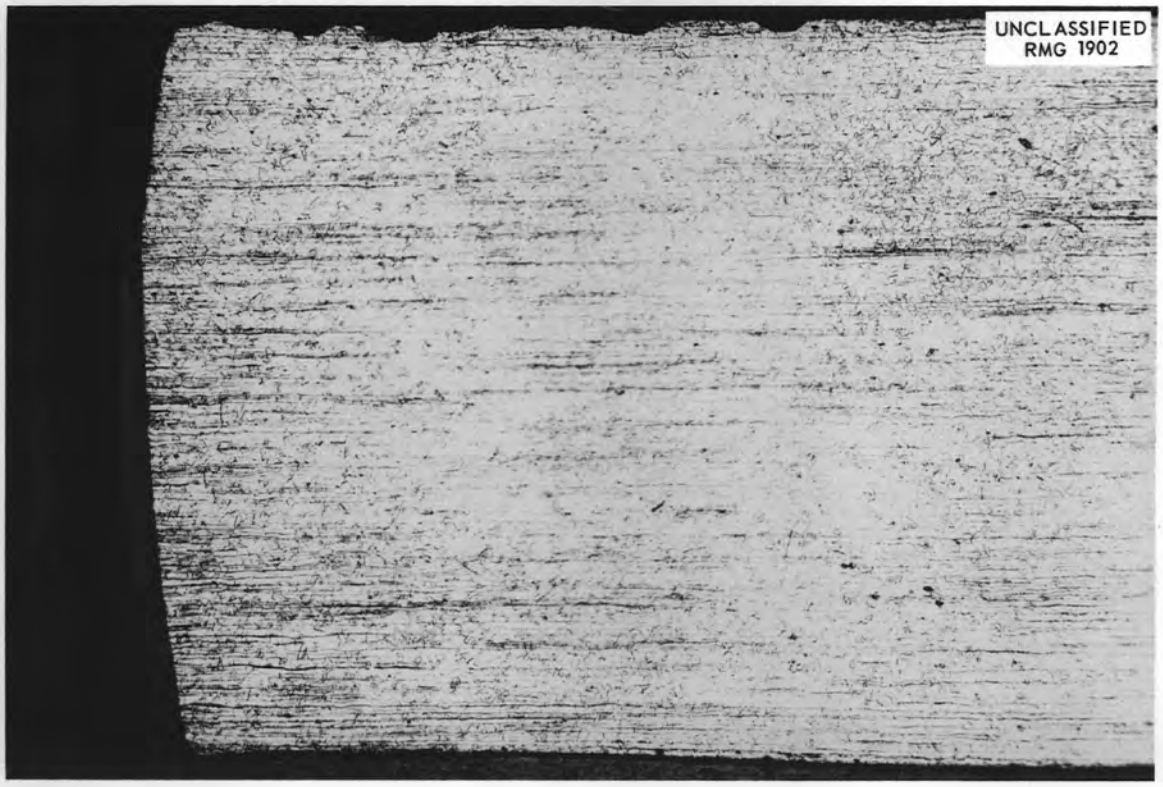

Fig. 35. Type 347 Stainless Steel CC Coupon 1069A (L-4-16). 50X.

Fig. 36. Zirconium–15% Nb–2% Pt CA Coupon 54-A-1 (L-4-16). 250X.

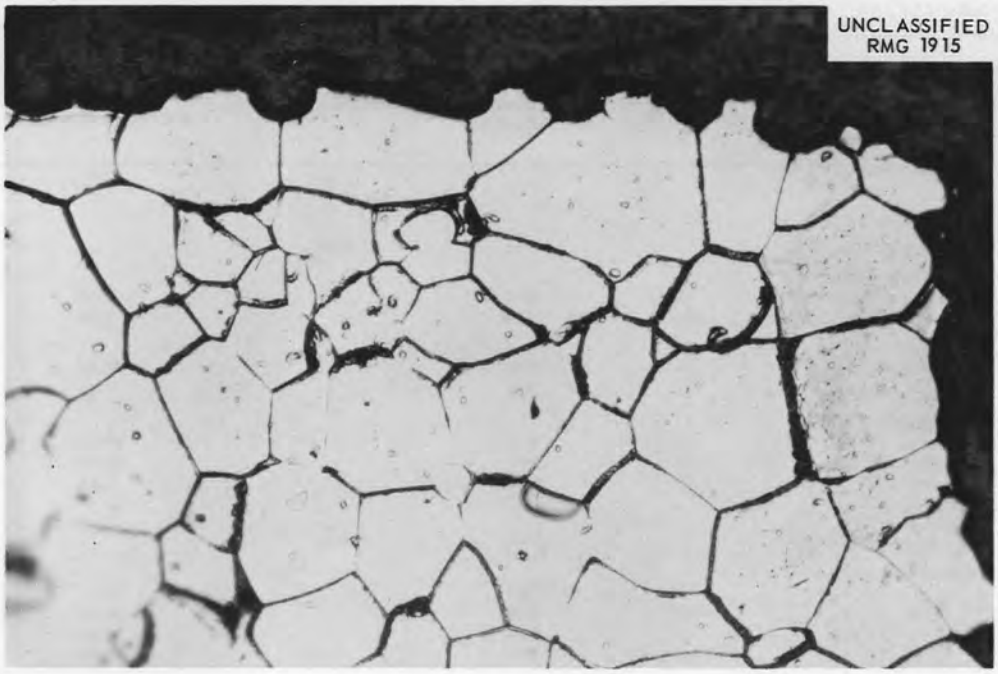

Fig. 37. Zirconium–33% Nb CA Coupon 42-A-1. 250X.

cross section and energy. The calculated fission power near each specimen is set forth in the weight data, Tables 21 and 22. The locations of the lines were estimated primarily from the values for the Zircaloy-2 specimens, since the Zircaloy-2 results have been employed to determine fluxes in other experiments and since Zircaloy-2 results are, in general, more reproducible than those for stainless steel. The indicated difference between annulus and channel locations in experiment L-4-16 is considered real and is ascribed to the high cross section presented by stainless steel channel holders.

A comparison between the fluxes in these and previous experiments is shown in Fig. 39.

4.8.2 Cesium-137

The results of Cs^{137} analyses are shown in Fig. 40 in terms of the average fission powers in a loop at an LITR power of 3 Mw calculated from the analytical results and the reactor energy accumulated during the total exposure preceding the time of sampling. A further illustration of the Cs^{137} data is shown in Fig. 41, where the data are plotted in terms of the average fission powers in the loop during the periods between adjacent samples as indicated by the difference between the Cs^{137} content of the samples.

As may be judged from the plots, the analytical data scattered appreciably. Within the indicated uncertainties there is no evidence that the actual fission rates changed significantly during the experiments. The L-2-15 results for the second solution charge probably reflect some carry-over of Cs^{137} produced in the original solution charge. It should be noted that the Cs^{137} analytical determinations were carried out with a gamma-ray spectrometer, whereas analyses in previous experiments were made by the beta-counting

Table 17. Induced Zr^{95}-Nb^{95} and Cr^{51} Activity in Specimens

Material and Specimen Number	Cleaned Weight when Counted (g)	Relative Zr^{95}-Nb^{95} Activity, 0.76-Mev Gamma (counts min^{-1} g^{-1})	Relative Cr^{51} Activity (counts min^{-1} g^{-1})	Exposure Time (hr) for Specimens: Circulation Time	Exposure Time (hr) for Specimens: Radiation Time	Cooling Time Before Analysis (hr)	Neutron Flux Observed (neutrons cm^{-2} sec^{-1})	Neutron Flux at 3 Mw (Calculated) (neutrons cm^{-2} sec^{-1})	Distance (in.)
				L-2-15			$\times 10^{12}$	$\times 10^{12}$	
Type 347 stainless steel									
Control (W-215)	0.9688		1.00	106.5		1872	8.32		
Core-channel coupons									
1240A	0.8788		1.94	717	544	2496		8.13	0.88
1258A	0.8941		1.20	717	544	2496		5.03	3.13
Core-annulus coupons									
1248A	0.8456		1.80	717	544	2496		7.54	1.10
1250A	0.7958		1.22	717	544	2496		5.11	3.10
Core-wall specimens									
A	0.4126		4.06	717	544	2496		17.00	−1.00
B	0.7712		3.12	717	544	2496		13.07	0.67
C	0.5585		1.30	717	544	2496		5.44	4.75
Zircaloy-2									
Control (W-122)	0.7966	1.00		106.5		2304	8.32		
Core-channel coupons									
ZB-11	0.5851	6.27		717	544	2928		13.81	0.38
ZB-13	0.6248	4.74		717	544	2928		10.44	1.88
ZB-16	0.7144	2.91		717	544	2928		6.41	3.63
ZB-17	0.7520	1.97		717	544	2928		4.34	4.88
Core-annulus coupons									
ZB-27	0.5921	6.34		717	544	2928		13.96	0.84
ZB-29	0.6255	3.87		717	544	2928		8.52	2.84
				L-4-16					
Type 347 stainless steel									
Control (W-217)	0.9489		1.00	105.8		1440	5.00		
Core-channel coupons									
1071A	0.6744		1.49	897	775	1680		1.90	1.63
1077A	0.7262		0.98	897	775	1680		1.26	3.13
1079A	0.9206		0.67	897	775	1680		0.85	4.38
1386A	0.8717		0.53	897	775	1680		0.68	5.13
Core-annulus coupons									
1388A	0.6475		0.95	897	775	1680		1.22	4.00
1411A	0.8246		0.92	897	775	1680		1.17	4.00
Core-wall specimens									
A	0.3485		4.54	897	775	1680		5.79	−1.00
B	0.2880		3.48	897	775	1680		4.44	0.68
C	0.3216		1.19	897	775	1680		1.52	4.75
Zircaloy-2									
Control (W-124)	0.7862	1.00		105.8		1584			
Core-channel coupons									
ZB-51	0.7481	4.69		897	775	1584		3.70	0.38
ZB-52	0.7477	4.64		897	775	1584		3.66	0.63
ZB-54	0.7780	2.64		897	775	1584		2.08	2.63
ZB-56	0.7882	2.10		897	775	1584		1.66	3.63
ZB-62	0.7687	1.28		897	775	1584		1.02	5.63
Core-annulus coupons									
ZB-83	0.7677	5.03		897	775	1584		3.97	0.46
ZB-57	0.7652	5.57		897	775	1584		4.39	0.46
ZB-58	0.7694	3.75		897	775	1584		2.96	2.21
ZB-84	0.7731	2.29		897	775	1584		1.81	3.71
85% sponge Zr–15% Nb									
Control (W-125)	0.8568	1.00		105.8		1464	5.00		
Core-annulus coupons									
Array I, position 11	0.8477	3.45		897	775	1704		2.75	2.96
67% crystal-bar Zr–33% Nb									
Control (W-126)	0.9152	1.00		105.8		1464	5.00		
Core-annulus coupons									
Array I, position 4	0.8800	4.85		897	775	1704		3.86	1.21
Array II, position 14	0.8571	2.72		897	775	1704		2.17	3.71

UNCLASSIFIED
ORNL-LR-DWG 75557

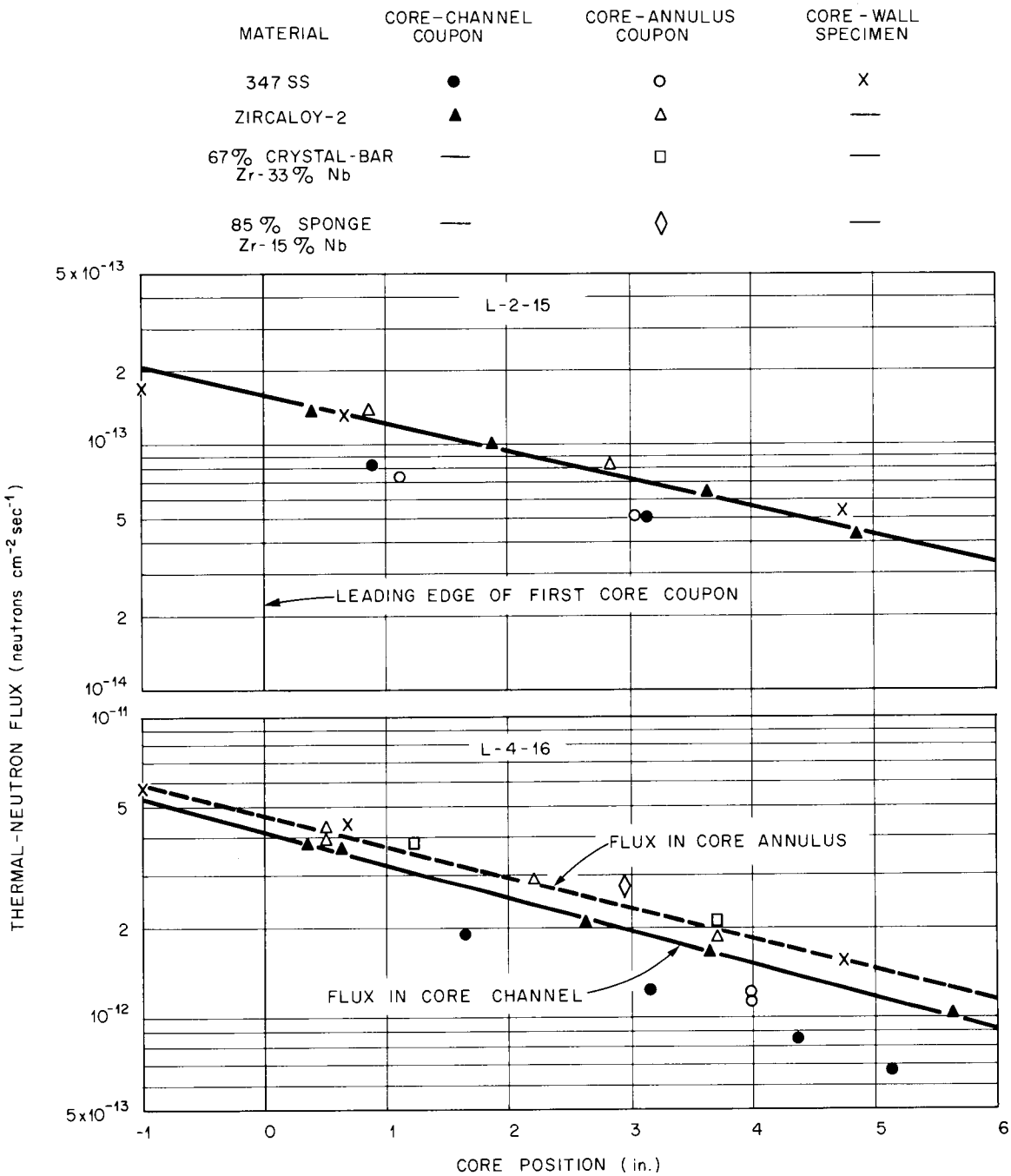

Fig. 38. Neutron Flux in Core vs Linear Position.

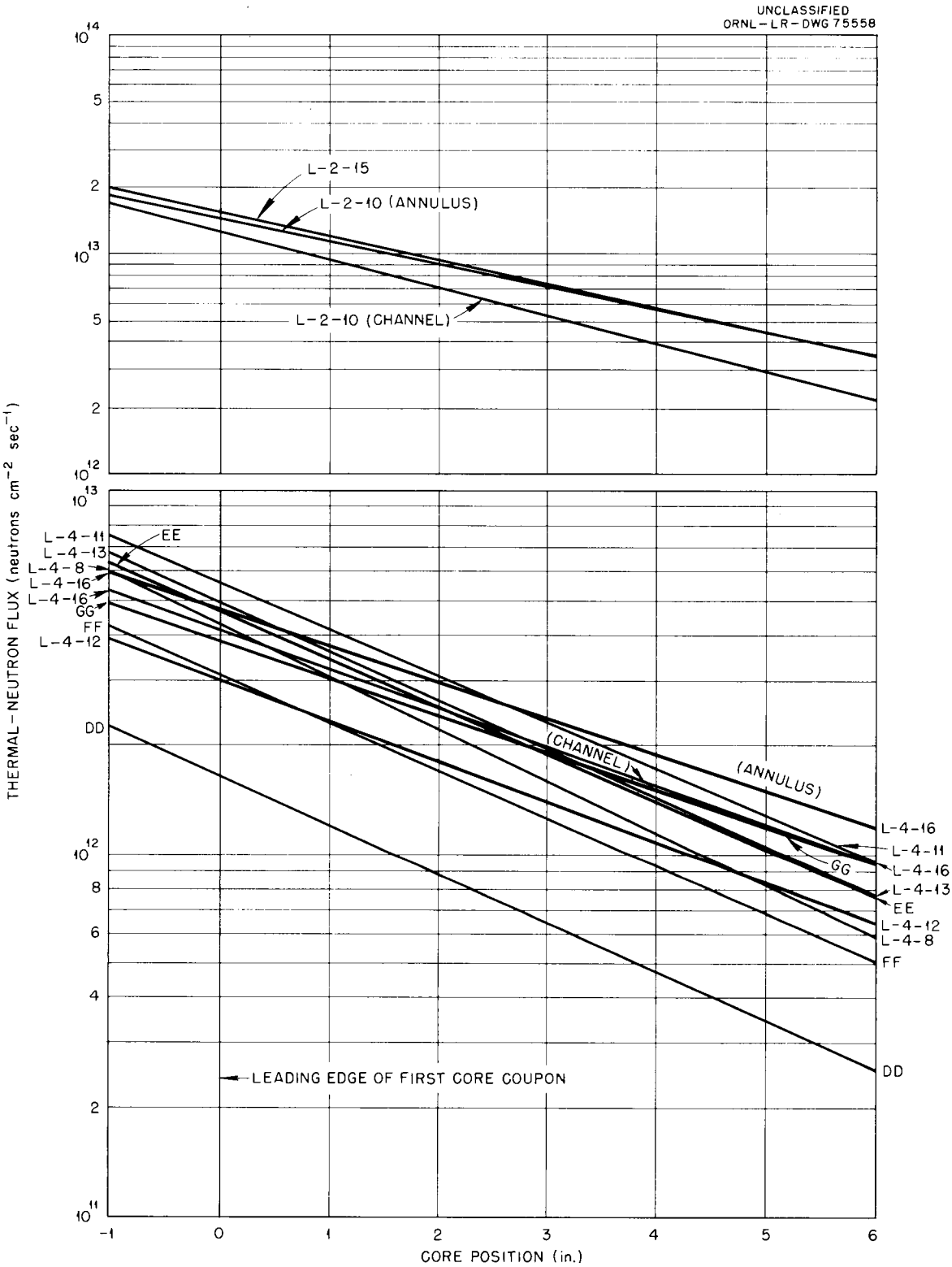

Fig. 39. Neutron Flux in Core vs Linear Position.

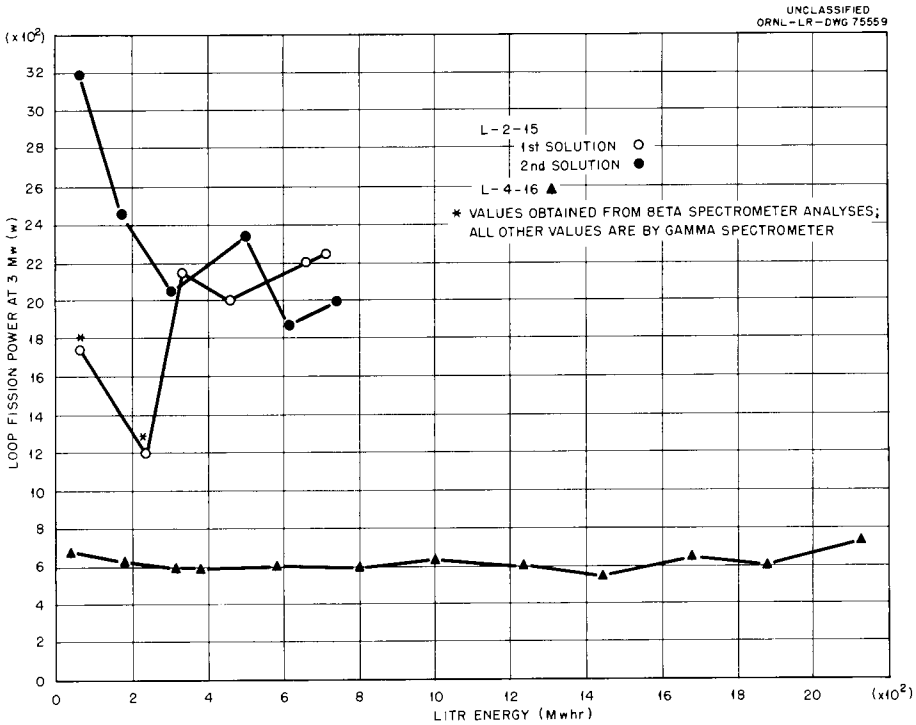

Fig. 40. Cumulative Average Fission Power at 3 Mw Based on Cs^{137} Analyses.

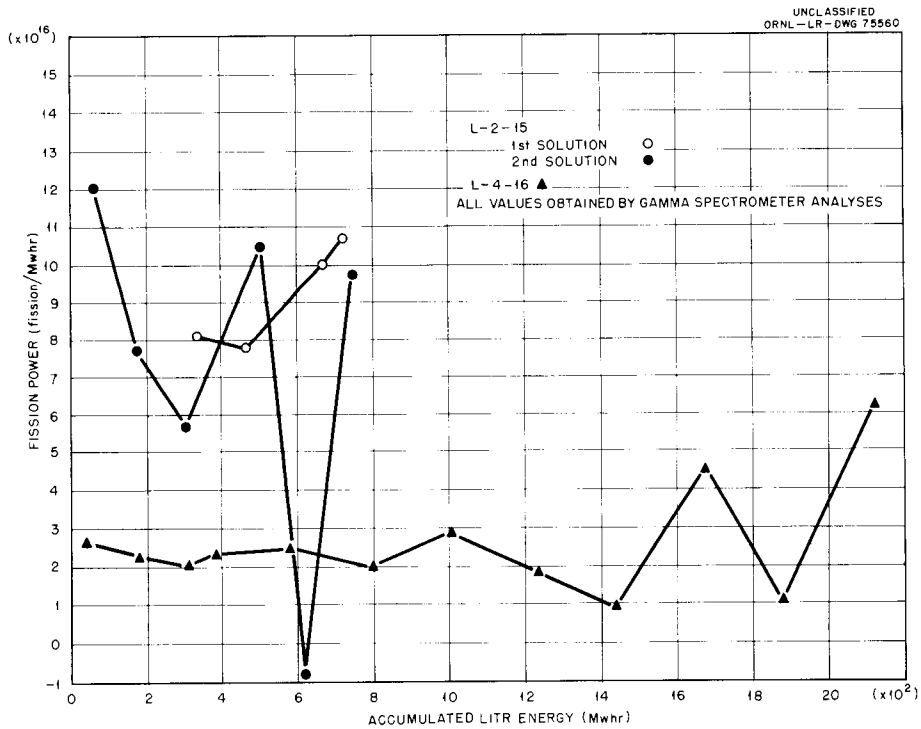

Fig. 41. Fission in Loop Solutions vs Accumulated LITR Energy.

technique.[18] Comparisons between the two counting techniques, which were made with the L-2-15 samples, showed that the gamma-counting results were consistently higher than the others by about 20%. The differences presumably resulted from differences in the fission standards employed. It is believed that the gamma-ray spectrometer results are the most nearly correct.

4.8.3 Heat from Absorption of Fission and Gamma-Ray Energy

The results of measurements of combined fission and gamma heat at 3-Mw reactor power, as determined from the difference between resistance-heater power requirements with the reactor down and at full power are shown in Fig. 13. The average values are 2749 ± 27 and 890 ± 17 w (90% confidence levels) for L-2-15 and L-4-16. There were no significant drifts or shifts of the heat values during either experiment.

The heat due to absorption of reactor gamma-ray energy in HB-2 is known to be about 700 w,[19] so that the heat due to fissioning in the L-2-15 loop core was about 2050 w. Assuming that the gamma heat in L-4-16 was approximately 200 w (i.e., assuming that in both HB-4 and HB-2 the gamma heat was proportional to the neutron flux), the heat due to fission in the L-4-16 core was about 700 w.

4.8.4 Comparison of Average Fission-Power Values from Cs^{137}, Gamma-Ray Heat, and Induced Activities

Values for the average fission power in the loop experiments at 3-Mw LITR power calculated from the results of the different types of measurements are compared in Table 18. The average of the Cs^{137} results in L-2-15 is the average of the final (cumulative average) values obtained with the two solution charges, as shown in Fig. 40. That for L-4-16 is the cumulative average for that experiment. The induced activity calculations employed the neutron fluxes shown in Fig. 38 and the average uranium concentrations listed in Table 10. A value of 200 Mev/fission was assumed throughout, and, for comparison here, the values obtained from the fission-heat measurements were multiplied by the ratio 200/170, since an estimated 170 Mev of energy per fission is absorbed in the loop.

[18] G. H. Jenks and J. E. Baker, *In-Pile Loop Corrosion Experiments with Uranyl Sulfate Solutions at 235 and 250°C*, ORNL-3131 (in press).

[19] G. H. Jenks and J. E. Baker, *In-Pile Loop Investigation of Corrosion of Zircaloy-2 and Other Possible Reactor Materials in 0.04 m UO_2SO_4 at 280°C*, ORNL-2962 (in press).

Table 18. Average Fission Power in Core of Experiment

Method of Determination	Average Fission Power in Core (w/ml)	
	L-2-15	L-4-16
Specimen activity	12.5	3.8
Fission and gamma heat	7.8[a]	2.6[b]
Cs^{137} analyses	6.9	2.3

[a] Assumes 700-w gamma heat.
[b] Assumes 200-w gamma heat.

The fission-heat value is higher than the Cs^{137} value by 13% in each experiment, but this difference is within the estimated uncertainty of some of the estimated heat values. There is poor agreement between the fission heats calculated from the specimen activity measurements and the other values. This poor agreement has been noted, and possible explanations have been discussed previously.[18] The Cs^{137} total power values are considered more reliable than those calculated from induced activities.

4.9 Results of Quantitative Examinations of Loops

4.9.1 Analyses of Scale from Low-Power-Density Regions

In an effort to determine the distribution of corrosion products throughout loop L-4-16, specimens of scale were scraped from the metal at the rear of the core, from the special in-line holder, from the pressurizer, and from the pump volute. These samples were analyzed for uranium and copper and for the corrosion products (chromium, nickel, iron, and zirconium). The results of these analyses are listed in Table 19. As shown, only small amounts of uranium were found in the samples, and the relative activities varied considerably.

Although the number of scale samples was insufficient to accurately establish the average composition of loop scales, a material balance for zirconium and nickel was made based on (1) the average results of the scale analyses, (2) estimates made from the oxygen consumption data of the total amount of iron in loop scales, (3) specimen weight results, and (4) solution analyses data.

The results, shown in Table 20, indicate that most of the zirconium which had been oxidized in the core was transferred to and deposited on surfaces outside the core. This result was expected since Zircaloy-2 surfaces exposed in the core are generally free of heavy scale. Observations in subsequent loop experiments and in the HRT have also shown that large fractions of the zirconium found in regions exposed to fissioning solutions are transported to regions relatively free of fissioning.[20] The nickel results indicate that appreciable amounts of this element are incorporated in the loop scales. Results of scale

[20] G. H. Jenks and J. E. Baker, *HRP Radiation Corrosion Studies: In-Pile Loop L-2-17*, ORNL-2974 (to be published).

Table 19. Chemical Analyses of Scale from Loop L-4-16

Position	Weight of Samples (mg)	Relative Gross Activity per mg	Analysis (wt %)					
			U	Cu	Cr[a]	Ni	Fe	Zr
Rear of core	13.6	0.04	0.029	0	7.0	6.0	50.7	5.1
Special in-line holder	12.7	0.68	0.039	0	4.5	7.4	43.9	10.7
Pressurizer	17.7	0.41	0.025	0.23	6.6	9.3	41.4	7.7
Pump volute	14.4	1	0.18	0	4.9	4.1	35.3	10.4

[a] These results are probably low because methods employed in dissolving scale may have led to volatilization of chromium chlorides.

analyses in subsequent experiments have confirmed this finding.[20] Also, in L-2-15 and other experiments, the difference between amounts of steel corrosion indicated by oxygen and dissolved-nickel data reveals that nickel is retained in the scales. These nickel results show that the amount of dissolved nickel cannot be used as an accurate measure of steel corrosion in these systems under irradiation.

4.9.2 Results of Specimen Weight Measurements

The results of weight measurement of specimens and other components are listed in Tables 21 and 22 together with other data, including average corrosion rate values calculated from weight data, solution fission-power densities near specimens, and brief descriptions of specimens. The rate values based on radiation time and total specimen areas are considered the most significant for the zirconium and titanium alloys, and these values are used in plots of the corrosion data. For stainless steel specimens, the rates based on radiation time and exposed surface areas (i.e., excluding areas covered in clamping or by adjacent specimens) have been considered the most nearly correct in treating data from past experiments and are employed in plots of these steel data. Density values employed in rate calculations are listed in Table 23.

(*a*) Zirconium Alloys. – The Zircaloy-2 and crystal-bar zirconium corrosion rate values are plotted vs fission-power density in solutions in Fig. 42. The impact and tensile specimens were not cathodically defilmed, and the plotted rate values were calculated from the "as-removed" weights. However, defilming of coupon specimens resulted in very small weight changes, and it is likely that defilming would have had negligible effects on the weight-change values. The in-line specimens exhibited weight gains even after defilming. Hence no estimates of rates for these specimens could be made, but it is believed that they corroded at very low rates.

Table 20. Experiment L-4-16 Material Balance of Scale Constituents

Element	Mass Ratio of Element to Iron in Scale[a]	Mass Ratio of Element to Iron in Stainless Steel	Amount in Solution[b] (g)	Amount Oxidized During Exposure (g)	Amount in Scale (g)	Excess in Scale over Amount Calculated from Corrosion Data[c] (g)
Zr	0.2		0.02	0.75[d]	0.91	0.17
Ni	0.16	0.187	0.39	0.78[e]	0.64	0.25
Fe	(1)	(1)	0.23	4.2[e]	4.0	(0)

Stainless Steel Oxidized Based on Oxygen Data (g)		
In-Pile Exposure	Preparatory Operation	Total
4.6	1.6	6.2

[a]Based on average of analytical results in Table 19.
[b]Sum of amounts found during preparatory and in-pile exposures.
[c]The amount in solution plus the amount in scale minus the amount oxidized during exposure.
[d]Based on specimen weight data.
[e]Based on data for oxygen uptake on steel.

Table 21. Data for Corrosion Specimens in Loop L-2-15

Sample Number	Position	Average Flow Velocity Across Specimen (fps)	Weight Data: Initial (g)	Weight Data: As Removed (g)	Weight Data: Defilmed (g)	Weight Data: Change (mg)	Exposed Sample Area (cm^2)	Corrosion Penetration (mils)	Corrosion Rate[a] (Exposed Area) (mpy): 792 hr	Corrosion Rate[a] (Exposed Area) (mpy): 544 hr	Total Area (cm^2)	Corrosion Penetration (mils)	Corrosion Rate[a] (Total Area) (mpy): 792 hr	Corrosion Rate[a] (Total Area) (mpy): 544 hr	Distance from Front of First Core-Channel Specimen to Center of Specimen (in.)	Thermal Neutron Flux at Specimen Locations (neutrons cm^{-2} sec^{-1})	Power Density at Specimen Locations (w/ml)	Strain (μ in./in.)	Stress (psi)	Remarks on Surface Appearance: As-Removed Surface	Remarks on Surface Appearance: Defilmed Surface
24 Core corrosion-sample coupons																$\times 10^{13}$					
Stainless steel, type 347																					
1240-A	4	11.9	0.9474	0.9294	0.9277	19.7	1.40	0.69	7.6	11.1	2.2	0.44	4.9	7.1	0.9	1.28	16.6			Uniform dark-brown scale on all surfaces	Clean; machine marks visible
1241-A	5	13.2	0.9697	0.9435	0.9416	28.1	1.40	0.99	10.9	15.9	2.2	0.63	6.9	10.1	1.1	1.20	15.6			Uniform dark-brown scale on all surfaces	Clean; machine marks visible
1256-A	7	16.6	0.9604	0.9450	0.9432	17.7	1.40	0.62	6.8	10.0	2.2	0.39	4.3	6.3	1.6	1.04	13.5			Uniform dark-brown scale on all surfaces	Some very thin film retained; machine marks visible
1257-A	10	28.9	0.9645	0.9570	0.9553	9.2	1.40	0.32	3.5	5.1	2.2	0.20	2.2	3.2	2.4	0.86	11.2			Uniform dark-brown scale on all surfaces	Some very thin film retained; slightly etched surfaces
1258-A	13	39.4	0.9487	0.9450	0.9434	5.3	1.40	0.19	2.1	3.1	2.2	0.12	1.3	1.9	3.1	0.71	9.2			Uniform dark-brown scale on all surfaces	Some film retained; machine marks visible
1259-A	18	19.9	0.9509	0.9505	0.9492	1.7	1.40	0.06	0.7	1.0	2.2	0.04	0.4	0.6	4.4	0.51	6.6			Uniform dark-brown scale on all surfaces	Some very thin film retained; machine marks visible
1260-A	21	13.1	0.9493	0.9491	0.9478	1.5	1.40	0.05	0.6	0.8	2.2	0.03	0.3	0.5	5.1	0.42	5.5			Uniform dark-brown scale on all surfaces	Some very thin film retained; machine marks visible
1261-A	24	9.7	0.9620	0.9616	0.9606	1.4	1.57	0.04	0.4	0.6	2.2	0.03	0.3	0.5	5.9	0.35	4.6			Uniform dark-brown scale on all surfaces	Some very thin film retained; machine marks visible
Zircaloy-2																					
ZB-11	2	9.9	0.7901	0.7692	0.7680	22.1	1.40	0.96	10.6	15.4	2.2	0.61	6.7	9.8	0.4	1.44	18.7			Thin gray film with overlying interference colors	Lightly etched surfaces; some very thin film retained
ZB-12	3	10.8	0.7880	0.7672	0.7662	21.8	1.40	0.94	10.4	15.1	2.2	0.60	6.6	9.6	0.6	1.35	17.5			Thin gray film with overlying interference colors	Lightly etched surfaces; some very thin film retained
ZB-13	8	19.4	0.7964	0.7800	0.7790	17.4	1.40	0.75	8.3	12.0	2.2	0.48	5.3	7.7	1.9	0.98	12.7			Thin gray film with overlying interference colors	Lightly etched surfaces; some very thin film retained
ZB-14	11	33.9	0.7964	0.7825	0.7812	15.2	1.40	0.66	7.3	10.6	2.2	0.42	4.6	6.7	2.6	0.80	10.4			Thin gray film with overlying interference colors	Lightly etched surfaces; some very thin film retained
ZB-15	14	43.6	0.7893	0.7778	0.7767	12.6	1.40	0.55	6.1	8.8	2.2	0.35	3.9	5.6	3.4	0.66	8.6			Thin gray film with overlying interference colors	Lightly etched surfaces; some very thin film retained
ZB-16	15	39.5	0.7892	0.7782	0.7772	12.0	1.40	0.52	5.7	8.4	2.2	0.33	3.6	5.3	3.6	0.62	8.1			Thin gray film with overlying interference colors	Lightly etched surfaces; some very thin film retained
ZB-17	20	14.7	0.7934	0.7847	0.7840	9.4	1.40	0.41	4.5	6.6	2.2	0.26	2.9	4.2	4.9	0.45	5.9			Thin gray film with overlying interference colors	Lightly etched surfaces; some very thin film retained
ZB-18	23	10.6	0.7941	0.7869	0.7856	8.5	1.40	0.37	4.1	5.9	2.2	0.24	2.6	3.8	5.6	0.37	4.8			Thin gray film with overlying interference colors	Lightly etched surfaces; some very thin film retained
Titanium-55AX																					
Ti-131	1	9.2	0.5390	0.5384	0.5366	2.4	1.57	0.13	1.4	2.1	2.2	0.09	1.0	1.4	0.1	1.52	19.8			Thin brass-colored film with machine marks visible	Some stain retained; machine marks visible
Ti-132	6	14.6	0.5385	0.5378	0.5365	2.0	1.40	0.12	1.3	1.9	2.2	0.08	0.9	1.3	1.4	1.11	14.4			Thin brass-colored film with machine marks visible	Some stain retained; machine marks visible
Ti-133	9	23.0	0.5316	0.5310	0.5298	1.8	1.40	0.11	1.2	1.8	2.2	0.07	0.8	1.1	2.1	0.92	12.0			Thin brass-colored film with machine marks visible	Clean; machine marks visible
Ti-134	12	36.3	0.5363	0.5358	0.5345	1.8	1.40	0.11	1.2	1.8	2.2	0.07	0.8	1.1	2.9	0.76	9.9			Thin brass-colored film with machine marks visible	Clean; machine marks visible
Ti-135	16	29.4	0.5378	0.5370	0.5360	1.8	1.40	0.11	1.2	1.8	2.2	0.07	0.8	1.1	3.9	0.58	7.5			Some spots of rustlike film over thin brass-colored film	Clean; machine marks visible
Ti-136	17	23.7	0.5350	0.5343	0.5333	1.7	1.40	0.11	1.2	1.8	2.2	0.07	0.8	1.1	4.1	0.55	7.2			Some spots of rustlike film over thin brass-colored film	Clean; machine marks visible
Ti-137	19	16.9	0.5360	0.5354	0.5345	1.5	1.40	0.09	1.0	1.4	2.2	0.06	0.7	1.0	4.6	0.48	6.2			Some spots of rustlike film over thin brass brass-colored film	Clean; machine marks visible
Ti-138	22	11.7	0.5349	0.5346	0.5329	2.0	1.40	0.12	1.3	1.9	2.2	0.08	0.9	1.3	5.4	0.39	5.1			Some spots of rustlike film over thin brass-colored film	Clean; machine marks visible
14 Core-annulus coupon specimens																					
Nickel- and platinum-clad Zircaloy-2																					
ZV-1	1		1.6048	1.4997	1.4815	123.3	2.8				4.0				0.9	1.24	16.1			Dull gray in color with plating breaking off in spots	Same as "as-removed"
ZV-2	14		1.6115	1.5223	1.5119	99.6	2.8				4.0				4.3	0.52	6.8			Dull gray with a lightly etched appearance	Some very thin film retained; machine marks visible; plating breaking off specimen
Zircaloy-2																					
ZB-27	2		0.7918	0.7616	0.7611	30.7	1.4	1.33	14.7	21.4	2.2	0.85	9.4	13.6	1.2	1.18	15.3			Thin gray film with overlying interference colors	Some very thin film retained on a lightly etched surface; machine marks visible
ZB-28	5		0.7943	0.7660	0.7657	28.6	1.4	1.24	13.7	19.9	2.2	0.79	8.7	12.7	1.9	0.96	12.5			Thin gray film with overlying interference colors	Some very thin film retained on a lightly etched surface; machine marks visible
ZB-29	10		0.7922	0.7710	0.7695	22.7	1.4	0.98	10.8	15.7	2.2	0.62	6.8	10.0	3.2	0.69	9.0			Thin gray film with overlying interference colors	Some very thin film retained on a lightly etched surface; machine marks visible
Stainless steel, type 347																					
1048-A	3		0.9703	0.8980	0.8911	79.2	1.4	2.78	30.7	44.6	2.2	1.77	19.5	28.4	1.4	1.10	14.3			Uniform dark-brown scale on all surfaces	One edge of specimen very heavily attacked
1249-A	6		0.9657	0.8745	0.8673	98.4	1.4	3.45	38.1	55.4	2.2	2.20	24.3	35.3	2.2	0.92	12.0			Uniform dark-brown scale on all surfaces	All surfaces show evidence of very heavy attack
1250-A	11		0.9515	0.8796	0.8524	99.1	1.4	3.47	38.3	55.7	2.2	2.21	24.4	35.5	3.4	0.65	8.5			Uniform dark-brown scale on all surfaces	All surfaces show evidence of very heavy attack
Titanium-110AT																					
TD-21	4		0.5355	0.5337	0.5330	2.5	1.4	0.15	1.7	2.4	2.2	0.10	1.1	1.6	1.7	1.03	13.4			Thin brass-colored film on all surfaces	Clean; some scratches visible
TD-22	8		0.5378	0.5373	0.5348	3.0	1.4	0.19	2.1	3.1	2.2	0.12	1.3	1.9	2.7	0.79	10.3			Thin brass-colored film on all surfaces	Clean; some scratches visible

Table 21 (continued)

Sample Number	Position	Average Flow Velocity Across Specimen (fps)	Weight Data: Initial (g)	Weight Data: As Removed (g)	Weight Data: Defilmed (g)	Weight Data: Change (mg)	Exposed Sample Area (cm^2)	Corrosion Penetration (mils)	Corrosion Rate[a] (Exposed Area) (mpy): 792 hr	Corrosion Rate[a] (Exposed Area) (mpy): 544 hr	Total Area (cm^2)	Corrosion Penetration (mils)	Corrosion Rate[a] (Total Area) (mpy): 792 hr	Corrosion Rate[a] (Total Area) (mpy): 544 hr	Distance from Front of First Core-Channel Specimen to Center of Specimen (in.)	Thermal Neutron Flux at Specimen Locations (neutrons cm^{-2} sec^{-1})	Power Density at Specimen Locations (w/ml)	Strain (μ in./in.)	Stress (psi)	Remarks on Surface Appearance: As-Removed Surface	Remarks on Surface Appearance: Defilmed Surface
Platinum																$\times 10^{13}$					
Pt-18	7		0.9030	0.9045	0.9035	+0.5	1.4				1.8				2.4	0.84	10.9			Clean on one side; heavy rustlike stain on the other	Clean; some scratches visible
Pt-19	12		0.8906	0.8910	0.8900	0.6	1.4	0.008	0.09	0.13	1.8	0.005	0.06	0.08	3.7	0.61	7.9			Some spots of stain scattered over clean surfaces	Clean
Stainless steel, type 309SCb																					
C-76	9		0.9653	0.9117	0.8967	68.6	1.4	2.45	27.0	39.3	2.2	1.56	17.2	25.1	2.9	0.74	9.6			Uniform dark-brown scale on all surfaces	Considerable roughening, particularly along edges; some scale retained
C-77	13		0.9303	0.7665	0.7297	200.6	1.4	7.16	79.0	115.0	2.2	4.56	50.3	73.2	3.9	0.57	7.4			Uniform dark-brown scale on all surfaces	Very severe roughening, particularly along edges; some scale retained
2 Core tensile specimen																					
Crystal-bar zirconium																					
918–919	F		15.3296	15.1917		137.9	18.1	0.46	5.1	7.4	21.2	0.39	4.3	6.3	2.7	0.79	10.3			Gray film on all surfaces; slightly roughened	
1014–1015	H		15.3046	15.1400		164.6	18.1	0.54	6.0	8.7	21.2	0.47	5.2	7.6	2.7	0.79	10.3			Gray film on all surfaces; slightly roughened	
4 Core impact specimen																					
Zircaloy-2																					
895	A		19.0946	18.8706		224.0	24.9	0.54	6.0	8.7	26.7	0.50	5.5	8.1	2.7	0.79	10.3			Thin gray film with overlying interference colors	Surface slightly roughened
898	C		18.9611	18.6842		276.9	24.9	0.67	7.4	10.8	26.7	0.63	7.0	10.1	2.7	0.79	10.3			Thin gray film with overlying interference colors	Surface slightly roughened
Crystal-bar zirconium																					
906	D		18.9146	18.6302		284.4	24.9	0.69	7.6	11.1	26.7	0.64	7.1	10.3	2.7	0.79	10.3			Uniform thin black shiny film on all surfaces	Surface slightly roughened
909	E		18.8760	18.6195		256.5	24.9	0.62	6.9	10.0	26.7	0.58	6.4	9.3	2.7	0.79	10.3			Uniform thin black shiny film on all surfaces	Surface slightly roughened
Core stress specimens and holders																					
Titanium-110AT specimens																					
TD-8			5.7621	5.7510	5.7458	16.3	19.5	0.08	0.88	1.29	20.0	0.08	0.88	1.29	2.8	0.76	9.9	4450	60,100	Thin brass-colored film on all surfaces	Some very thin film retained; machine marks visible
TD-9			5.6323	5.6199	5.6127	19.6	19.5	0.10	1.10	1.61	20.0	0.10	1.10	1.61	2.8	0.76	9.9	4775	64,450	Thin brass-colored film on all surfaces	Some very thin film retained; machine marks visible
Titanium-55AX holders																					
40			6.5056	6.4982	6.4960	9.6					20.0	0.05	0.54	0.79	0.8	1.30	16.9			Thin brass-colored film on all surfaces	Clean; machine marks visible
43			6.0413	6.0378	6.0341	7.2					20.0	0.04	0.40	0.59	3.2	0.69	8.9			Thin brass-colored film on all surfaces	Clean; machine marks visible
24 In-line corrosion-sample coupons																					
Stainless steel, type 347																					
1361-A	4	11.9	0.9558	0.9598	0.9540	1.8	1.40	0.06	0.66	1.01	2.2	0.04	0.44	0.64						Uniform brown scale on all surfaces	Clean with slight staining; machine marks visible
1364-A	5	13.2	0.9513	0.9558	0.9492	2.1	1.40	0.07	0.77	1.18	2.2	0.05	0.55	0.75						Uniform brown scale on all surfaces	Clean with slight staining; machine marks visible
1365-A	7	16.6	0.9480	0.9525	0.9473	0.7	1.40	0.02	0.22	0.39	2.2	0.02	0.22	0.25						Uniform brown scale on all surfaces	Clean with slight staining; machine marks visible
1367-A	10	28.9	0.9385	0.9436	0.9370	1.5	1.40	0.05	0.58	0.84	2.2	0.03	0.37	0.53						Uniform brown scale on all surfaces	Clean with slight staining; machine marks visible
1369-A	13	39.4	0.9537	0.9581	0.9534	0.3	1.40	0.01	0.11	0.17	2.2	0.01	0.11	0.11						Uniform brown scale on all surfaces	Clean with slight staining; machine marks visible
1371-A	18	19.9	0.9547	0.9584	0.9538	0.9	1.40	0.03	0.33	0.51	2.2	0.02	0.22	0.32						Uniform brown scale on all surfaces	Clean with slight staining; machine marks visible
1376-A	21	13.1	0.9530	0.9555	0.9515	1.5	1.40	0.05	0.58	0.84	2.2	0.03	0.37	0.53						Uniform brown scale on all surfaces	Clean with slight staining; machine marks visible
1378-A	24	9.7	0.9524	0.9551	0.9505	1.9	1.57	0.06	0.65	0.95	2.2	0.04	0.44	0.60						Uniform brown scale on all surfaces	Clean with slight staining; machine marks visible
Zircaloy-2																					
ZB-19	2	9.9	0.7897	0.7924	0.7924	+2.7	1.40				2.2									Uniform brown scale on all surfaces	Uniform dark-brown scale over all surfaces
ZB-20	3	10.8	0.7976	0.8022	0.8022	+4.6	1.40				2.2									Uniform brown scale on all surfaces	Uniform dark-brown scale on all exposed surfaces
ZB-21	8	19.4	0.7988	0.8047	0.8039	+5.1	1.40				2.2									Uniform brown scale on all surfaces	Uniform dark-brown scale over all surfaces
ZB-22	11	33.9	0.7861	0.7903	0.7898	+3.7	1.40				2.2									Uniform brown scale on all surfaces	Uniform dark-brown scale over all surfaces
ZB-23	14	43.6	0.7873	0.7906	0.7900	+2.7	1.40				2.2									Uniform brown scale on all surfaces	Uniform dark-brown scale over all surfaces
ZB-24	15	39.5	0.7892	0.7925	0.7922	+3.0	1.40				2.2									Uniform brown scale on all surfaces	Uniform dark-brown scale over all surfaces
ZB-25	20	14.7	0.7823	0.7848	0.7845	+2.2	1.40				2.2									Uniform brown scale on all surfaces	Uniform dark-brown scale over all surfaces
ZB-26	23	10.6	0.7828	0.7849	0.7840	+1.2	1.40				2.2									Uniform brown scale on all surfaces	Uniform dark-brown scale over all surfaces
Titanium-55AX																					
Ti-140	1	9.2	0.5375	0.5404	0.5394	+1.9	1.57				2.2									Uniform brown scale on all surfaces	Scale flaked off in spots; dark film underneath
Ti-142	6	14.6	0.5396	0.5442	0.5432	+3.6	1.40				2.2									Uniform brown scale on all surfaces	Scale flaked off in spots; dark film underneath
Ti-143	9	23.0	0.5389	0.5440	0.5432	+4.3	1.40				2.2									Uniform brown scale on all surfaces	Scale flaked off in spots; dark film underneath
Ti-144	12	36.3	0.5343	0.5386	0.5343	+0.0	1.40				2.2									Uniform brown scale on all surfaces	Scale flaked off in spots; dark film underneath; machine marks visible
Ti-146	16	29.4	0.5370	0.5409	0.5395	+2.5	1.40				2.2									Uniform brown scale on all surfaces	Scale flaked off in center; dark film underneath
Ti-147	17	23.7	0.5424	0.5460	0.5450	+2.6	1.40				2.2									Uniform brown scale on all surfaces	Scale flaked off in center; dark film underneath
Ti-148	19	16.9	0.5356	0.5392	0.5376	+2.0	1.40				2.2									Uniform brown scale on all surfaces	Scale flaked off in spots; dark film underneath
Ti-149	22	11.7	0.5383	0.5410	0.5390	+0.7	1.40				2.2									Uniform brown scale on all surfaces	Scale flaked off in spots; dark film underneath

Table 21 (continued)

Sample Number	Position	Average Flow Velocity Across Specimen (fps)	Weight Data: Initial (g)	Weight Data: As Removed (g)	Weight Data: Defilmed (g)	Weight Data: Change (mg)	Exposed Sample Area (cm^2)	Corrosion Penetration (mils)	Corrosion Rate[a] (Exposed Area) (mpy): 792 hr	Corrosion Rate[a] (Exposed Area) (mpy): 544 hr	Total Area (cm^2)	Corrosion Penetration (mils)	Corrosion Rate[a] (Total Area) (mpy): 792 hr	Corrosion Rate[a] (Total Area) (mpy): 544 hr	Distance from Front of First Core-Channel Specimen to Center of Specimen (in.)	Thermal Neutron Flux at Specimen Locations (neutrons cm^{-2} sec^{-1})	Power Density at Specimen Locations (w/ml)	Strain (μ in./in.)	Stress (psi)	Remarks on Surface Appearance: As-Removed Surface	Remarks on Surface Appearance: Defilmed Surface
																$\times 10^{13}$					
14 In-line annulus coupon specimens																					
Nickel- and platinum-clad Zircaloy-2																					
ZV-3	1-F		1.6083	1.5518	1.5492	59.1	2.8				4.0									Uniform brown scale on all surfaces	Light gray surfaces, with plating breaking free from specimen
ZV-4	14-F		1.6191	1.5536	1.5504	68.7	2.8				4.0									Uniform brown scale on all surfaces	
Zircaloy-2																					
ZB-30	2-F		0.7882	0.7889	0.7887	+0.5	1.4				2.2									Uniform brown scale on all surfaces	Thin gray scale over all surfaces flaked off in places
ZB-81	5-F		0.7966	0.7970	0.7970	+0.4	1.4				2.2									Uniform brown scale on all surfaces	Thin gray scale over all surfaces flaked off in places
ZB-82	10-F		0.7949	0.7956	0.7953	+0.4	1.4				2.2									Uniform brown scale on all surfaces	Thin brown scale over all surfaces flaked off in places
Stainless steel, type 347																					
1252-A	3-F		0.9538	0.9550	0.9525	1.3	1.4	0.05	0.50	0.73	2.2	0.03	0.32	0.46						Uniform brown scale on all surfaces	Clean, with slight staining; machine marks visible
1253-A	6-F		0.9519	0.9528	0.9511	0.8	1.4	0.03	0.31	0.45	2.2	0.02	0.20	0.29						Uniform brown scale on all surfaces	Clean, with dark staining; machine marks visible
1254-A	11-F		0.9606	0.9614	0.9591	1.5	1.4	0.06	0.58	0.84	2.2	0.04	0.37	0.53						Uniform brown scale on all surfaces	Heavy dark staining; machine marks visible
Titanium-110AT																					
TD-23	4-F		0.5333	0.5342	0.5314	1.9	1.4	0.12	1.30	1.89	2.2	0.08	0.83	1.20						Uniform brown scale on all surfaces	Dark stain on all surfaces; machine marks visible
TD-24	8-F		0.5563	0.5571	0.5549	1.4	1.4	0.09	0.96	1.39	2.2	0.06	0.61	0.88						Uniform brown scale on all surfaces	Dark stain on all surfaces; machine marks visible
Platinum																					
Pt-20	7-F		0.7788	0.7786	0.7781	0.7	1.4	0.009	0.10	0.15	1.8	0.007	0.08	0.12						Uniform brown scale on all surfaces	Clean; some scratches visible
Pt-21	12-F		0.8433	0.8442	0.8428	0.5	1.4	0.007	0.07	0.11	1.8	0.005	0.05	0.09						Uniform brown scale on all surfaces	Clean; some spots of stain retained
Stainless steel, type 309SCb																					
C-78	9		0.9382	0.9396	0.9378	0.4	1.4	0.01	0.16	0.23	2.2	<0.01	0.10	0.15						Uniform brown scale over all surfaces	Heavily stained surfaces; machine marks visible
C-79	13		0.9190	0.9202	0.9176	1.4	1.4	0.05	0.55	0.80	2.2	0.03	0.35	0.51						Uniform brown scale over all surfaces	Heavily stained surfaces; machine marks visible
1 In-line tensile specimen																					
Crystal-bar zirconium																					
1016–1017	A		15.2796	15.3027		+23.1	18.1				21.2									Uniform brown scale on all surfaces	
3 In-line impact specimens																					
Zircaloy-2																					
896	E		18.7900	18.8203		+30.3	24.9				26.7									Uniform brown scale on all surfaces	
Crystal-bar zirconium																					
907	C		18.8564	18.8902		+33.8	24.9				26.7									Uniform brown scale on all surfaces	
910	D		18.8633	18.8929		+29.6	24.9				26.7									Uniform brown scale on all surfaces	
In-line stress specimens and holders																					
Titanium-110AT specimens																					
TD-6	B		5.7914	5.8094	5.7876	3.8	19.5	0.02	0.22	0.32	20.0	0.02	0.22	0.32				4450	60,100	Uniform dark-brown scale on all surfaces	Some very thin film retained; machine marks visible
TD-7	B		5.5370	5.5491	5.5337	3.3	19.5	0.02	0.22	0.32	20.0	0.02	0.22	0.32				4280	57,800	Uniform dark-brown scale on all surfaces	Some very thin film retained; machine marks visible
Titanium-55AX holders																					
27			6.1065	6.1156	6.1049	1.6														Uniform dark-brown scale on all surfaces	Clean; machine marks visible
35			6.1940	6.2054	6.1938	0.2														Uniform dark-brown scale on all surfaces	Clean; machine marks visible
Tapered channel coupon holders (Zircaloy-2)																					
Core (No. 107)																					
A			82.8151	82.2520	82.2323	582.8					90.0	0.39	4.3	6.3	3.0	0.72	8.8			White metallic appearance on inlet end ranging to a light brown on outlet end; etched appearance	Clean; interference colors ranging from light rose to light blue; slightly etched appearance
B											90.0				3.0	0.72	8.8			White metallic appearance on inlet end ranging to a light brown on outlet end; etched appearance	
In-line (No. 18)																					
A																				Heavy brown film on inlet end ranging to a thin brown film on other end; black underlay	
B			95.9863	96.1417	96.1198	+133.5														Heavy brown film on inlet end ranging to a thin brown film on other end; black underlay	Very thin brown scale on the outside; inside a gray scale or film with a dark appearance on both ends

[a]Two corrosion rates are presented: one based on the total operation time of 792 hr and the other based on the total radiation time of 544 hr (3 Mwhr of reactor time equivalent to 1 hr of total radiation time).

Table 22. Data for Corrosion Specimens in Loop L-4-16

Sample Number	Position	Average Flow Velocity Across Specimen (fps)	Weight Data: Initial (g)	Weight Data: As Removed (g)	Weight Data: Defilmed (g)	Weight Data: Change (mg)	Exposed Sample Area (cm^2)	Corrosion Penetration (mils)	Corrosion Rate[a] (Exposed Area) (mpy): 1032 hr	Corrosion Rate[a] (Exposed Area) (mpy): 775 hr	Total Area (cm^2)	Corrosion Penetration (mils)	Corrosion Rate[a] (Total Area) (mpy): 1032 hr	Corrosion Rate[a] (Total Area) (mpy): 775 hr	Distance from Front of First Core-Channel Specimen to Center of Specimen (in.)	Thermal Neutron Flux at Specimen Locations (neutrons cm^{-2} sec^{-1})	Power Density at Specimen Locations (w/ml)	Remarks on Surface Appearance: As-Removed Surface	Remarks on Surface Appearance: Defilmed Surface
																$\times 10^{12}$			
Core coupons																			
Stainless steel, type 347																			
1069-A	4	12.2	0.9665	0.9600	0.9600	−6.5	1.4	0.23	1.93	2.57	2.2	0.15	1.23	1.64	0.9	3.35	4.4	Dark rustlike film on all surfaces	Some stain retained; machine marks visible
1070-A	5	13.4	0.9600	0.9549	0.9548	−5.2	1.4	0.18	1.54	2.06	2.2	0.11	0.98	1.31	1.1	3.14	4.1	Dark rustlike film on all surfaces	Some stain retained; machine marks visible
1071-A	7	16.9	0.9742	0.9701	0.9701	−4.1	1.4	0.14	1.22	1.62	2.2	0.09	0.78	1.03	1.6	2.77	3.6	Dark rustlike film on all surfaces	Some stain retained; machine marks visible
1076-A	10	29.5	0.9699	0.9671	0.9671	−2.8	1.4	0.10	0.83	1.11	2.2	0.06	0.53	0.71	2.4	2.30	3.0	Dark rustlike film on all surfaces	Some stain retained; machine marks visible
1077-A	13	40.1	0.9621	0.9611	0.9611	−1.0	1.4	0.04	0.30	0.40	2.2	0.03	0.19	0.25	3.1	1.90	2.5	Dark rustlike film on all surfaces	Some stain retained; machine marks visible
1079-A	18	20.2	0.9743	0.9742	0.9736	−0.7	1.4	0.02	0.21	0.28	2.2	0.01	0.13	0.18	4.4	1.40	1.8	Heavy dark rustlike film on all surfaces	A few spots of scale retained; machine marks visible
1386-A	21	13.2	0.9676	0.9678	0.9670	−0.6	1.4	0.02	0.18	0.24	2.2	0.01	0.11	0.15	5.1	1.15	1.5	Heavy dark rustlike film on all surfaces	A few spots of scale retained; machine marks visible
1387-A	24	9.9	0.9574	0.9577	0.9566	−0.8	1.57	0.03	0.21	0.28	2.2	0.02	0.15	0.20	5.9	0.95	1.3	Heavy dark rustlike film on all surfaces	A few spots of scale retained; machine marks visible
Zircaloy-2																			
ZB-51	2	10.2	0.7937	0.7844	0.7844	−9.3	1.4	0.40	3.41	4.54	2.2	0.26	2.17	2.89	0.4	3.8	5.0	Thin dark-gray film with slightly roughened surface	Etched surface; some film retained
ZB-52	3	11.1	0.7848	0.7756	0.7756	−9.2	1.4	0.40	3.37	4.49	2.2	0.25	2.14	2.86	0.6	3.55	4.7	Thin dark-gray film with slightly roughened surface	Etched surface; some film retained
ZB-53	8	19.7	0.7891	0.7822	0.7822	−6.9	1.4	0.30	2.53	3.36	2.2	0.19	1.61	2.14	1.9	2.6	3.4	Thin dark-gray film with slightly roughened surface	Lightly etched surface; some film retained
ZB-54	11	34.5	0.7915	0.7856	0.7856	−5.9	1.4	0.26	2.16	2.88	2.2	0.16	1.37	1.83	2.6	2.15	2.8	Thin dark-gray film with slightly roughened surface	Lightly etched surface; some film retained
ZB-55	14	44.4	0.7910	0.7859	0.7859	−5.1	1.4	0.22	1.87	2.49	2.2	0.14	1.19	1.58	3.4	1.78	2.3	Thin dark-gray film with slightly roughened surface	Lightly etched surface; some film retained
ZB-56	15	40.3	0.7988	0.7938	0.7938	−5.0	1.4	0.21	1.83	2.44	2.2	0.14	1.16	1.55	3.6	1.53	2.0	Thin dark-gray film with slightly roughened surface	Lightly etched surface; some film retained
ZB-61	20	14.9	0.7963	0.7924	0.7922	−4.1	1.4	0.18	1.50	2.00	2.2	0.11	0.95	1.27	4.9	1.22	1.6	Thin dark-gray film with slightly roughened surface	Lightly etched surface; some film retained
ZB-62	23	10.8	0.7918	0.7881	0.7880	−3.8	1.4	0.16	1.39	1.85	2.2	0.10	0.88	1.18	5.6	0.98	1.3	Thin dark-gray film with slightly roughened surface	Lightly etched surface; some film retained
Titanium-55AX																			
Ti-203	1	9.4	0.5416	0.5411	0.5409	−0.7	1.57	0.04	0.33	0.44	2.2	0.03	0.24	0.31	0.1	4.05	5.3	Thin brass-colored film on all surfaces	Some stain retained; machine marks visible
Ti-204	6	14.9	0.5348	0.5344	0.5344	−0.4	1.4	0.02	0.21	0.28	2.2	0.02	0.13	0.18	1.4	2.94	3.9	Thin brass-colored film on all surfaces	Some stain retained; machine marks visible
Ti-205	9	23.3	0.5412	0.5410	0.5410	−0.2	1.4	0.01	0.10	0.14	2.2	0.01	0.06	0.09	2.1	2.44	3.2	Thin brass-colored film on all surfaces	Some stain retained; machine marks visible
Ti-213	12	37.1	0.5416	0.5416	0.5408	−0.8	1.4	0.05	0.42	0.56	2.2	0.03	0.27	0.36	2.9	2.02	2.7	Thin brass-colored film on all surfaces	Some stain retained; machine marks visible
Ti-214	16	30.0	0.5418	0.5418	0.5411	−0.7	1.4	0.04	0.37	0.49	2.2	0.03	0.24	0.31	3.9	1.58	2.1	Thin brass-colored film on all surfaces	Some stain retained; machine marks visible
Ti-215	17	24.2	0.5413	0.5415	0.5405	−0.8	1.4	0.05	0.42	0.56	2.2	0.03	0.27	0.36	4.1	1.48	2.0	Thin brass-colored film on all surfaces	Some stain retained; machine marks visible
Ti-216	19	18.1	0.5373	0.5375	0.5371	−0.2	1.4	0.01	0.10	0.14	2.2	0.01	0.06	0.09	4.6	1.32	1.7	Thin brass-colored film on all surfaces	Some stain retained; machine marks visible
Ti-219	22	11.9	0.5304	0.5303	0.5303	−0.1	1.4	<0.01	0.05	0.07	2.2	<0.01	0.03	0.05	5.4	1.08	1.4	Thin brass-colored film on all surfaces	Some stain retained; machine marks visible
Core-annulus coupons																			
Stainless steel, type 347																			
1388-A	15(1)		0.9619	0.9617	0.9613	−0.6	1.4	0.02	0.18	0.24	2.2	0.01	0.11	0.15	3.9	1.89	2.5	Dark rustlike film on all surfaces	Some stain retained; machine marks visible
1411-A	15(2)		0.9652	0.9651	0.9648	−0.4	1.4	0.01	0.12	0.16	2.2	<0.01	0.08	0.10	3.9	1.89	2.5	Dark rustlike film on all surfaces	Some stain retained on all surfaces
Zircaloy-2																			
ZB-83	1(1)		0.7925	0.7801	0.7790	−13.5	1.4	0.58	4.94	6.58	2.2	0.37	3.14	4.19	0.4	4.20	5.5	Thin dark-gray film with slightly roughened surface	Some very thin film retained
ZB-57	1(2)		0.7889	0.7740	0.7740	−14.9	1.4	0.64	5.45	7.26	2.2	0.41	3.47	4.62	0.4	4.20	5.5	Thin dark-gray film with slightly roughened surface	Some film retained on edges; specimen heavily etched
ZB-58	8(2)		0.7900	0.7797	0.7792	−10.8	1.4	0.46	3.95	5.26	2.2	0.30	2.51	3.35	2.2	2.80	3.7	Thin dark-gray film with slightly roughened surface	Some film retained specimen heavily etched
ZB-84	14(1)		0.7858	0.7802	0.7785	−7.3	1.4	0.31	2.67	3.56	2.2	0.20	1.70	2.27	3.7	1.99	2.6	Thin dark-gray film with slightly roughened surface	Some very thin film retained; specimen heavily etched
85% sponge Zr, 15% Nb[b]																			
2	2(2)		0.8396	0.8292	0.8292	−10.4	1.4	0.43	3.63	4.84	2.2	0.27	2.31	3.08	0.7	3.95	5.2	Thin dark scale on all surfaces	Thin dark film retained in spots
21-1	11(1)		0.8774	0.8727	0.8719	−5.5	1.4	0.23	1.92	2.56	2.2	0.14	1.22	1.63	2.9	2.35	3.1	Dark scale with overlying interference colors	Thin dark film retained; machine marks visible
85% sponge Zr, 15% Nb[c]																			
21A-1	3(2)		0.8679	0.8483	0.8483	−19.6	1.4	0.81	6.84	9.12	2.2	0.52	4.35	5.80	0.9	3.75	4.9	Rust-colored scale over all surfaces	Thin dark film retained in spots
83% crystal-bar Zr, 15% Nb, 2% Pd[b]																			
2	4(2)		0.8480	0.8419	0.8419	−6.1	1.4	0.25	2.10	2.79	2.2	0.16	1.34	1.78	1.2	3.50	4.6	Thin dark scale on all surfaces	Thin dark film retained in spots
27-1	12(1)		0.8578	0.8554	0.8552	−2.6	1.4	0.11	0.90	1.19	2.2	0.07	0.57	0.76	3.2	2.21	2.9	Dark scale over all surfaces, flaked in spots	Some spots of scale retained on all surfaces
83% crystal-bar Zr, 15% Nb, 2% Pd[c]																			
27A-1	5(2)		0.8252	0.8142	0.8142	−11.0	1.4	0.45	3.79	5.03	2.2	0.29	2.42	3.21	1.4	3.35	4.4	Thin black scale on all surfaces	Thin dark film retained in spots; machine marks visible
95% crystal-bar Zr, 5% Pd[b]																			
30-1	10(1)		0.8015	0.7949	0.7938	−7.7	1.4	0.32	2.70	3.60	2.2	0.20	1.72	2.29	2.7	2.49	3.3	Black scale over all surfaces, flaked in spots	Thin dark film retained; grain pattern of alloy is visible
2	10(2)		0.7726	0.7652	0.7643	−8.3	1.4	0.34	2.91	3.88	2.2	0.22	1.85	2.47	2.7	2.49	3.3	Black scale over all surfaces, flaked in spots	Thin dark film retained; grain pattern of alloy is visible
67% crystal-bar Zr, 33% Nb[b]																			
42-1	4(1)		0.9333	0.9228	0.9217	−11.6	1.4	0.45	3.85	5.12	2.2	0.29	2.45	3.26	1.2	3.50	4.6	Dark gray scale with overlying interference colors	Some scale retained in spots on all surfaces; machine marks visible
2	14(2)		0.8912	0.8837	0.8837	−7.5	1.4	0.29	2.49	3.31	2.2	0.19	1.58	2.11	3.7	1.99	2.6	Uniform rust-colored scale on all surfaces	Some scale retained in spots on all surfaces; machine marks visible
67% crystal-bar Zr, 33% Nb[c]																			
42A-1	5(1)		0.8900	0.8619	0.8601	−29.9	1.4	1.17	9.90	13.19	2.2	0.74	6.29	8.39	1.4	3.35	4.4	Dark scale with overlying interference colors	Some spots of dark scale retained; machine marks visible
80% crystal-bar Zr, 15% Nb, 5% Pt[b]																			
53-1	2(1)		0.8852	0.8791	0.8784	−6.8	1.4	0.25	2.14	2.85	2.2	0.16	1.36	1.81	0.7	3.95	5.2	Black shiny scale flaked off in spots	Some scale retained on all surfaces; machine marks visible
2	13(2)		0.8979	0.8946	0.8939	−4.0	1.4	0.15	1.26	1.68	2.2	0.09	0.80	1.06	3.4	2.10	2.8	Black shiny scale over all surfaces	Some scale retained on all surfaces
80% crystal-bar Zr, 15% Nb, 5% Pt[c]																			
53A-1	3(1)		0.8804	0.8694	0.8674	−13.0	1.4	0.48	4.09	5.45	2.2	0.31	2.60	3.46	0.9	3.75	4.9	Black scale over all surfaces	Some scale retained in spots on all surfaces; machine marks visible

Table 22 (continued)

Sample Number	Position	Average Flow Velocity Across Specimen (fps)	Weight Data: Initial (g)	Weight Data: As Removed (g)	Weight Data: Defilmed (g)	Weight Data: Change (mg)	Exposed Sample Area (cm^2)	Corrosion Penetration (mils)	Corrosion Rate[a] (Exposed Area) (mpy): 1032 hr	Corrosion Rate[a] (Exposed Area) (mpy): 775 hr	Total Area (cm^2)	Corrosion Penetration (mils)	Corrosion Rate[a] (Total Area) (mpy): 1032 hr	Corrosion Rate[a] (Total Area) (mpy): 775 hr	Distance from Front of First Core-Channel Specimen to Center of Specimen (in.)	Thermal Neutron Flux at Specimen Locations (neutrons cm^{-2} sec^{-1})	Power Density at Specimen Locations (w/ml)	Remarks on Surface Appearance: As-Removed Surface	Remarks on Surface Appearance: Defilmed Surface
																$\times 10^{12}$			
Titanium-55AX																			
Ti-230	12	37.1	0.5388	0.5413	0.5386	−0.2	1.4	0.01	0.10	0.14	2.2	0.01	0.06	0.09				Uniform brown rustlike scale on all surfaces	Thin film with interference colors on all surfaces; machine marks visible
Ti-232	16	30.0	0.5382	0.5409	0.5378	−0.4	1.4	0.02	0.21	0.28	2.2	0.02	0.13	0.18				Uniform brown rustlike scale on all surfaces	Thin film with interference colors on all surfaces; machine marks visible
Ti-233	17	24.2	0.5325	0.5347	0.5321	−0.4	1.4	0.02	0.21	0.28	2.2	0.02	0.13	0.18				Uniform brown rustlike scale on all surfaces	Thin film with interference colors on all surfaces; machine marks visible
Ti-235	19	18.1	0.5409	0.5429	0.5406	−0.3	1.4	0.02	0.16	0.21	2.2	0.01	0.10	0.13				Uniform brown rustlike scale on all surfaces	Thin film with interference colors on all surfaces; machine marks visible
Ti-236	22	11.9	0.5420	0.5440	0.5418	−0.2	1.4	0.01	0.10	0.14	2.2	0.01	0.06	0.09				Uniform brown rustlike scale on all surfaces	Thin film with interference colors on all surfaces; machine marks visible
In-line annulus coupons																			
Stainless steel, type 347																			
1412-A	15		0.9875	0.9881	0.9868	−0.7	1.4	0.02			2.2							Uniform brown rustlike scale on all surfaces	Some stain retained on all surfaces; machine marks visible
Zircaloy-2																			
ZB-59	1		0.7909	0.7913	0.7913	+0.4	1.4				2.2							Uniform brown rustlike scale on all surfaces	Uniform thin dark scale retained on all surfaces
ZB-60	14		0.7815	0.7825	0.7817	+0.2	1.4				2.2							Uniform brown rustlike scale on all surfaces	Uniform thin dark scale retained on all surfaces
85% sponge Zr, 15% Nb[b]																			
21-3	4		0.8586	0.8601	0.8601	+1.5	1.4				2.2							Uniform brown rustlike scale on all surfaces	Uniform thin dark scale retained on all surfaces
85% sponge Zr, 15% Nb[c]																			
21A-2	5		0.8668	0.8686	0.8682	+1.4	1.4				2.2							Uniform brown rustlike scale on all surfaces	Uniform thin dark scale retained on all surfaces
83% crystal-bar Zr, 15% Nb, 2% Pd[b]																			
27-3	6		0.8620	0.8636	0.8630	+1.0	1.4				2.2							Uniform brown rustlike scale on all surfaces	Uniform thin dark scale retained on all surfaces
95% crystal-bar Zr, 5% Pd[b]																			
30-3	12		0.7788	0.7837	0.7825	+3.7	1.4				2.2							Uniform brown rustlike scale on all surfaces	Uniform thin dark scale retained on all surfaces
67% crystal-bar Zr, 33% Nb[b]																			
42-3	9		0.9180	0.9190	0.9190	+1.0	1.4				2.2							Uniform brown rustlike scale on all surfaces	Uniform thin dark scale retained on all surfaces
67% crystal-bar Zr, 33% Nb[c]																			
42A-2	10		0.9245	0.9267	0.9253	+0.8	1.4				2.2							Uniform brown rustlike scale on all surfaces	Uniform thin dark scale retained on all surfaces
80% crystal-bar Zr, 15% Nb, 5% Pt[b]																			
53-3	8		0.8964	0.8997	0.8966	+0.2	1.4				2.2							Uniform brown rustlike scale on all surfaces	Uniform thin dark scale retained on all surfaces
83% crystal-bar Zr, 15% Nb, 2% Pt[b]																			
54-3	7		0.9008	0.9031	0.9019	+1.1	1.4				2.2							Uniform brown rustlike scale on all surfaces	Uniform thin dark scale retained on all surfaces
95% crystal-bar Zr, 5% Pt[b]																			
55-3	13		0.8245	0.8263	0.8255	+1.0	1.4				2.2							Uniform brown rustlike scale on all surfaces	Uniform thin dark scale retained on all surfaces
85% crystal-bar Zr, 15% Nb[b]																			
69-3	2		0.7867	0.7885	0.7881	+1.4	1.4				2.2							Uniform brown rustlike scale on all surfaces	Uniform thin dark scale retained on all surfaces
85% crystal-bar Zr, 15% Nb[c]																			
69A-3	3		0.7378	0.7397	0.7395	+1.7	1.4				2.2							Uniform brown rustlike scale on all surfaces	Uniform thin dark scale retained on all surfaces
75% crystal-bar Zr, 20% Nb, 5% Pd[b]																			
64-3	11		0.9153	0.9167	0.9156	+0.3	1.4				2.2							Uniform brown rustlike scale on all surfaces	Uniform thin dark scale retained on all surfaces
In-line impact specimens																			
Titanium-110AT[c]																			
923	E		13.1281	13.1351		+7.0	24.9				26.7							Uniform dark rustlike scale over all surfaces	
Zircaloy-2[e]																			
Zr-2 Line	C		19.0765	19.1020		+25.5	24.9				26.7							Uniform dark rustlike scale over all surfaces	
85% crystal-bar Zr, 15% Nb[b]																			
Zr-71	F		19.2662	19.2927		+26.5	24.9				26.7							Uniform dark rustlike scale over all surfaces	
In-line tensile specimens																			
Titanium-110AT[c]																			
110AT line	A		10.8144	10.8241		+9.7	18.1				21.2							Uniform dark rustlike scale over all surfaces	
In-line tapered channel coupon holder (type 347 stainless steel)																			
A			113.8130								90.0							Dark-brown film over all surfaces	
B			113.3262								90.0							Dark-brown film over all surfaces	

[a]Two corrosion rates are presented: one based on the total operation time of 1032 hr and the other based on the total radiation time of 775 hr (3 Mwhr of reactor time equivalent to 1 hr of total radiation time).
[b]Held at 900°C for 3 hr, water-quenched.
[c]Held at 900°C for 3 hr, water-quenched; held 600°C for 48 hr, air-cooled.
[d]Commercial anneal.
[e]Held at 650°C for 30 min.
[f]Held at 900°C for 3 hr, water-quenched; held 600°C for 3 hr, water-quenched.

Table 22 (continued)

Sample Number	Position	Average Flow Velocity Across Specimen (fps)	Weight Data: Initial (g)	Weight Data: As Removed (g)	Weight Data: Defilmed (g)	Weight Data: Change (mg)	Exposed Sample Area (cm^2)	Corrosion Penetration (mils)	Corrosion Rate[a] (Exposed Area) (mpy): 1032 hr	Corrosion Rate[a] (Exposed Area) (mpy): 775 hr	Total Area (cm^2)	Corrosion Penetration (mils)	Corrosion Rate[a] (Total Area) (mpy): 1032 hr	Corrosion Rate[a] (Total Area) (mpy): 775 hr	Distance from Front of First Core-Channel Specimen to Center of Specimen (in.)	Thermal Neutron Flux at Specimen Locations (neutrons cm^{-2} sec^{-1})	Power Density at Specimen Locations (w/ml)	Remarks on Surface Appearance: As-Removed Surface	Remarks on Surface Appearance: Defilmed Surface
																$\times 10^{12}$			
83% crystal-bar Zr, 15% Nb, 2% Pt[b]																			
2	6(2)		0.8896	0.8834	0.8831	−6.5	1.4	0.26	2.18	2.90	2.2	0.16	1.39	1.85	1.7	3.11	4.1	Heavy black scale on all surfaces	Some scale retained in spots
54-1	13(1)		0.8989	0.8956	0.8953	−3.6	1.4	0.14	1.21	1.61	2.2	0.09	0.77	1.02	3.4	2.10	2.8	Black scale flaked off in spots	Some scale retained in spots
83% crystal-bar Zr, 15% Nb, 2% Pt[c]																			
54A-1	7(2)		0.8817	0.8660	0.8655	−16.2	1.4	0.65	5.43	7.23	2.2	0.40	3.46	4.61	1.9	2.99	3.9	Heavy black scale on all surfaces	Some scale retained on all surfaces
95% crystal-bar Zr, 5% Pt[b]																			
55-1	8(1)		0.8082	0.8011	0.8006	−7.6	1.4	0.29	2.50	3.32	2.2	0.19	1.59	2.11	2.2	2.80	3.7	Uniform black scale over all surfaces	Spots of black scale retained on all surfaces
55-2	12(2)		0.8127	0.8056	0.8050	−7.7	1.4	0.29	2.53	3.36	2.2	0.19	1.61	2.14	3.2	2.21	2.9	Uniform black scale over all surfaces	Spots of black scale retained on all surfaces
85% crystal-bar Zr, 15% Nb[b]																			
69-1	6(1)		0.7714	0.7640	0.7629	−8.5	1.4	0.35	2.97	3.96	2.2	0.22	1.89	2.52	1.7	3.11	4.1	Gray-to-brown scale on all surfaces	Spots of dark scale retained; machine marks visible
2	11(2)		0.7901	0.7850	0.7846	−5.5	1.4	0.23	1.92	2.56	2.2	0.14	1.22	1.63	2.9	2.35	3.1	Black scale on all surfaces, flaked off in spots	Spots of dark scale retained
85% crystal-bar Zr, 15% Nb[c]																			
69A-1	7(1)		0.7718	0.7580	0.7569	−14.9	1.4	0.61	5.21	6.94	2.2	0.39	3.31	4.42	1.9	2.99	3.9	Uniform dark scale with overlying interference colors	Spots of dark scale retained
75% crystal-bar Zr, 20% Nb, 5% Pd[b]																			
64-1	9(1)		0.9027	0.8962	0.8958	−6.9	1.4	0.27	2.28	3.04	2.2	0.17	1.45	1.93	2.4	2.67	3.5	Uniform black scale over all surfaces	Some spots of glossy black scale retained
2	9(2)		0.9148	0.9094	0.9087	−6.1	1.4	0.24	2.02	2.69	2.2	0.15	1.28	1.71	2.4	2.67	3.5	Uniform black scale over all surfaces	Some spots of glossy black scale retained
Core-impact specimens																			
Titanium-110AT[d]																			
922	F		13.0980	13.0858		12.2	24.9	0.04	0.34	0.45	26.7	0.04	0.34	0.45	2.3	2.71	3.5	Thin brass-colored film on all surfaces; machine marks visible	
Titanium-55AX[d]																			
929	G		13.0006	12.9846		16.0	24.9	0.06	0.51	0.68	26.7	0.05	0.42	0.57	2.3	2.71	3.5	Thin brass-colored film on all surfaces; machine marks visible	
Zircaloy-2[e]																			
ZR-2 core	D		19.1052	18.9389		166.3	24.9	0.40	3.4	4.5	26.7	0.38	3.2	4.3	2.3	2.71	3.5	Thin dark-gray film on all surfaces	
85% crystal-bar Zr, 15% Nb[b]																			
ZR-70	H		19.7425	19.5731		169.4	24.9	0.40	3.4	4.5	26.7	0.37	3.1	4.2	2.3	2.71	3.5	Dark-gray film with overlying interference colors	
85% crystal-bar Zr, 15% Nb[f]																			
ZR-72A	C		19.5655	19.3783		187.2	24.9	0.43	3.6	4.9	26.7	0.40	3.4	4.5	2.3	2.71	3.5	Dark-gray film with overlying interference colors	
Core tensile specimens																			
Titanium-110AT[d]																			
110AT core	B		10.7425	10.7357		6.8	18.1	0.03	0.25	0.34	21.2	0.03	0.25	0.34	2.3	2.71	3.5	Thin brass-colored film on all surfaces; some machine marks visible	
Core-tapered channel holder (type 347 stainless steel)																			
A											90.0				3.0	2.31	3.0	Front end deep blue ranging along holder to a metallic bronze, with a heavy film of deep rose; purple interference colors; machine marks visible	Purple-to-rose interference colors; scattered spots of scale
B			97.9859	97.8397	97.8312	154.7					90.0	0.08	0.70	0.94	3.0	2.31	3.0		
In-line coupons																			
Stainless steel, type 347																			
1389-A	4	12.2	0.9715	0.9734	0.9706	−0.9	1.4	0.03	0.27	0.36	2.2	0.02	0.17	0.23				Uniform brown rustlike scale on all surfaces	Some stain retained; machine marks visible on all surfaces
1390-A	5	13.4	0.9628	0.9656	0.9623	−0.5	1.4	0.02	0.15	0.20	2.2	0.02	0.09	0.13				Uniform brown rustlike scale on all surfaces	Some stain retained; machine marks visible on all surfaces
1391-A	7	16.9	0.9695	0.9720	0.9683	−1.2	1.4	0.04	0.36	0.48	2.2	0.03	0.23	0.31				Uniform brown rustlike scale on all surfaces	Some stain retained; machine marks visible on all surfaces
1408-A	10	29.5	0.9686	0.9711	0.9671	−1.5	1.4	0.05	0.45	0.60	2.2	0.04	0.29	0.39				Uniform brown rustlike scale on all surfaces	Some stain retained; machine marks visible on all surfaces
1409-A	13	40.1	0.9641	0.9666	0.9622	−1.9	1.4	0.06	0.57	0.76	2.2	0.05	0.37	0.49				Uniform brown rustlike scale on all surfaces	Some stain retained; machine marks visible on all surfaces
1414-A	18	20.2	0.9686	0.9702	0.9675	−1.1	1.4	0.03	0.33	0.44	2.2	0.03	0.21	0.28				Uniform brown rustlike scale on all surfaces	Some stain retained
1418-A	21	13.2	0.9628	0.9636	0.9610	−1.8	1.4	0.05	0.54	0.72	2.2	0.05	0.34	0.46				Uniform brown rustlike scale on all surfaces	Some stain and small spots of scale retained; machine marks visible
1419-A	24	9.9	0.9437	0.9451	0.9423	−1.4	1.57	0.04	0.37	0.49	2.2	0.03	0.26	0.35				Uniform brown rustlike scale on all surfaces	Some stain retained; machine marks visible
Zircaloy-2																			
ZB-63	2	10.2	0.7976	0.8000	0.7988	+1.2	1.4				2.2							Uniform brown rustlike scale on all surfaces	Some scale flaked off in spots; dark film visible in these areas
ZB-64	3	11.1	0.7978	0.8012	0.7992	+1.4	1.4				2.2							Uniform brown rustlike scale on all surfaces	Some scale flaked off in spots; dark film visible in these areas
ZB-65	8	19.7	0.7876	0.7904	0.7897	+2.1	1.4				2.2							Uniform brown rustlike scale on all surfaces	Some scale flaked off in spots; dark film visible in these areas
ZB-66	11	34.5	0.7902	0.7929	0.7917	+1.5	1.4				2.2							Uniform brown rustlike scale on all surfaces	Some scale flaked off in spots; dark film visible in these areas
ZB-67	14	44.4	0.7956	0.7982	0.7970	+1.4	1.4				2.2							Uniform brown rustlike scale on all surfaces	Some scale flaked off in spots; dark film visible in these areas
ZB-68	15	40.3	0.7929	0.7962	0.7950	+2.1	1.4				2.2							Uniform brown rustlike scale on all surfaces	Some scale flaked off in spots; dark film visible in these areas
ZB-69	20	14.9	0.7833	0.7850	0.7841	+0.8	1.4				2.2							Uniform brown rustlike scale on all surfaces	Some scale flaked off in spots; dark film visible in these areas
ZB-70	23	10.8	0.7993	0.8021	0.8007	+1.4	1.4				2.2							Uniform brown rustlike scale on all surfaces	Some scale flaked off in spots; dark film visible in these areas
Titanium-55AX																			
Ti-224	1	9.4	0.5340	0.5356	0.5328	−1.2	1.57	0.07	0.56	0.75	2.2	0.04	0.36	0.48				Uniform brown rustlike scale on all surfaces	Some small spots of scale retained; interference colors on all surfaces; machine marks visible
Ti-225	6	14.9	0.5339	0.5358	0.5340	+0.1	1.4											Uniform brown rustlike scale on all surfaces	Some scale flaked off in spots; black film visible in these areas
Ti-226	9	23.3	0.5393	0.5422	0.5388	−0.5	1.4	0.03	0.30	0.40	2.2	0.02	0.19	0.25				Uniform brown rustlike scale on all surfaces	Flakes of scale retained on all surfaces; black film visible in these areas

Table 23. Corrosion Penetration Factors

Material	Density (g/cc)	Factor [(mg of material) cm^{-2} (mil penetration)$^{-1}$]
Stainless steel, type 347	8.02	20.37
Zircaloy-2	6.50	16.51
Ti-110AT	4.46	11.33
Ti-55AX	4.54	11.53
85% Zr, 15% Nb	6.81	17.30
83% Zr, 15% Nb, 2% Pd	6.92	17.58
95% Zr, 5% Pd	6.78	17.22
67% Zr, 33% Nb	7.18	18.24
80% Zr, 15% Nb, 5% Pt	7.56	19.20
83% Zr, 15% Nb, 2% Pt	7.11	18.06
95% Zr, 5% Pt	7.25	18.41
75% Zr, 20% Nb, 5% Pd	7.19	18.26

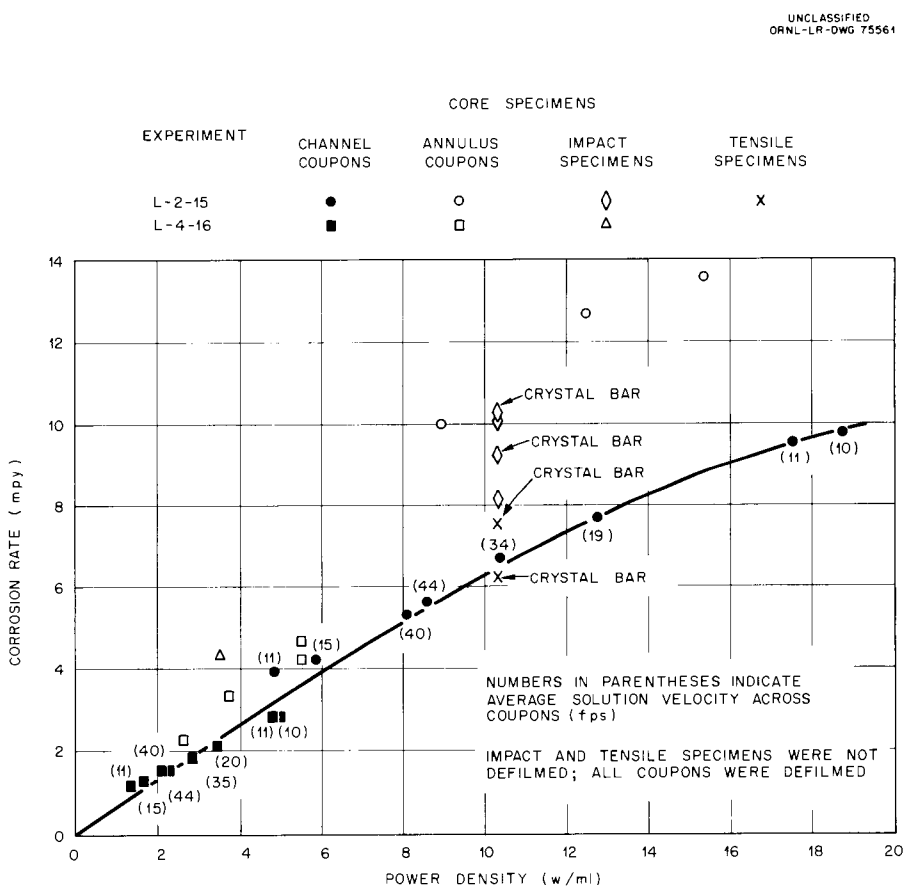

Fig. 42. Zircaloy-2 Core Specimen Corrosion Rates vs Solution Fission-Power Density.

The rate values for Zr-Nb alloys located in the core annulus of L-4-16 are plotted and compared with similarly located Zircaloy-2 specimens in Fig. 43. In connection with this comparison, it should be noted that the surface preparations employed with the Zr-Nb coupons differed from those for the Zircaloy-2 (Table 3*a*). The latter were machined, while the former were chemically polished. Impact and tensile specimens of all materials were machined.

UNCLASSIFIED
ORNL-LR-DWG 75562

MATERIAL	* HEAT TREATMENT			
	A	B	C	D
ZIRCALOY-2			X	
85 SPONGE ZIRCONIUM-15 Nb	△	⊕		
83 CRYSTAL-BAR ZIRCONIUM-15 Nb-2 Pd	▲	⊕		
95 CRYSTAL-BAR ZIRCONIUM-5 Pd	▽			
67 CRYSTAL-BAR ZIRCONIUM-33 Nb	▼	⊕		
80 CRYSTAL-BAR ZIRCONIUM-15 Nb-5 Pt	◊	⊕		
83 CRYSTAL-BAR ZIRCONIUM-15 Nb-2 Pt	⧫	⊙		
95 CRYSTAL-BAR ZIRCONIUM-5 Pt	□			
85 CRYSTAL-BAR ZIRCONIUM-15 Nb	■	⊕		●
75 CRYSTAL-BAR ZIRCONIUM-20 Nb-5 Pd	○			

ALL COUPONS DEFILMED
IMPACT SPECIMENS NOT DEFILMED

* A - 900°C, 3 hr, WATER QUENCHED
B - 900°C, 3 hr, WATER QUENCHED; 600°C, 48 hr, AIR COOLED
C - 650°C, 30 min
D - 900°C, 3 hr, WATER QUENCHED; 600°C, 3 hr, WATER QUENCHED

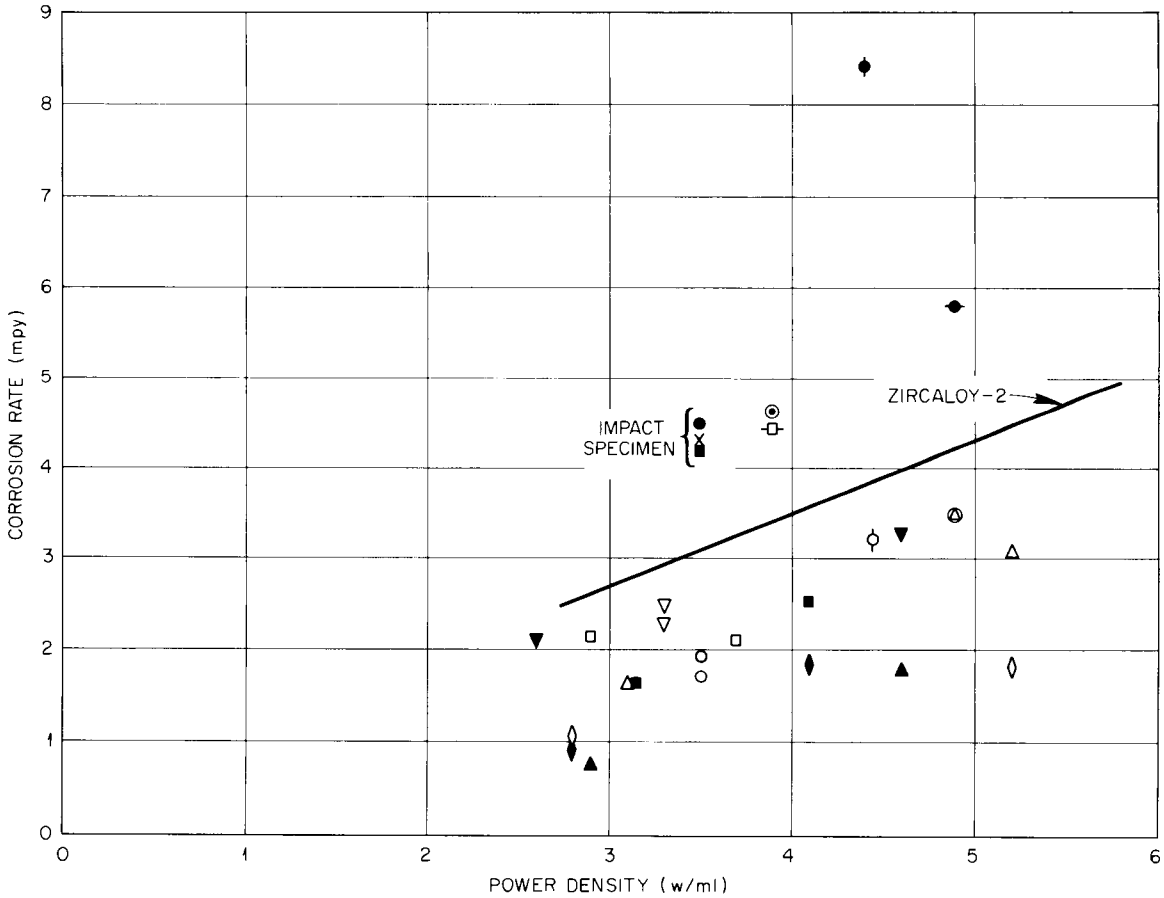

Fig. 43. Corrosion Rates of Zirconium-Alloy CA Coupons vs Solution Fission-Power Density.

The rates for the beta-quenched Zr-Nb alloys were, with the exception of the impact specimen, lower than those for Zircaloy-2 at the same power density. However, the heat-treated alloys generally showed higher rates. The rates for the impact specimens of Zircaloy-2 and beta-quenched Zr–15 Nb were in near agreement. All in-line specimens of these alloys showed weight gains after defilming.

(*b*) Titanium Alloys. – The titanium alloy specimen results are shown in Fig. 44. The in-line specimens in experiment L-4-16 exhibited weight losses after defilming, and the average of the calculated rates for these specimens is shown. In experiment L-2-15, only the 110AT CA coupons showed weight losses. The calculated average rate values for each of these specimens are shown in Fig. 44.

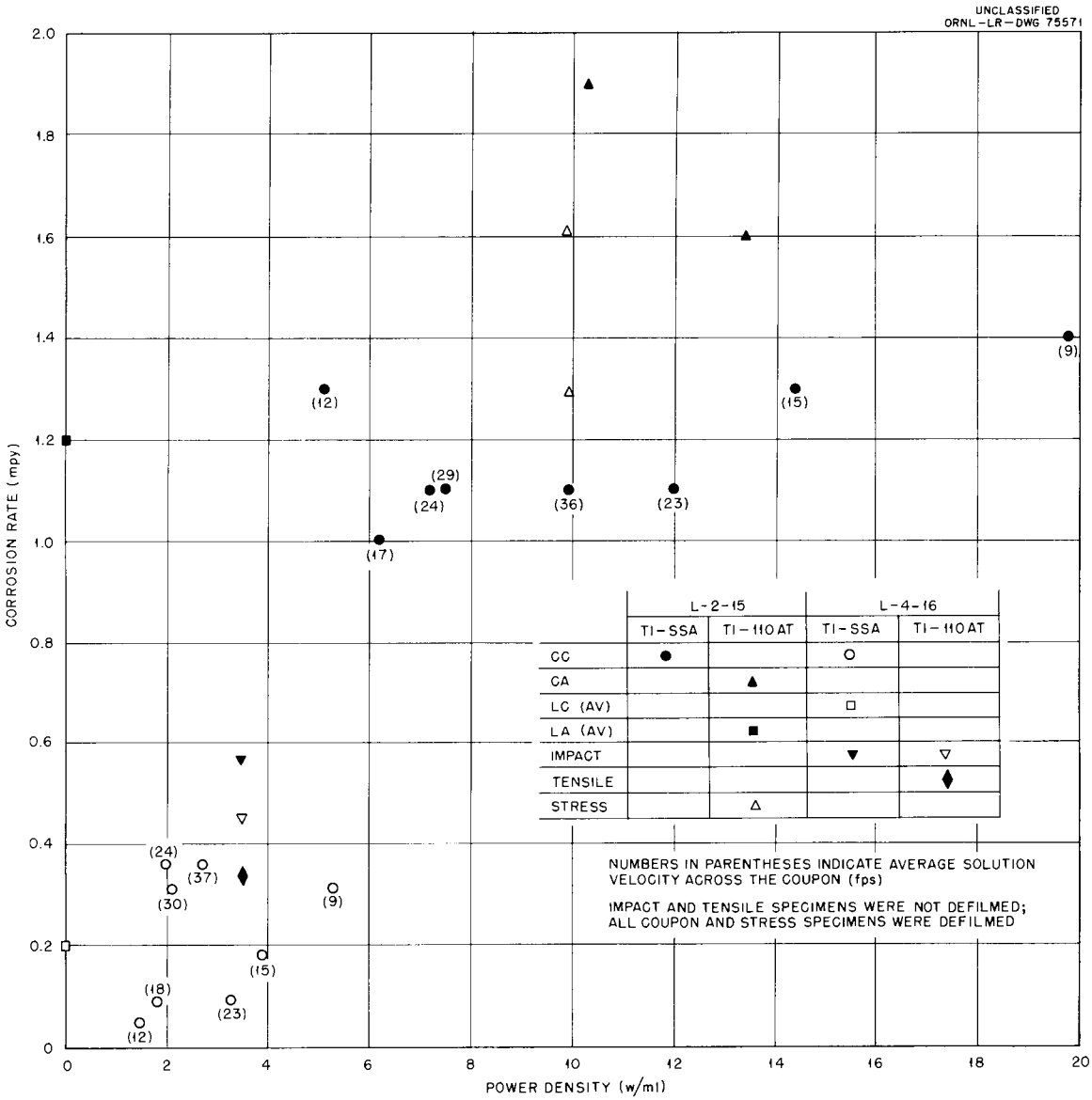

Fig. 44. Corrosion Rate of Titanium Alloys vs Solution Fission-Power Density.

(*c*) Stainless Steel. – The stainless steel specimen results are plotted in Fig. 45. For the in-line specimens of type 347 stainless steel, only the average values are shown. The corrosion rates of in-line specimens of type 309SCb in L-2-15 were about the same as those for type 347 in comparable locations.

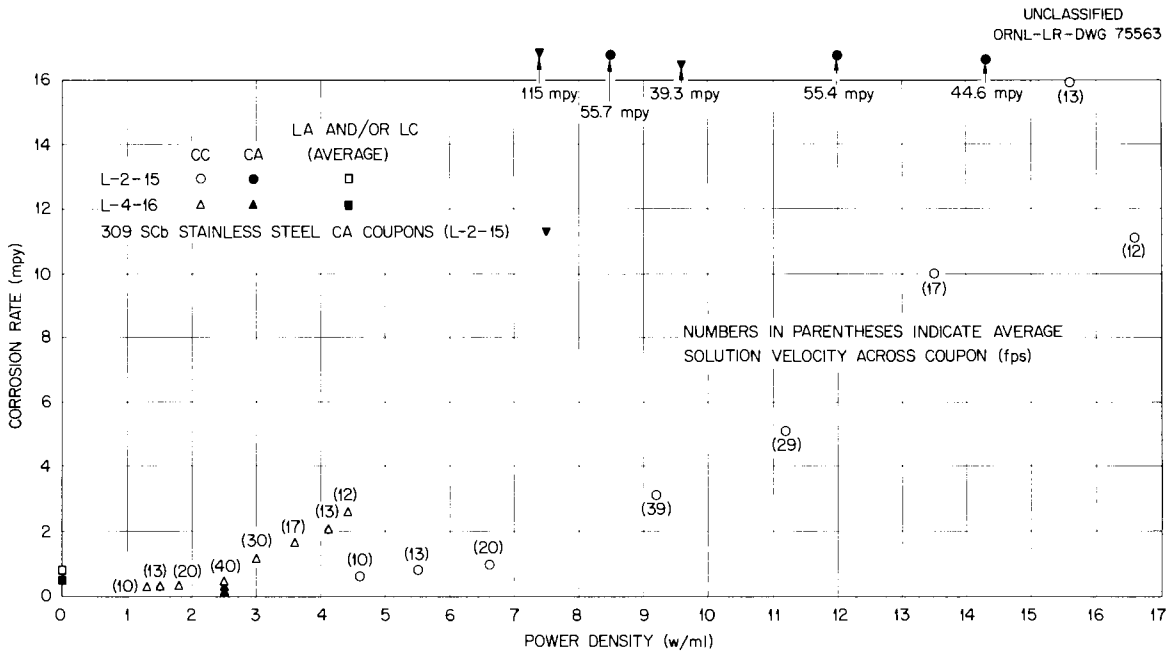

Fig. 45. Corrosion Rates of Type 347 Stainless Steel Core Coupons vs Solution Fission-Power Density.

5. SUMMARY AND DISCUSSION OF RESULTS

5.1 Solution Composition and Stability

In a previous report the results of solution analyses in a group of several loop experiments at 250°C were analyzed and discussed in detail.[18] A less complete analysis of the L-2-15 and L-4-16 results shows many similarities between these and the previous areas. Conclusions and comments drawn for the L-2-15 and L-4-16 results are based in part on the previous data analyses.

For the L-2-15 and L-4-16 experiments the average value for the sample dilution factor based on Li_2SO_4 tracer was probably high by amounts ranging up to 10–12%. A possible explanation for this is that the wash water in the sample lines was vaporized during gas-flushing, thus concentrating the Li_2SO_4 solution remaining in the lines. Within the limits of the considerable uncertainty arising from the dilution factor uncertainty, there were no significant losses of uranium, sulfate, or copper from any of the solutions. For uranium and copper, this was also indicated by the constancy of the values for fission and gamma heat and radiolytic-gas pressures and by the small amounts of these elements in the samples of heavy scale in L-4-16. This conclusion with respect to copper differs from that for the lower-temperature experiments, where some decrease in copper concentration occurred.

The free-acid values determined from pH measurements were generally lower than those determined from direct analyses for hydrogen ion (Figs. 11 and 12). The pH measurements indicated that the acid concentrations remained fairly constant at about 0.02 *m* throughout the radiation exposures but that the acidities dropped from about 0.03 to 0.02 *m* prior to the initiation of exposure. The free-acid analysis values indicated a fairly constant concentration of about 0.03 *m* throughout the exposure in L-2-15 and an increase from about 0.023 to 0.03 *m* in L-4-16. Possible explanations exist for the variations in acidity indicated by each type of measurement, so that there is no apparent reason to consider one set of values more accurate than the other.

The amounts of nickel found in solution in each experiment were less than those expected from the data for oxygen consumption by steel, assuming that all oxidized nickel entered solution. That found in solution in L-2-15 was very much less. Comparisons between the amounts of nickel expected and recovered are shown in Table 24. Possible explanations for low recovery of nickel in solution have been considered previously. It is believed that the nickel is incorporated in the heavy corrosion scales as indicated by the results of scale analyses in L-4-16 (Tables 19 and 20) and in other experiments.

In general agreement with previously reported and discussed observations, little or no manganese was found in solution. Iron, zirconium, and chromium were found in all samples in amounts which exceeded 100 ppm in some cases. Chlorine was not detected in the loop solutions.

The results of the analyses for zirconium in the bulk scales indicated that most or all of the zirconium oxide formed in the core was transported to and deposited on surfaces outside the core. The clean appearance of Zircaloy-2 specimens in the core supported this conclusion. Evidence for transport of appreciable fractions of the oxide has also been observed in other experiments.

Table 24. Comparison of Total Amount of Steel Corrosion Determined from Oxygen Consumption and Dissolved-Nickel Data

Experiment	Time (hr)	Calculated Oxygen Consumption on Steel		Ratio of Consumption from Oxygen Data to That from Nickel Data
		From Oxygen Consumption Data (cc, STP)[a]	From Nickel Data (cc, STP)[a, b]	
L-2-15	701	2200	1000[c]	2.2
L-4-16	952	1230	1110	1.2

[a]From graphs shown in Fig. 7.

[b]Assuming (1) no selective oxidation of any steel constituent, (2) all oxidized nickel in solution, and (3) 12.5% nickel in the stainless steel.

[c]Corresponds to about 350 mg of nickel in solution. Probably 30 to 50% of this amount was oxidized from the four Ni-Pt-plated Zircaloy-2 specimens during in-pile exposure. Hence the agreement between values for oxygen consumption on steel is poorer than indicated.

5.2 Zirconium Alloys

The Zircaloy-2 data have been analyzed and included in a general discussion of Zircaloy-2 radiation corrosion.[21] For convenience, the conclusions from that discussion which are pertinent to the present experiment will be summarized here.

The Zircaloy-2 data from the present experiments, as well as all other 280°C in-pile loop and autoclave experiments, can be expressed by the following equation:

$$1/R = 2.23/P\alpha + 1/40 \ , \tag{1}$$

where

R = corrosion rate, mpy ,

P = fission-power density in solution, w/ml ,

α = factor by which the effective power density is greater than the solution power density due to uranium sorption near or on the corroding surface.

In general, the value of α in solutions of the same composition decreases with increasing solution velocity and, in the venturi-shaped channel specimen holders, with decreasing value of the angle included between the center line and the walls. Appreciable fractions of the areas of all specimens were in close proximity to other surfaces (where they were clamped in the holders and where they were in contact with other specimens), and thus exposed to essentially stagnant solution. The α value for a "covered" surface is expected to be greater than that for the exposed surface of the same specimen. The corrosion rates determined from weight measurements were thus averages of the two different rates for the covered and exposed surfaces. In analyzing the results of these experiments for the effects of velocity on α, it was assumed that the corrosion rate for the covered surfaces of a channel specimen was the same as that for the low-velocity annulus specimen exposed at the same solution power density.

Reciprocal solution power-density–corrosion-rate plots for L-2-15 and L-4-16 data are reproduced in Figs. 46 and 47. The calculated corrosion rates for the exposed surfaces of the channel specimens are also shown. It was concluded that the α value for the surfaces of those specimens exposed in the convergent portion of the channel holder was near unity at all velocities tested (10 to 44 fps). Those in the divergent section were probably greater than unity. The lines through the average corrosion rate values, in general, do not extrapolate to the value of 40 mpy at infinite power density. This is an expected result when different portions of a specimen corrode at different rates.

The average corrosion rates for the impact and tensile specimens were generally lower than those for the annulus specimens in L-2-15 (Fig. 42); that for the impact specimens in L-4-16 was greater. The explanations for these differences are unknown, since information on the histories of those specimens is incomplete. Differences in material and surface preparation may be partial explanations. In the case of the L-2-15 results, the relatively low rates for the impact and tensile specimens may have resulted, in part, from the fact that nearly all the surfaces of these specimens were exposed to the flowing solution, while a large fraction of the areas of the corrosion coupons were exposed to stagnant solution.

---

[21] G. H. Jenks, *A Model for the Effects of Irradiation on Zircaloy-2 Corrosion and a Review and Correlation of In-Pile Zircaloy-2 Corrosion Data*, ORNL-3039 (July 6, 1961).

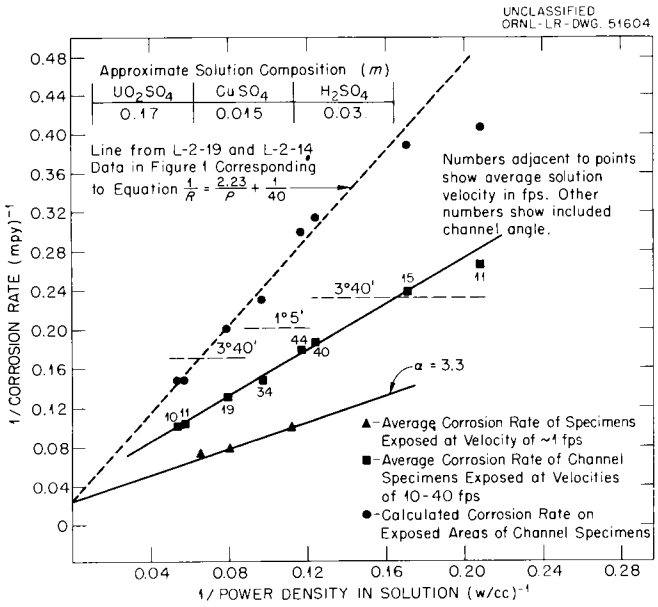

Fig. 46. Zircaloy-2 Corrosion, In-Pile Loop Experiment L-2-15 at 280°C.

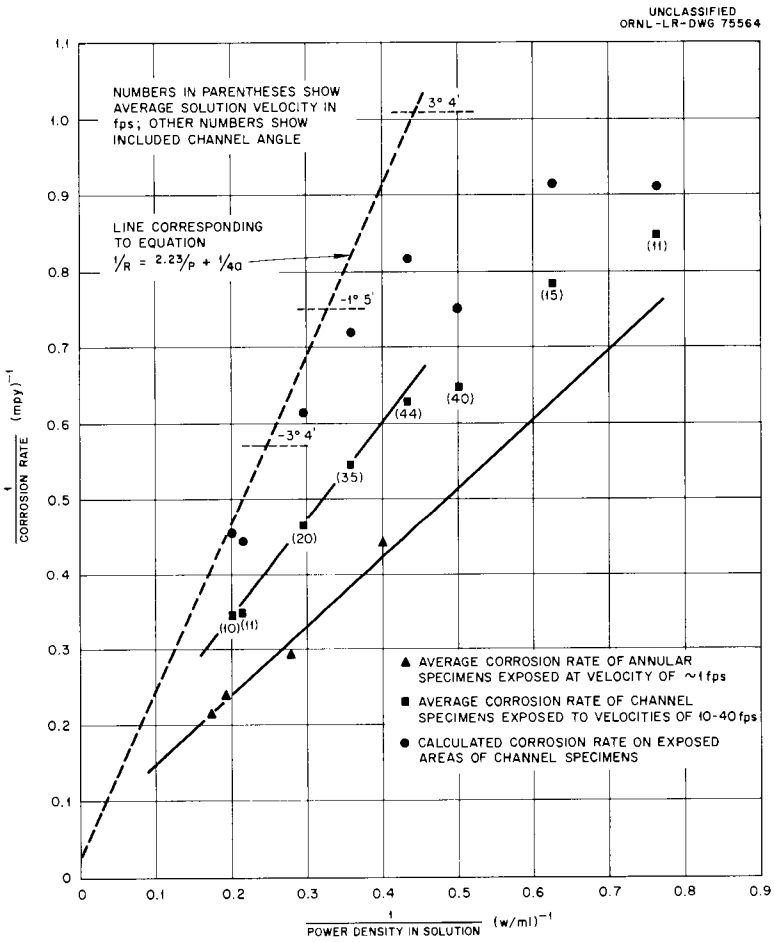

Fig. 47. Zircaloy-2 Corrosion, In-Pile Loop Experiment L-4-16 at 280°C.

5.3 Other Zirconium Alloys

As shown in Tables 21 and 22 and in Fig. 43, specimens of various other alloys of zirconium exposed in the core annulus of experiment L-4-16 corroded at varying rates. The effect of heat treatment on the corrosion resistance of these alloys was quite pronounced. All specimens of the alloys that were held at 900°C for 3 hr and water-quenched exhibited, with one exception, appreciably lower rates than observed for the commercially annealed Zircaloy-2 CA coupons. The rates varied from 0.4 to 0.9 of those exhibited by the Zircaloy-2 coupons. The exception, an impact specimen of 85 crystal-bar zirconium–15 Nb, exhibited a rate 1.3 times that for Zircaloy-2. With two exceptions, all specimens of the alloys that were held at 900°C for 3 hr, water-quenched, and then held at 600°C for an additional 48 hr and air-cooled, exhibited appreciably higher rates than observed for the Zircaloy-2 CA coupons. The rates for these coupons varied from 1.3 to 2.3 of those exhibited by the Zircaloy-2 coupons. The exceptions, coupons of 83 crystal-bar zirconium–15 Nb–2 Pd and of 80 crystal-bar zirconium–15 Nb–5 Pt, exhibited rates 0.8 and 0.9 times that of Zircaloy-2. In general, the relative rates for those several zirconium alloys are similar to those observed in other experiments.

5.4 Nickel- and Platinum-Clad Zircaloy-2

Metallographic examination of the Zircaloy-2 specimens plated with nickel and then platinum and exposed in the L-2-15 experiment showed the nickel layer to be missing from all coupons. The platinum appeared to remain in place. The nickel was exposed to the solution on one or more edges as a result of the method of fabrication. Zircaloy-2 corrosion rates of 10.5 and 4.8 mpy at 16.1 and 6.8 w/ml were estimated, assuming that the platinum on these specimens underwent no corrosive attack and that the weight losses were attributable to the loss of all the nickel and part of the Zircaloy-2. These rates are a little lower than those expected for CA positions in this experiment. This suggests that the Zircaloy-2 surfaces were unexposed during the initial period of the in-pile operation.

5.5 Titanium Alloys

The rate values determined for Ti-55A and Ti-110AT core specimens were plotted vs solution power density in Fig. 44. Average values for in-line specimens of Ti-55A in L-4-16 and of the Ti-110AT in L-2-15 are shown. (In-line specimens of the 55A in L-2-15 exhibited weight gains.) These results are considered in support of the conclusions drawn previously that the corrosion of titanium is accelerated during in-pile exposure by some change which occurs throughout the solution under irradiation, so that surfaces in and out of the core are affected to about the same extent. Comparisons of the L-4-16 and L-2-15 results show that the titanium rates increase with increasing average corrosion fission-power density in solution. The Ti-110AT probably corroded at slightly higher rates than the Ti-55A.

5.6 Stainless Steel

Steel corrosion in the in-pile loops has been found to be affected by a number of experimental variables, as reviewed briefly in the following paragraphs.

1. The effects of radiation on steel corrosion are confined to the core. Corrosion outside the core is about the same as that expected in the absence of radiation. The corrosion of specimens at the rear of the core is generally about the same as that found with in-line specimens. Above certain levels for fission-power density in solution adjacent to specimens, the average rate of attack is greater than expected out-of-radiation and the degree of attack increases with increasing power density. The power-density level above which the corrosion rate is affected varies from one experiment to another.

2. Some variations in attack, both positive and negative, with velocity of solution flow past specimens have been observed. To explain the positive and negative effects, it has been postulated that the solution flow may accelerate the attack by mechanisms comparable to those prevailing out-of-radiation, but that it may also reduce the amount of sorbed uranium and, hence, the effective fission-power density at a corroding surface.

3. Some evidence for increased corrosion of specimens in contact with zirconium, titanium, and, in particular, platinum has been obtained.

4. The corrosion of steel in the core is usually markedly increased upon the initiation of radiation exposure with a fresh fuel solution. The average rate drops off during continued exposure and usually reaches and levels off at a value about the same as that for in-line surfaces. A careful analysis of the results of a group of 250°C experiments employing solutions of 0.17 *m* UO_2SO_4, 0.03 *m* $CuSO_4$, and varying concentrations of acid has shown that the oxygen consumption rate in the core is dependent upon the acid and $NiSO_4$ concentrations. Plots of the total oxygen consumption by steel vs radiation exposure time showed a marked decrease in consumption rate after initial periods of varying length of time, and the time of occurrence of the change in rate was correlated with a decrease in acidity and/or increase in nickel concentration to a value for the factor $[H_2SO_4] - [NiSO_4]$ of about 0.01 *m*. Plots of the rate of oxygen consumption per unit steel area in the core and per unit power density during radiation exposure showed near agreement between the results of various experiments. The rate dropped to the background level when the value for the factor $[H_2SO_4] - [NiSO_4]$ was about 0.01.

5. Corrosion of steel surfaces proceeds by formation of pits of about 1 mil in depth. These spread out laterally to yield fairly uniform corrosion of a surface.

6. Since the rate of corrosion in the core decreases with exposure time, the results of weight-loss measurements yield rate values which are averages of a range of values.

7. The relative effects and interrelations of the several variables affecting corrosion are uncertain, so that the corrosion rate under a given set of conditions in the core cannot be accurately predicted.

In general, the results of these L-4-16 and L-2-15 experiments provide additional evidence in support of most of the above items but do not throw much additional light on the interpretation of these effects. With respect to item 4, the results also show that corrosion of steel in the core decreased with exposure time, but, as discussed in more detail below, there does not appear to be any correlation between the concentration of excess acid and the changes in corrosion rates.

The plots of total oxygen consumption on steel vs radiation time (Fig. 12) show the same general characteristics as those observed for the 250°C experiments, although the time to the change in slope was very short for L-4-16. The results obtained in the 250°C experiment EE, which employed a solution having

an initial composition 0.16 *m* UO_2SO_4, 0.020 *m* H_2SO_4, and 0.028 *m* $CuSO_4$, are illustrated for comparison. The results for the oxygen consumption rates on steel during radiation exposure varied with radiation time in a manner also qualitatively similar to that observed at the lower temperature. This is illustrated by the plots in Fig. 48, where the rate values are average values for the steel surfaces in the core calculated by assuming that all oxygen consumption by steel was on these surfaces. Again, the results of the 250°C experiment EE are shown for comparison.

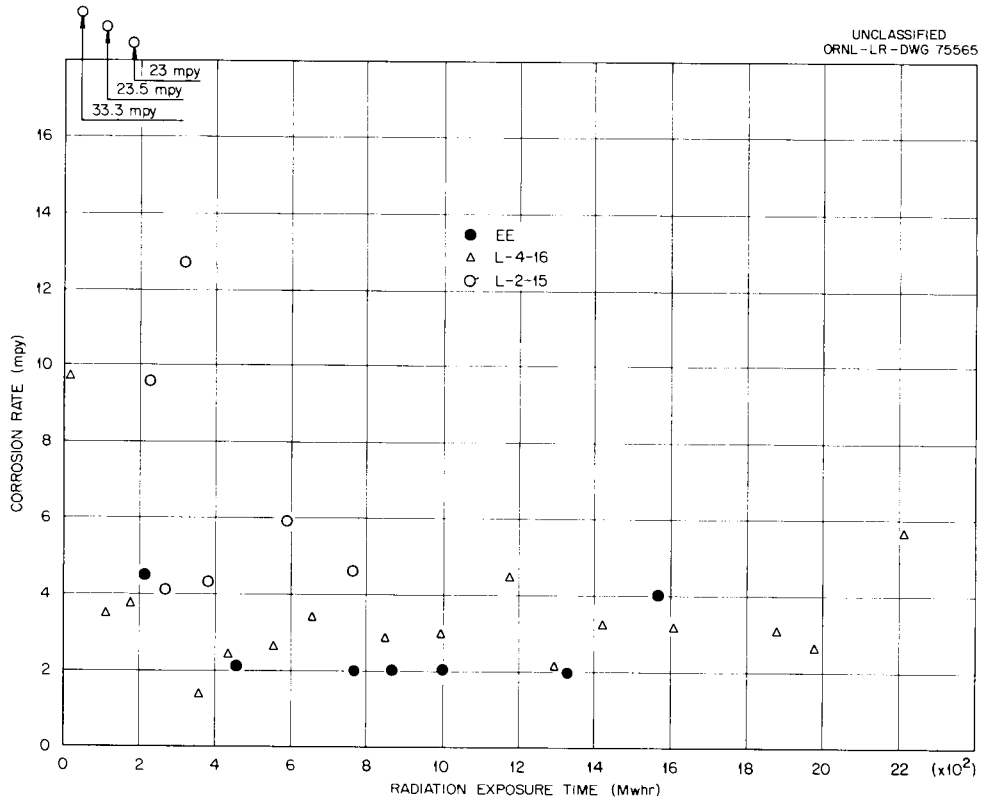

Fig. 48. Comparison of Average Corrosion Rates on Steel Surfaces in Core for Experiments L-4-16, L-2-15, and the 250°C Experiment EE – O_2 Consumption Data.

As discussed in previous paragraphs, the concentration of excess acid in the L-4-16 and L-2-15 experiments probably remained fairly constant throughout radiation exposure in each case. The concentrations of nickel were generally negligibly small in comparison with the acid. Hence, there is no correlation between the reduction in rates observed during the early portion of the exposures and reductions in the acid concentrations. The explanation for the decrease in rates following the initiation of exposure with fresh solution is unknown. The lack of effect of changes in acid concentration and the leveling off of the rates of oxygen consumption while the concentrations were 0.02 *m* or greater show that the tolerance to acid was much greater in these experiments employing solutions of 0.17 *m* UO_2SO_4 and 0.015 *m* $CuSO_4$ in addition to the acid than in those at 250°C employing solutions of 0.17 *m* UO_2SO_4 and 0.03 *m* $CuSO_4$. The difference in acid tolerance is probably a result of the increased temperature, since a similar beneficial effect of temperature occurs out-of-pile.

ORNL-3099
UC-25 – Metals, Ceramics, and Materials
TID-4500 (20th ed.)

INTERNAL DISTRIBUTION

1. C. E. Larson
2. Biology Library
3–4. Central Research Library
5–6. ORNL Y-12 Library, Document Reference Section
7. Reactor Division Library
8–27. Laboratory Records Department
28. Laboratory Records, ORNL R.C.
29. J. E. Baker
30. R. E. Biggers
31. E. G. Bohlmann
32. G. E. Boyd
33. W. E. Clark
34. E. L. Compere
35. W. R. Grimes
36. G. H. Jenks
37. G. W. Keilholtz
38. C. J. McHargue
39. W. R. Musick
40. A. R. Olsen
41. M. L. Picklesimer
42. M. J. Skinner
43. L. E. Stanford
44. J. A. Swartout
45. D. B. Trauger
46. A. M. Weinberg
47. F. Daniels (consultant)
48. F. T. Gucker (consultant)
49. F. T. Miles (consultant)

EXTERNAL DISTRIBUTION

50. Research and Development Division, AEC, Washington
51. Research and Development Division, AEC, ORO
52. Reactor Development Division, AEC, Washington
53. Reactor Development Division, AEC, ORO
54–632. Given distribution as shown in TID-4500 (20th ed.) under Metals, Ceramics, and Materials category (75 copies – OTS)